

# A Survey of Methods for 3D Histology Reconstruction

Jonas Pichat<sup>a,\*</sup>, Juan Eugenio Iglesias<sup>a</sup>, Tarek Yousry<sup>b</sup>, Sébastien Ourselin<sup>a,c</sup>, Marc Modat<sup>a,c</sup>

<sup>a</sup>Translational Imaging Group, CMIC, University College London, UK

<sup>b</sup>Department of Brain Repair and Rehabilitation, UCL Institute of Neurology, UK

<sup>c</sup>Dementia Research Centre, UCL Institute of Neurology, London, UK

---

## Abstract

Combining histology and non-invasive imaging has long attracted the attention of the medical imaging community due to its potential to relate macroscopic information with the underlying microscopic properties of tissues. On the one hand, histology is an invasive procedure which breaks the tissue spatial arrangement due to slicing, but enables its investigation at a cellular level. On the other hand, macroscopic imaging allows for non-invasive acquisition of volumetric data but does not provide microscopic details. Through the establishment of spatial correspondences between histological sections and volumetric medical images, it is possible to relate micro- and macro-scale information so as to gain insight into what affects the signals used to construct medical images, recover the original topology of histology and lost relationships, or build high resolution anatomical atlases.

This survey article synthesises almost three decades of registration methods between two-dimensional (2D) histological slices and volumetric (3D) medical images. The problem is equivalent to reconstructing histological volumes using structural ground truth and calls for mono- and multi-modal image registration techniques. We first summarise the process that produces digitised sections from a tissue specimen in order to understand the peculiarity of data, associated artefacts and possible ways to minimise them. We then delve into the description of methods for histological reconstruction with and without the help of external information. We finally attempt to identify the trends and challenges that the field is facing, many of which are derived from the cross-disciplinary nature of the problem as it involves the collaboration between physicists, histologists, computer scientists and physicians.

*Keywords:* Histology, Medical imaging, MRI, 3D reconstruction, Image registration

---

## 1. Introduction

Histology is concerned with the various methods of microscopic examination of a thin tissue section (Culling, 2013). Cutting through a specimen reveals its internal topography and staining the sections permits the observation of complex differentiated structures. The digitisation of histological sections (referred to as digital pathology) makes high-resolution microscope sections available for image computing and machine learning algorithms. These allow for disease detection, characterisation and prediction so as to complement the opinion of the pathologist (Madabhushi and Lee, 2016; Gurcan et al., 2009), and constitute the field of histopathological image analysis.

When extending such examinations to the third dimension, one faces a substantial challenge: volume slicing breaks the spatial relations between structures. This results in partial understanding about physiology, since a tissue is an object that lives in the 3D space: it is made of an ensemble of cells which, together, carry out a specific function; in turn, organs and basic structures are made of multiple tissues, and only looking at 2D fragments results in narrower understanding of anatomy.

Hence, working with individual 2D histological slices comes with a serious challenge: identifying 3D structures using 2D samples. In this regard, Gagnier and Shipley (2013) showed that

it is complicated to determine how features progress into a volume when only a single face is available. In addition, structures are uniquely altered due to the histology process itself (Figure 1). This may cause anatomically different structures to look similar in microscope slides and conversely, slicing may cause one same structure to have different views if not consistently cut parallel. Other variations due to staining result in objects that may disappear or become highly salient from section to section. Although our ability to represent and mentally transform the shapes of objects is impressive (Atit et al., 2013; Frick et al., 2014), it worsens when structures are interconnected within a dense and complicated environment or subject to complex transformations.

Reconstructing histological volumes from serial 2D sections helps gaining knowledge about spatial environments while accessing microscopic information about tissues. In this respect, the Swiss anatomist Wilhelm His Sr. (1831-1904) explained that just looking through sections does not enable one to build three-dimensional images in the mind and those who wish to grasp anatomical structures must actively engage in working through a reconstruction, reproducing the relationships they wish to understand (Hopwood, 1999).

When using histology alone, reconstruction algorithms aim to restore continuity and usually exploit the fact that the biological specimens shape changes smoothly across sections. They provide a representation of structures and their environment in three dimensions, although one needs to bear in mind that the original

---

\*Corresponding author:

Email address: jonas.pichat.13@ucl.ac.uk (Jonas Pichat)

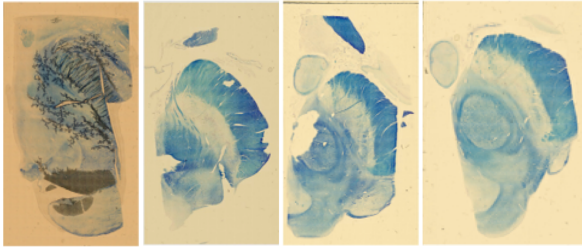


**Figure 1:** Artefacts related to the preparation of tissue sections (wax-embedded here). Those include (but are not limited to) intensity inhomogeneities, stain diffusion, tears, missing pieces, debris, air bubbles, various orientations and locations on glass slides, and spatial distortions.

shape is unattainable without prior knowledge. For illustration purposes, [Malandain et al. \(2004\)](#) pointed out that if a banana is sliced, an ellipsoid will be reconstructed through pairwise alignment of adjacent slices, rather than the original fruit. This is called the “banana effect” or “z-shift”.

The most direct way of recovering volumes from sets of 2D histological slices is by optimising the spatial alignment of every pair of adjacent slices using image registration techniques. Composing the transformations from every slice to a reference slice completes the process—the reference slice is picked for its high contrast, few artefacts, and preferably but not necessarily its location in the middle of the stack. A consequence is that any registration failure (or misalignment) between any two slices impacts the final reconstruction since errors propagate due to the sequential nature of the process. Methods have therefore been developed to minimise these effects by looking at neighbourhoods rather than single slices and attention has also been directed towards preprocessing tissue slices owing to their highly variable quality.

A remedy to the incorrectness of the histological reconstruction is the use of volumetric medical images, such as magnetic resonance imaging (MRI). By providing structural ground truth, they reduce the space of solutions although registration itself still remains an ill-posed problem. Blockface photographs (i.e., pictures of the tissue face taken prior to cutting) and needles may also be used to help reconstruction. While the former provides images of the tissue free of cutting artefacts, the latter allows for straightforward extraction and matching of landmarks in both medical imaging and histology.

Volumetric medical imaging, besides guiding reconstruction, constitutes an invaluable source for accurate, non-invasive study of biological structures and their functions. Relative to histology, [Fischl \(2013\)](#) listed three advantages: the possibility of imaging the exact same tissue with multiple contrasts (e.g., T1 or T2 MRI, MTR, etc.); imaging large samples (e.g., whole-brain or whole-hemisphere) with much less effort than e.g., whole-brain or prostate whole-mount histology; preserving the geometry of the sample and avoiding irreversible damage and distortions induced by processing, cutting, mounting and staining during the histological preparation.

However, resolution-wise, 3D medical imaging is outperformed by histology ( $< 1\mu\text{m}$ ). In addition, for many pathological disorders, there is still no contrast mechanism that allows

imaging to be a full substitute for histology. This is due to the poorly understood relationships between histological and magnetic properties of tissues. Directly predicting what a given histological signature will appear as (when it does) in medical imaging is therefore extremely complex. Practically, this results in that multiple pathologies can share a common imaging phenotype ([Gore, 2015](#)). For example, [Filippi et al. \(2012\)](#) noted that in proton density, FLAIR and T2w MRI scans, Multiple Sclerosis (MS) lesions appeared as non-specific focal areas of signal increase and, therefore, resembled many other types of pathology. This makes it difficult to differentiate them with imaging only. Additionally, some cortical MS lesions can still be missed with conventional MRI sequences ([Seewann et al., 2012](#)). Direct comparisons with histology helps interpret images better and derive more information. They may also correct or adjust existing imaging protocols in order to optimally visualise e.g., lesions in the grey matter of patients with MS.

One of the many benefits of combining histology and medical imaging is to confirm non-invasive measures with baseline information on the actual properties of tissues ([Annese, 2012](#)). By combining 3D medical imaging with digital pathology, it is possible to simultaneously obtain both the rich structural information of the former and the chemical and cellular information of the latter, which may allow for more complete characterisation and understanding of e.g., diseases ([Mori, 2016](#)). One can also derive more accurate segmentations of architectonic boundaries used in the creation of atlases ([Ding et al., 2016](#); [Oh et al., 2014](#); [Amunts et al., 2013](#); [Hawrylycz et al., 2012](#); [Yushkevich et al., 2009](#)) and brain mapping ([Amunts and Zilles, 2015](#)). Note that a more realistic histological reconstruction is obtained as a byproduct of multimodal registration with clinical imaging, when a sufficient number of histological slices is available. Such undertakings are intended to eventually bridge the gap between *in vivo* and *post mortem* studies.

One lasting, sufficient correlation method between many histopathological findings and imaging observations has been by general (visual) comparison. On that matter though, it was recently mentioned in the context of prostate cancer assessment that due to variations in imaging technology, contouring procedure and data analysis, available volume correlation studies had yielded conflicting results ([Priester et al., 2016](#)). Such contradictions were explained by the worrying observation that nearly all prior attempts to define MRI/pathological relationships had relied on imprecise techniques such as manual registration, volume approximation, and 2D measurements. Following the same line of thought—two decades before, correlation was proved to be optimised when the alignment between data had first been carefully taken care of by use of a combination of linear and non-linear transformations ([Mazziotta et al., 1995](#)). In other words, ensuring the comparison of like with like is of utmost importance ([Madabhushi and Lee, 2016](#)).

Multimodal image registration permits the automation of the alignment process and allows to redefine “visual closeness” as the optimisation of a certain matching criterion. It also accounts for the complex transformations that affect histological sections individually and grants higher reproducibility with less or no human effort. Careful use of registration techniques can establish



**Figure 2:** Modalities that may be involved in the registration process. From left to right, a screenshot of a T2w *ex vivo* slice ( $0.1 \times 0.1 \times 0.4\text{mm}^3$ ), a visually corresponding blockface photograph (tissue surrounded by wax) and a Nissl-stained histological section.

more accurate correspondences between histology and volumetric medical imaging i.e., produce histological reconstructions closer to reality, and contribute to more sound data analyses. To this end, it is common to use intermediate modalities (Figure 2) in the process of relating *in vivo* to *post mortem*, so as to keep track on the deformations that the tissue undergoes during its changes of state.

The objective of this paper is to survey the past 30 years of literature on registering histology and clinical imaging. The paper is structured according to the multidisciplinary nature of the problem. Sections 2 and 3 explain the preparation of histological slices, list artefacts associated with every step of the process and cover preprocessing methods in order to best cope with image deteriorations. Section 4 proposes a classification of histological reconstruction methods from 2D serial slices and Section 5 reviews pipelines that aim to combine histological and clinical imaging information by spatially aligning them. Section 6 presents approaches used to validate the correctness of reconstructions—with or without the help of external information—and Section 7 enumerates the clinical applications of such techniques. Finally, Section 8 returns on a few methodological points, discusses some of the remaining challenges in the field and highlights the importance of cross-disciplinary knowledge in solving a biological question.

## 2. From fresh tissue to digital pathology

A pathologist receiving fresh tissue has three options: keeping it fresh, stabilising it in a fixative, or freezing it. Biological tissue is too soft for direct sectioning (although a vibrating blade might do the job), so it is most commonly either embedded in a hardening material and sectioned using a microtome, or frozen and sectioned in a cryostat (a microtome inside a freezer). Sections are then mounted on glass slides and stained before being observed under the microscope by the histopathologist, and/or digitised using flatbed scanners (Dubois et al., 2007) for all sorts of image processing and analyses.

We first briefly describe the two most common processes to obtain sections, namely formalin-fixed paraffin-embedded (FFPE) sections (Section 2.1)—henceforth referred to as paraffin sections—and frozen sections (Section 2.2). Further details can be found in the thorough presentation of histological techniques by Bancroft and Gamble (2008). Then, we briefly present several types of microscopy examinations and the process of digitisation

(Section 2.3). Finally, we highlight the most common artefacts for both types of sections (Section 2.4).

### 2.1. Paraffin sections

FFPE tissue sections stained with H&E are the gold standard (Buesa, 2007) as they provide with generic information in very little time and cost (Rosai, 2007). Their widespread use also relates to the familiarity histopathologists have with the method: the *artefact* it produces at any stage during tissue handling and processing is recognisable and well-documented. In contrast, observing new patterns with other dyes requires time and training (Bancroft and Gamble, 2008). The above-mentioned artefact is to be taken in the sense that it describes a structure that is not naturally present in the living state of the tissue but is rather the product of a series of preparation steps (see also Hardy (1899); throughout the rest of the paper, the definition of *artefact* is narrowed down to image degradations). Knowledge of the steps relative to tissue preparation and diverse staining patterns is not only essential for diagnosis and risk assessment—and this is still an active area of research (Kakar et al., 2015)—but also for all subsequent image analysis steps. In the following, we briefly describe the different stages of FFPE sections preparation.

*Fixation.* It is the most important step when performing histological specimen preparation (Rolls, 2012). Fixation is critical for several reasons: (i) it prevents the tissue from autolysis; (ii) it keeps the tissue close to its living state, without loss of arrangement; (iii) it minimises changes in shape or volume in subsequent procedures and (iv) it yields clear staining of sections. Formaldehydes, such as formalin—which is the most common of all—are routinely used for chemical fixation, such as in Yang et al. (2013); Chen et al. (2003); Bürgel et al. (1999); Weninger et al. (1998); Schormann and Zilles (1998); Streicher et al. (1997). Among others, glutaraldehydes may be used (Baheerathan et al., 1998).

*Tissue processing.* Since most fixatives are water-based and thus not miscible with wax, the tissue must be processed to enable impregnation. This process follows three steps. (i) *Dehydration:* it removes water by immersion in gradients of alcohol. (ii) *Clearing:* it replaces the dehydrating fluid with a wax solvent (the wax solvent has the effect of raising the refractive index of the tissue, making it appear clear, hence the name). Note that long-term clearing creates distortions. Xylene is routinely used for short schedules and blocks less than 4mm thick. Among others, toluene is also used and has similar properties. (iii) *Impregnation:* it replaces the clearing agent with the embedding medium.

*Embedding.* The specimen infiltrated with wax is put in a mould covered with liquefied wax and topped with a cassette. The specimen should lay flat at the bottom of the mould as its orientation conditions the plane of sectioning (an important consideration when flatness is assumed for the comparison with clinical imaging). The ensemble then cools on a cold plate and makes a solid block for microtomy (blocks may also be stored at room temperature for decades, which forms an important archive in

retrospective analyses). Paraffin was used for example, in [Axer et al. \(2011\)](#); [Alic et al. \(2011\)](#); [Bajcsy et al. \(2006\)](#); [Breen et al. \(2005b\)](#); [Schormann et al. \(1995\)](#). Celloidin, more difficult to remove, was used in [Li et al. \(2009\)](#); [Gefen et al. \(2008\)](#); [Beare et al. \(2008\)](#).

*Cutting (or microtomy).* It is performed with a microtome, to which the cassette with the wax-embedded tissue block is clamped. It begins with “trimming”, which consists of removing the surplus of wax until a full section of tissue is available. It requires great care since tissue of diagnostic importance may be removed or the block surface damaged. Cutting is then processed at a certain thickness and the quality of the resulting sections depends upon several factors such as the knife angle, blade quality, speed of sectioning etc., as well as all the previous preparation steps. Thin sections (1–20 $\mu\text{m}$ ) were cut in [Samavati et al. \(2011\)](#); [Zhan et al. \(2007\)](#); [Burton et al. \(2006\)](#). Thick sections (> 20 $\mu\text{m}$ ) were cut in [Jiang et al. \(2013\)](#); [Osechinskiy and Kruggel \(2010\)](#); [Mazaheri et al. \(2010\)](#); [Singh et al. \(2008\)](#).

*Floating, drying.* The thin sections are picked up from the microtome and put in a flotation bath, filled with warm water in order to flatten. Then, they are collected on a glass slide and dried.

*Staining, cover-slipping.* It is the process of colouring and differentiating certain structures in the tissue. Hematoxylin and eosin (H&E) stain is the most common stain in histopathology laboratories. It was used for instance in [Le Nobin et al. \(2015\)](#); [Nir et al. \(2014\)](#); [Gibson et al. \(2012\)](#); [Ward et al. \(2012\)](#); [Arganda-Carreras et al. \(2010\)](#); [Ou and Davatzikos \(2009\)](#); [Meyer et al. \(2006\)](#). H&E method shows a wide range of normal and abnormal cell and tissue components and is easy to perform using either paraffin or frozen sections. Other popular stains include Cresyl violet (Nissl staining), as used in [Adler et al. \(2014\)](#); [Yang et al. \(2012\)](#); [Mailly et al. \(2010\)](#); [Johnson et al. \(2010\)](#); [Chakravarty et al. \(2006\)](#); [Ali and Cohen \(1998\)](#), and methylene blue ([Annese et al., 2006](#)) for nervous tissue sections, silver and gold methods to demonstrate e.g., cell processes in neurones, toluidine blue ([Handschuh et al., 2010](#)) to stain acidic components, Masson’s trichrome ([Song et al., 2013](#)) to stain connective tissue and Alcian blue ([Magee et al., 2015](#)) to stain certain types of mucin. If immunohistochemical staining is to be performed, it requires antigen retrieval (heat- or enzyme-induced) due to loss of antigenicity during fixation ([Shi et al., 1991](#)). Immunohistochemistry (IHC) was performed in [Capek et al. \(2009\)](#); [Groen et al. \(2010\)](#).

After the slice has been stained, it is cover-slipped: a smaller sheet of glass covers the tissue mounted on the glass slide. This creates even thickness for viewing and prevents the microscope lens from touching the tissue. The slide can then be observed under the microscope and/or digitised.

## 2.2. Frozen sections

Frozen sections are quicker to produce than paraffin sections but it is a very demanding process: good section quality (in terms of preservation of tissue morphology) is achieved through

great care and expertise ([Peters, 2003](#)). Although there are conflicting reports about how much freezing may degrade cell morphology and reduce the readability of histological specimens, rapid freezing is known for limiting ice crystal formation and minimising morphological damage. Among disadvantages, it is harder to make the tissue lay flat; frozen sections are also more difficult to cut than paraffin sections and inconvenient to store. The main advantages of using them are the shortcuts in the process (e.g., no dehydration is needed), and their better preservation of antigens for immunohistochemistry. They were used in [Annese et al. \(2014\)](#); [Stille et al. \(2013\)](#); [Annese \(2012\)](#); [Choe et al. \(2011\)](#); [Palm et al. \(2010, 2008\)](#); [Dauguet et al. \(2007c\)](#). In the following, we present the different stages of frozen sections preparation.

*Cryo-protection/embedding.* The limiting factor involved in cryosectioning is the cutting consistency of the block and the freezing damages from ice crystals. Thus, the tissue may require cryoprotection to make it less brittle ([Barthel and Raymond, 1990](#)). Cryoprotecting the tissue is not necessary and consists of fixation (formaldehyde), rinsing and infiltration in increasing series of sucrose solutions. The addition of sucrose provides a smoother cutting block and minimises freezing artefacts. It also happens that sections are prepared from fresh, rapid-frozen tissue but cutting can be incredibly hard without any fixation. Then, optimal cutting temperature (OCT) compound is used to embed the tissue prior to frozen sectioning. OCT helps conduct heat away from the specimen during freezing, protects the tissue from drying during storage, and supports the tissue during sectioning.

*Rapid freezing (or flash/snap freezing).* Once embedded in a particular orientation e.g., face-up, the tissue sample needs to be rapidly frozen to minimise freezing artefacts resulting from ice crystal formation as water freezes in the tissue ([Peters, 2010](#)). One method is to use dry ice (–70° Celsius) on its own. It is simple and safe but creates freezing artefacts that break cell membranes. An alternative is the immersion of the sample in a freezing medium, like a mixture of dry ice and 2-methyl butane (isopentane), which achieves very rapid freezing. Note that direct freezing would cause the tissues or blocks to crack, which would make them very difficult to cut. Tissues with fat often produce poor quality sections since fat freezes at lower temperatures and thus remains too soft to cut; further decreasing temperature may weaken the sample and cause cracks. Tissues with substantial water content, such as the brain, often yield ice crystals during the freezing in the cryostat and result in e.g., non-representative architecture of tumour growth or inflammatory infiltrate ([Taxy, 2009](#)). Snap freezing with liquid nitrogen is often employed to mitigate these artefacts. The frozen tissue can then be stored in a –80° Celsius freezer for future cutting.

*Cutting.* This is similar to paraffin-embedded sections except it is performed in a cryostat. It also starts with trimming of the block. Frozen sections are usually cut between 3–10 $\mu\text{m}$  thick (5 $\mu\text{m}$  thick sections provide adequate morphology). Ultra-thin sections (< 1 $\mu\text{m}$ ) were cut in [Yushkevich et al. \(2006\)](#) (0.25 $\mu\text{m}$ ).

Thin sections ( $1 - 20\mu\text{m}$ ) were cut in [Dubois et al. \(2007\)](#); [Humm et al. \(2003\)](#). Thick sections ( $> 20\mu\text{m}$ ) were cut in [Palm et al. \(2010\)](#); [Malandain et al. \(2004\)](#).

*Retrieving, drying.* Retrieving is the process of picking up the cut frozen section and putting it on a glass microscope slide. Tissue sections can be either picked up from the cryostat stage or from the block directly. From the time the tissue section touches a warm slide, it starts to develop a drying artefact. Air drying frozen section slides will however allow the sections to better adhere to the slide as complex staining procedures cause greater tendency for the tissue to come off the slide during staining.

*Fixation.* Sections of fresh frozen tissue should be fixed immediately unless they are going to be stored for future study. A standard histology fixative: 4% neutral buffered formalin, is the most suitable fixative for frozen sections. Sections of fresh frozen tissue will rapidly dry if exposed to warm air, and this will result in cellular artefact.

*Staining.* Slides prepared by frozen section technique can be successfully stained by many of the staining procedures used for routine paraffin embedded tissues. For example Nissl-stained sections were used in [Yushkevich et al. \(2006\)](#); [Yelnik et al. \(2007\)](#); [Dubois et al. \(2007\)](#) and H&E stained sections were used in [Humm et al. \(2003\)](#). Frozen sections are usually preferred for immunohistochemical staining due preserved antigenicity. This a specific type of stain, in which a primary antibody is used to bind specifically to a particular protein for the purpose of detecting and measuring it. Then, a secondary antibody (which carries a colorimetric or fluorescent detection tag) is used to bind to the primary antibody and reveal its bounding location. IHC was performed in [Seeley et al. \(2014\)](#); [Stille et al. \(2013\)](#); [Lockwood-Estrin et al. \(2012\)](#); [Lebenberg et al. \(2010\)](#).

### 2.3. Microscopy and digitisation

Major types of light (or optical) microscopy include bright-field ([Wang et al., 2014](#)), phase contrast, fluorescence ([Dauguet et al., 2007c](#)) and confocal ([Wang et al., 2015](#)). Electron microscopy encompasses transmission electron microscopy ([Dauguet et al., 2007a](#)) and scanning electron microscopy, the latter being mainly used in the context of serial blockface imaging ([Mikula and Denk, 2015](#); [Denk and Horstmann, 2004](#)). The preparation of tissue specimens for light microscopy follows the steps from Sections 2.1 and 2.2. The preparation of tissues for transmission electron microscopy is described in [Graham and Orenstein \(2007\)](#).

As for immunocytochemistry and immunohistochemistry ([Yelnik et al., 2007](#)), the reaction of antibody with antigen in can be examined and photographed with a fluorescence microscope. Histochemical and cytochemical procedures (based on e.g., specific binding of a dye, a fluorescent dye-labeled antibody or enzymatic activity), can be used with both light microscopic and electron microscopic preparations. Light and electron microscopes produce high resolution micrographs (orders of magnitude of  $0.1\mu\text{m}$  and  $1\text{nm}$  respectively).

Autoradiography—or rather radioautography ([Belanger and LeBlond, 1946](#)), can be observed with both light and transmission electron microscopes and reflects the rate of the energy consumption required to support cellular activity. It is quantified using tracers of glucose metabolism incorporated by living cells and tissues. They generate a labelled product allowing for example, to measure circulating glucose in the blood or radioactivity concentrations. The specimen is then killed and a sample is processed for histology and sectioned. Sections are placed against an X-ray film to produce autoradiographs. The exact 3D localisation of the radiation source is however unknown and thus requires the reconstruction of autoradiographic volumes ([Schubert et al., 2016](#)). Reconstruction is also a pre-requisite for comparison against other three-dimensional modalities such as functional imaging.

Although in the context of multimodal image registration, computer scientists usually work with histological images at a fixed resolution similar to that of a clinical image—most high-resolution detail in histology is biological noise for the purpose of registration—digital pathology should allow the histopathologist to scroll through any level of details of a “virtual” microscopic slide for its examination at any time and anywhere (i.e. not under a microscope), should it be on its own, against another histological section or a 3D medical image plane. This process of digitisation is fundamental ([Ghaznavi et al., 2013](#)) and brings together the fields of virtual microscopy, digital whole slide imaging and telepathology ([Weinstein et al., 2009](#)).

### 2.4. Artefacts

In histology, an artefact is the result of the alteration of a tissue from its living state, caused by the very process of dying and the histological preparation. Artefacts affect different structures from one same tissue section independently, and one *same* structure in adjacent tissue sections differently. Artefacts may compromise both image analysis for accurate diagnosis and image registration for precise alignment. One challenge is to be able to identify artefacts and not confuse them with normal tissue components or pathological changes. This means understanding the causes of such deteriorations as well as their expression in order to provide relevant corrections. Whether paraffin or frozen sections are used, some artefacts have similar characteristics despite having different causes. This makes some preprocessing methods applicable to both types of sections. An exhaustive list of artefacts encountered in paraffin sections, along with ways to minimise them is available in [Rolls et al. \(2008\)](#) and we present some of the most common in the following.

*Loss of detail.* In paraffin sections, delayed fixation may cause poorly defined nuclei and imprecise cytoplasmic details. Improper draining of sections before drying may lead to out-of-focus areas, and imperfect dehydration before clearing, which leaves tiny water droplets in the tissue, may cause opaque areas. Similarly for frozen sections, drying (which starts as soon as the tissue is in contact with a warm glass slide) may blur nuclear details and cytoplasmic borders (due to the leakage of fluids from the cytoplasm), and a loss of contrast. Drying artefacts are

described as cells melting and spreading on the slide by [Peters \(2010\)](#).

*Changes in morphology.* In paraffin sections, the use of an overheated forceps (beyond the melting point of wax) can cause local heat damage and changes in morphology of structures in the area surrounding the contact point. In frozen sections, drying may cause enlargement of cells and nuclei.

*Uneven staining.* In paraffin sections, it may be result from incomplete fixation of the specimen (which leads to zonal fixation), incomplete slide dewaxing (which results in slides containing patches of residual wax and produces unstained, or unevenly stained areas) and excessive heat in the slide drier. Approximate timing as well as different storage conditions also produce inconsistent results across sections. Poor quality formalin results in a “formalin pigment” formation in sections by reaction with haemoglobin, leading to unwanted colouration. As for frozen sections, issues may arise due to over-agitation of loosely adherent tissue in the staining solution.

*Folds and wrinkles.* In paraffin sections, they may be due to poor fixation and/or processing, too large a clearance angle of the microtome, too thin sections, low temperature of the flotation bath (which may not allow sections to flatten properly) or mechanical damages (when attempting to remove a fold in the section with a brush). In frozen sections, the tissue can fold, stretch or tear if too rough during retrieving.

*Cracks and holes.* In paraffin sections, they may happen due to over-processing (which makes the tissue very brittle), under-processing (which makes the tissue poorly supported and therefore fragmented), flotation on a water bath that is too warm, prolonged drying at too high a temperature, too quick sectioning, insufficient clearance angle or a damaged cutting blade during microtomy. As for frozen sections, freezing blocks (instead of cooling them down) can make them crack during cutting. Another challenge is faced with large blocks of tissue, such as whole organs: liquid nitrogen will freeze faster and create a shell around the exterior of the tissue. Then, the organ is likely to crack when the interior expands due to slower freezing.

*Contaminants.* In paraffin sections, this may happen when the water from the flotation bath is not replaced regularly, which favours contaminants that may end up on the slide under the section. Dust, organisms and other contaminants on the glass slide can also spoil otherwise good sections.

*Compression and distortion.* In paraffin sections, they may be due to under-processing (which results in the shrinkage of the specimen); inappropriate size of the container compared to the size of the specimen (which means using an insufficient amount of fixative or squashing the specimen inside); rough handling; poor quality embedding wax (which produces blocks that are difficult to cut); suboptimal knife tilt angle during microtomy and wrong blade type; delay before cutting the final sections of a block (which makes the block warmer); and overheated flotation bath and sections left too long in it (which

cause over-expansion). It is also important to be aware that paraffin sections are unlikely to be of even thickness as the first couple of sections are the widest (due to the thermal expansion of the block during the first passes across the knife) and the least compressed; however as the block warms the sections get narrower and more compressed. As for frozen sections, compression and distortion will most likely result from ice crystal formation—the more water a tissue contains, the more chances artefacts will occur. As water freezes, the expansion of ice crystals compresses cellular tissues (compression artefacts) and distort histopathological correlations. They usually have the appearance of bubbles (ice crystals “bubbles” artefacts). The knife used in cryosectioning can also create cutting artefacts (shearing of the tissue).

In the end, artefacts are unavoidable but also surmountable as pathologists learn to read around them. However, it is very important to try to minimise their impact on subsequent steps, which heavily rely on the tissue quality: for example, sections with cracks and holes often have to be manually discarded because they cannot be registered. Artefacts hamper image computing methods by reducing comparability between supposedly similar structures within or across modalities. For this reason, preprocessing methods have been developed.

### 3. Preprocessing of digital pathology

Among the artefacts resulting from histological preparation, loss of detail and changes in morphology burden image analysis. Not much can be done about them as content is hardly retrievable from lost or corrupted information without any prior knowledge. When due to scanning, though (local poor focusing can cause blurred regions in images), loss of detail is surmountable but at the cost of time-consuming review by the scanner operator. In the context of whole slide imaging, [Lopez et al. \(2013\)](#) automatically identified tiles that required additional focus points. Specifically, they compared the ability of several features in discriminating between blurred and sharp regions of images and showed that the Haralick contrasts and gradient-based features best performed at this task. Compression and distortion are usually taken care of by the process of registration. As for the rest of them, namely: inhomogeneous intensity distributions within and across slices; folding and crumpling; cracks and holes; as well as other artefacts including contaminants and vignetting, or techniques for stitching, dedicated preprocessing methods are presented in the following paragraphs.

*Inhomogeneous slices appearance.* Ideally, the absolute colour of a slide reveals the biological component that a pathologist wishes to retrieve. For example, in the case of H&E, the colour value quantifies the amount of nucleic acids (blue-purple) Hematoxylin has bound to, and the amount of proteins (in pink) Eosin has bound to. However, for the reasons listed in Section 2.4—and/or because of the microscope and the camera used for imaging ([Yagi and Gilbertson, 2005](#))—slides exhibit different colours. Improved feature classification, segmentation and visualisation require the reduction of these variations as well as some sort of

standardisation of the imaging protocols (Badano et al., 2015). This calls for transforming the appearance of a source image into that of a target image preferred by an expert.

In general, histological reconstruction methods use greyscale images for intensity standardisation (or the channel that provides the best contrast in an RGB image). Most techniques are based on histogram matching (Gonzalez and Woods, 2002). One representative method, used for example in Yelnik et al. (2007) and Alegro et al. (2016), was proposed by Malandain and Bardinnet (2003). Using Parzen windowing, they first computed continuous probability density functions from the discrete intensity histograms of two input slices—a Gaussian kernel was also used in Ceritoglu et al. (2010) and Casero et al. (2017). Then, Malandain et al. estimated the optimal affine intensity transformation between them (though higher order polynomial fits may be used). This type of method can be applied in different ways and the reference slice is usually picked for its relative smooth intensity variation of staining and high-contrasted structures (Gaffling et al., 2009; Yang et al., 2013). Adler et al. (2014) optimised the parameters of a global affine intensity transformation using white and grey matter masked images jointly. The central slice was taken as a reference. Yang et al. (2012) used histogram equalisation, in which case a flat histogram is implicitly used as reference for matching. Equalisation is however not robust because it highly depends on the extremal values of the intensity histogram (Malandain and Bardinnet, 2003).

Attempts at decreasing the bias introduced by selecting a single reference slice have been proposed: Li et al. (2009) applied to each slice a transformation that was a weighted sum of transformations from that slice to a set of references (experimentally, one slice every 30 slices). Weights were based on its distance to the corresponding reference slices. Chakravarty et al. (2003) used least trimmed square technique to calculate two third order polynomials for every slice, each of which mapped its intensity profile to that of its predecessor and successor. These polynomials were then averaged and applied to the single slice. Chakravarty et al. (2006) extended their previous work (Chakravarty et al., 2003) by adding an extra layer that accounted for local variations, in which the same averaging process (though restricted to linear fitting) was applied to patches of every slice. This approach however depends on where it starts in the stack. Pichat et al. (2015) computed an unbiased average intensity profile to which the intensity distributions of all slices were matched.

Should it be using a single, a set of, or an average reference distribution, normalisation always depends on the set of histological slices at hands. Hence, the goal of standardising slices appearance is, in general, more to bring visual consistency and help with subsequent segmentation and classification tasks, than being representative of tissue behaviours relative to staining.

The idea of computing a standard histogram allows for a standardisation that is not “stack-specific”. This was proposed in Nyul and Udupa (1999) within the context of clinical imaging, where a standard histogram was computed from a training dataset made of images coming from several acquisition protocols. A similar principle was used in Bagci and Bai (2010). The method developed in Dauguet et al. (2004) followed the same effort, although standard values of each class of tissues had to

be user-defined.

Within the field of histopathological image analysis, the importance of the consistency of *colour* has long been known and is still an objective of research: computational methods, referred to as *colour normalisation*, have been developed to cope with inter-slice colour variations. Two ways of addressing the problem stand out: (i) *colour modification* methods represent the mathematical transformations applied to the source images to match the characteristics of a target image—they are similar to previously described intensity standardisation methods for grey-scale images; (ii) *colour separation* (or deconvolution) methods, concerned with first extracting the main components (i.e., the stains) constituting the original image (relying on the manual delineation of regions of interest, non-negative matrix factorizations, plane fitting in the optical density domain or other colour models), then normalising them individually and finally recombining them, such as in Macenko et al. (2009); Magee et al. (2009); Khan et al. (2014); Vicory et al. (2015); Vahadane et al. (2016); Bejnordi et al. (2016). These methods apply to sections stained with more than one dye, mostly H&E stained images, and are still actively developed. Colour modification was introduced in Shirley (2001), who proposed to match the colour distribution of one image to that of a reference image by use of a linear transform in Lab colour space (a more perceptual colour model than RGB) so as to match the means and standard deviations of each colour channel in the two images in that colour space. This was applied to histological data in Wang et al. (2007). In order to account for scanner-induced variations, Bautista et al. (2014) proposed to use a colour-calibration slide made in-house to derive a colour correction matrix. Bautista and Yagi (2015) showed that it is possible to achieve consistent and accurate segmentations with simple classifiers by accounting for the staining conditions of the slides using dye amount tables.

The use of such colour normalisation methods in the (multimodal) histological reconstruction literature is, to the best of our knowledge, sparse: Braumann et al. (2005) used them and linearly transformed the three RGB colour channels of every image to match the histogram statistics (i.e., mean and standard deviation) of a manually selected reference slice.

*Folds.* They are defined as regions containing multiple layers of stained tissue. This results in regions with higher saturation and lower luminance. As already established, Kothari et al. (2013) used the difference between colour saturation and luminance to detect them. They developed a model that adaptively finds the difference-value range of tissue folds in order to account for the high variability of colour saturation and intensity in different slides. Bautista et al. (2010) enhanced folds and limited the changes in hue by using the difference value between saturation and luminance as a shifting factor for pixel values. Palokangas et al. (2007) used *k*-means clustering on HSI-transformed images (although only saturation and intensity components were said to be discriminative enough). However, such clustering assumes that there are always folds in the images and the method relies on careful initialisation of cluster centres. Simple thresholds are said to be less effective because a tissue fold in a lightly stained image can look similar to e.g., a tumour in a darkly

stained image (Kothari et al., 2013; Palokangas et al., 2007). Similarly to intensity/colour normalisation, fold detection and masking were shown to improve subsequent feature extraction and classification tasks.

The correction of folds may be one of the most difficult problem to solve here, mainly because of the interference of constituents caused by the overlap of different parts of the tissue. Although modelling of developable surfaces has been proposed in computer graphics (Solomon et al., 2012), the reconstruction of unfolded tissue section is difficult as it supposes the separation of structures belonging to different overlapping bits of the tissue section—the number of folded layers is also unknown *a priori*.

*Tears (or cracks) and holes.* Such artefacts are more frequently addressed than folds but their correction remains sparse. Cracks require, in general, manual delineation of the torn area (Breen et al., 2005b) as it is challenging to automatically tell whether a piece of tissue is missing or if the tissue has effectively opened up without loss of material. Yang et al. (2012) filled up the missing sections and missing parts and corrected folds using a procedure described in Qiu et al. (2009). Choe et al. (2011) used a two-stage process involving manual contouring of the torn area was performed and filling by vertical translation of pixel values (columns of the image). Such a process however makes a strong assumption about the horizontality of tears. A similar protocol was followed in Kindle et al. (2011). Breen et al. (2005a) used correspondences between landmarks to stitch the torn piece back: a first thin-plate splines (TPS) warping (Bookstein, 1989) was performed between histology and blockface photograph using manually defined sets of corresponding landmark points. Then, another set of landmarks was found at the borders of the torn piece of tissue in histology and in the intact corresponding piece of the blockface photo (both were overlaid to ease the process). Finally, a separate TPS warping was applied to register the torn piece of tissue back. Correspondences between sets of landmarks were found using the “live-wire” algorithm developed by Falcão et al. (1998); Mortensen et al. (1992). One could also approach the problem of tear correction as jigsaw puzzle solving (Kong and Kimia, 2001; Paikin and Tal, 2015), although it has failed in Yigitsoy and Navab (2013) because these methods rely on borders and medical images usually have low signal and distortions at their boundaries. The tearing/cracking of thin sheets has been subject to extensive studies within the fields of statistical physics (Holmes and Crosby, 2010) or computer vision (Pfaff et al., 2014).

*Masking.* In order to discard various contaminants in the background or edges of the glass slide, which could have an influence in subsequent registration steps, tissue is usually separated from the background. Thresholding is widely used (Nikou et al. (2003); Malandain et al. (2004); Lee et al. (2005); Dauguet et al. (2007b); Palm et al. (2010); Goubran et al. (2013); Stille et al. (2013) and it is usually complemented by mathematical morphology operations (Malandain and Bardin, 2003; Dauguet et al., 2007b; Palm et al., 2010). Dubois et al. (2007) used iterative Gaussian smoothing of histograms for automatic threshold computation: following Mangin et al. (1998), they tracked the positions of

modes in the scale-space and the two modes that remained across most scales were picked as those representing background and tissue. Region growing was then applied in the histogram using previously computed upper and lower bounds. Masking was performed with mathematical morphology (successive erosions using *a priori* knowledge of the tissue surface) and the largest connected component was extracted. Yushkevich et al. (2006) used active contour segmentation with region competition (Zhu and Yuille, 1996) followed by mathematical morphology to refine the masks: opening (which is less destructive than erosion but still removes foreground bright pixels) was performed and the largest connected component was kept as final mask. Level-sets were used with a dynamic speed function in Li et al. (2009), and in Uberti et al. (2009) (based on Li et al., 2005). They incorporated higher level constraints obtained from prior knowledge and understanding of mouse brain anatomy. Palm et al. (2010) used *k*-means clustering on the “a” channel, after transformation from RGB to CIELab colour space, to segment tissue in blockface photographs. This was followed by a hole-filling algorithm. Adler et al. (2014) used Atropo (Avants et al., 2011), an *n*-class Markov random field segmentation software package for tissue foreground segmentation. They used three labels: grey matter, white matter and background—grey matter and white matter labels were united into foreground tissue mask, from which the largest connected component was retained.

*Vignetting (or shading).* A common problem irrespective of the type of camera and method of microscope attachment is uneven illumination at the edges of the image (Leong et al., 2003). In general, it occurs in most imaging sensors due to an uneven illumination of the scene being imaged. As a consequence, images are usually lighter near the optical centre and darker at image borders (i.e., a shading artefact). This effect is particularly evident when stitching images into a mosaic in order to increase the field of view of the microscope to obtain e.g., whole-slide images. Correction of uneven illumination in histological slices has borrowed ideas from intensity inhomogeneity correction in MRI (Sled et al., 1998; Vovk et al., 2007). The correction of vignetting was addressed in Peng et al. (2014); Piccinini et al. (2013b) and the interested reader may also refer to Reyes-Aldasoro (2009); Yu (2004). In the (multi-modal) histological reconstruction literature, shading correction was performed as preprocessing in Bürgel et al. (1999) using methods from Gonzalez (1987). Arganda-Carreras et al. (2010) developed a background correction algorithm based on a phantom (Fernandez-Gonzalez et al., 2004) that was used to correct the mosaic-like effect of the images caused by uneven illumination of the field of view of the microscope. Capek et al. (2009) also applied methods for compensation of such a light variability, further described in Čapek et al. (2006). Hsu et al. (2008) accounted for colour difference and optical degradation by means of a Gaussian-like model and a wavelet-based image blending.

*Stitching (or mosaicing).* It is needed when the field of view of the classical microscope is too narrow to allow for the visualisation of the entire tissue. The section can either be physically cut into several pieces that are isolated in the image (see Chappelow

et al. (2011b), or Ou and Davatzikos (2009), who simulated it), or spatial tiles can be obtained by moving the microscope stage (Capek et al., 2009). The latter protocol however introduces overlapping between adjacent fields of view. Overlap is recommended to account for field curvature-induced artefacts in the image and avoid loss of detail at the edges between images; Gareau et al. (2008) included 10% overlap in the translation step distance. Spatial rearrangement of the pieces relative to each other is required in both situations to recover an image of the full tissue section for subsequent volume reconstruction or registration with other modalities. This is usually performed through image registration. Capek et al. (2009) performed stitching by first positioning the tiles using landmark points, and then optimising a similarity measure in the parameter space of translations using  $n$ -step search (Tekalp, 1995). This method was implemented in GlueMRC (Karen et al., 2003). Hsu et al. (2008) solved mosaicing by matching features detected in adjacent histological tiles. Those were extracted using wavelet-based edge correlation and pairs of corresponding features were then identified by maximisation of the normalised correlation coefficient. Saalfeld et al. (2012) solved mosaicing of ssTEM images based on previous work (Saalfeld et al., 2010) using SIFT features.

There exist several softwares that automatically perform the task (Piccinini et al., 2013a): in ImageJ, the Stitching<sup>1</sup> plug-in (Preibisch et al., 2009); Autostitch<sup>2</sup> (Brown and Lowe, 2007); MosaicJ<sup>3</sup> (Thévenaz and Unser, 2007); XuvTools<sup>4</sup> (Emmenlauer et al., 2009); HistoStitcher and AutoStitcher<sup>5</sup> (Chappelow et al., 2011b; Penzias et al., 2016). Only a few studies, such as Ma et al. (2007) using Autostitch, have been accounting for vignetting (Piccinini et al., 2013a). Piccinini et al. (2013a) developed MicroMos<sup>6</sup> and ensured their tiles had all been flat-field corrected prior to stitching them back together.

An automatic mosaic acquisition and processing system for multiphoton microscopy was described in Chow et al. (2006), along with the importance of normalisation to avoid shading artefacts at the border of tiles. Methods that extend the tiles beyond their boundaries by propagating available structures were also developed in Jia and Tang (2008) and Yigitsoy and Navab (2013). Stitching is extensively studied in the general computer vision literature (Brown and Lowe, 2007).

#### 4. 3D histological reconstruction

Histological reconstruction methods aim to restore the loss of continuity due to volume slicing. They are based on the fact that the shape of a biological specimen changes smoothly across sections, but suffers from various artefacts that affect every section independently during its preparation. When using histology

alone, reconstruction algorithms provide representations of structures and their environment in three dimensions—which help with subsequent segmentation and classification tasks (McCann et al., 2015)—but one needs to bear in mind that the original shape is unattainable without prior or external knowledge.

Reconstruction algorithms from serial histological slices rely on image registration and consist of optimising the spatial alignment of variously oriented 2D slices relative to each other, while being robust to artefacts following histological preparation. The most straightforward way is to register every slice with its direct neighbour and repeat the process with the following pairs, but this is not robust to errors. First efforts towards the reconstruction and visualisation of volumes from 2D sections relied on this technique and were initiated in the early 1970s (Levinthal and Ware, 1972; Lopresti et al., 1973). A list of company/academic softwares and plugins for histological reconstruction from serial sections is available in Table 1.

Registration is the process of bringing two images (one usually referred to as “reference, fixed or target” and the other as “floating, moving or source”) into spatial alignment and deforming the floating image such that it looks like the reference image (for transformations others than rigid-body). The objective is to estimate the transformation that optimises an energy function. It is usually made of two terms, one referred to as the matching criterion (a distance measure, in a broad sense) and a regulariser, either implicit (by restricting the type of transformation) or explicit (e.g., deformation field filtering, penalty terms, etc.), which controls the transformation and prevents excessive or unrealistic deformations. This definition holds for the rest of the paper. Further details can be found in reviews about (medical) image registration (Maintz and Viergever, 1998; Hill et al., 2001; Zitova and Flusser, 2003; Sotiras et al., 2013) and a report was recently presented in Viergever et al. (2016) to assess whether the goals of the field were met. A list of open-source toolkits for medical image registration is available in Table 2.

Histological reconstruction is obtained by the composition of every single pairwise transformation with respect to a certain reference. The quality of the resulting volume highly depends upon the choice of that reference slice. It is usually an arbitrary choice made by an expert, who selects a slice that exhibits little deformations, few artefacts and high contrast. Although the first slice (Lee et al., 2005; Colchester et al., 2000) is sometimes chosen as reference (Chen et al., 2003; Krinidis et al., 2003a), it may be preferable to select it around the centre of the stack (Ourselin et al., 2001b; Pitiot et al., 2006; Cifor et al., 2011). This minimises the propagation of errors due to slight misalignments (let aside registration failures), which may produce skewed or helicoidal stacks. To the best of our knowledge, only Bagci and Bai (2010) proposed to automate the process of selecting the *best* reference slice by considering the information content in feature space.

Without any information about the true shape, volume reconstruction remains an ill-posed problem i.e., although there exists a solution, it is not unique (and the *true* one is unknown); for example, changing the initial arrangement of slices relative to one another will lead to a different reconstruction. Whichever way it is addressed, the process tends to straighten up structures:

<sup>1</sup>[http://imagej.net/Image\\_Stitching](http://imagej.net/Image_Stitching)

<sup>2</sup><http://www.autostitch.net/>

<sup>3</sup><http://bigwww.epfl.ch/thevenaz/mosaicj/>

<sup>4</sup><http://www.xuvtools.org/doku.php>

<sup>5</sup><http://engineering.case.edu/centers/ccipd/content/software>

<sup>6</sup><https://sourceforge.net/projects/micromos/>

**Table 1:** Company/academic softwares and plugins for histological reconstruction from serial sections and their use in the literature.

softwares/plugins	institution	non-rigid warping	references	used in
TrakEM2 (ImageJ)	Uni of Zürich (CHE)	no	(Cardona et al., 2012)	(Chklovskii et al., 2010)
StackReg (ImageJ)	EPFL (CHE)	no	(Thevenaz et al., 1998)	(Micheva and Smith, 2007)
AutoAligner	Bitplane (CHE)	no	-	(Friedrich and Beutel, 2010)
Voloom	TU München (DEU)	yes	(Feuerstein et al., 2011)	(Fónyad et al., 2015)
BrainView	LIN (DEU)	yes	(Lohmann et al., 1998)	(Dubois et al., 2007)
Free-D	INRA (FRA)	yes	(Andrey and Maurin, 2005)	(Bonnet et al., 2013)
BrainVISA	CEA I <sup>2</sup> BM (FRA)	yes	(Cointepas et al., 2001)	(Dubois et al., 2007)
AlignSlices (Amira)	FEI VSG (FRA)	no	-	(Andersson et al., 2008; Cornillie et al., 2008)
3DHISTECH	(HUN)	-	-	(Onozato et al., 2013)
poSSum	Nencki Institute (POL)	yes	(Majka and Wójcik, 2015)	(Majka and Wójcik, 2015)
ImageRegistration (ImageJ)	NTUST (TWN)	yes	(Wang et al., 2014)	(Wang et al., 2014)
BioVis3D	(URY)	-	-	(Dezsó et al., 2012)
HistoloZee	UPenn (USA)	yes	(Adler et al., 2014)	(Yushkevich et al., 2016)
Protomo	Florida SU (USA)	no	(Winkler, 2007)	(Singh et al., 2016)
Reconstruct	Boston Uni (USA)	yes	(Fiala, 2005)	(Mathiisen et al., 2010)
IMOD	Uni of Colorado (USA)	yes	(Kremer et al., 1996)	(Mishchenko, 2009)
ImageJ	NIH (USA)	no	(Schneider et al., 2012)	(Le Nobin et al., 2015)
NIH Image	NIH (USA)	no	(Rasband and Bright, 1995)	(Laissue et al., 1999)

a banana-like original volume, cut and reconstructed, will end up looking like an ellipsoid—hence its name, the “banana effect” or “z-shift” effect (Malandain et al., 2004).

Some works tried to bypass registration failures through graph theoretic approaches (Yushkevich et al., 2006; Adler et al., 2014; Pichat et al., 2015), which formulate the reconstruction problem as a shortest path problem in order to identify the best sequence of transformations. Alternatively, most recent works commonly proceed by aligning every slice with a set of neighbouring slices (as opposed to considering only one neighbour) in order to smooth out potential errors and improve continuity (Mertzanidou et al., 2016; Rusu et al., 2015; Saalfeld et al., 2012; Feuerstein et al., 2011; Nikou et al., 2003).

We classify works aiming to reconstruct volumes based on the registration method they used. This yields two categories: registration using geometric features (Section 4.1) and registration using voxel comparison (Section 4.2). While the former may be fast (because it uses a subset rather than the whole image domain), the latter is more accurate but slower and requires careful initialisation as methods tend to settle in local optima.

#### 4.1. Geometric methods (landmark-based)

Geometric methods aim to register two images by minimising a criterion that takes into account landmark information. The first step in geometric registration is to obtain points of interest (Section 4.1.1). Those are usually noticeable locations in the image, under the assumption that saliency at the image level is equivalent to relevant anatomical regions. After finding correspondences between landmarks, a smooth transformation is sought so that their alignment is respected (Section 4.1.2). Further details can be found in Sotiras et al. (2013).

##### 4.1.1. Detecting points of interest

Processing histological images is complex when it comes to using points of interest: the appearance of slices vary greatly

and adjacent sections expose *similar* rather than the *same* constituents. Consequently, their description should be flexible enough to grant matching, while peculiar enough to disambiguate between close potential candidates. Besides, the very task of locating reliable landmarks remains an open problem, and it is still an active area of research (Sotiras et al., 2013). In this section, we use interchangeably the terms landmark, key-point and point of interest. Points of interest fall into three categories: manually extracted landmarks, needle tracks, and automatically extracted landmarks.

*Manual landmark selection.* It is usually carried out by experienced histopathologists and benefits from the rich details that high resolution histological images provide. The main advantage of manual selection is that it allows for accurate, consistent selection of anatomically relevant landmarks. The task is however very time-consuming and subject to inter- and intra-user variability, and was for example performed in Gaffling et al. (2011). Zhao et al. (1993) manually segmented the contours of the autoradiographs, which is a special case of landmark extraction as points may be sampled along those contours or curves used as such for boundary matching.

*Needle tracks as landmarks.* Needles can either be inserted in the fresh tissue, or in the embedding medium by placing ink marks (Simonetti et al., 2006). The marks can then be manually or automatically isolated, such as in Colchester et al. (2000) who identified centres of labelled needles tracks using Hough transform. Although the technique is known to be invasive, recent advances allow to minimise damages to the tissue (Hughes et al., 2013)

*Automatic feature extraction.* Within the context of histology, we identified three main types of features associated with automated methods to extract and describe them, namely Fourier-based, blob-like and object-level features.

**Table 2:** List of open-source registration toolkits/software used for histological reconstruction (L and NL stand for linear and non-linear registrations respectively).

softwares/packages/plugins	institution	type of transformation(s)	references	used in
<b>ANIMAL</b>	McGill (CAN)	NL	(Collins et al., 1994, 1995)	(Chakravarty et al., 2006)
<b>TurboReg</b> (ImageJ)	EPFL (CHE)	L	(Thevenaz et al., 1998)	(Riddle et al., 2011)
<b>UnwarpJ</b> (ImageJ)	EPFL (CHE)	NL	(Sorzano et al., 2005)	(Wang et al., 2015)
<b>MERIT (MeVisLab)</b>	Fraunhofer MEVIS (DEU)	L/NL	(Boehler et al., 2011)	(Schwier et al., 2013)
<b>bUnwarpJ</b> (ImageJ)	UAM (ESP)	NL	(Arganda-Carreras et al., 2008)	(Kindle et al., 2011)
<b>Elastix</b>	UMC Utrecht (NDL)	NL	(Klein et al., 2010)	(Alic et al., 2011; Stille et al., 2013)
<b>NiftyReg</b>	UCL (UK)	L/NL	(Modat et al., 2010, 2014)	(Pichat et al., 2015)
<b>VTK CISC</b>	KCL (UK)	L/NL	(Hartkens et al., 2002)	(Benetazzo et al., 2011)
<b>AIR</b>	USC (USA)	L/NL	(Woods et al., 1998a,b)	(Brey et al., 2002; Beare et al., 2008)
<b>ITK</b>	NLM (USA)	L/NL	(Yoo et al., 2002)	(Mosalganti et al., 2006; Gijtenbeek et al., 2006)
<b>ANTs</b>	UPenn (USA)	NL	(Avants et al., 2009)	(Adler et al., 2014)
<b>DRAMMS</b>	UPenn (USA)	NL	(Ou and Davatzikos, 2009)	(Ou and Davatzikos, 2009)

**Fourier-based features:** Hsu (2011) adjusted the method they used earlier in the context of mosaicing (Hsu et al., 2008) for histological reconstruction, based on work from Hsieh et al. (1997). The detection of edges was handled by wavelet transforms. The robustness to noise was achieved using edge correlation, as introduced in Xu et al. (1994). Reliability of feature points was increased by means of multiscale edge confirmation, which filtered out the noise since mostly features remain across multiple scales (unlike noise). The reader may also refer to Mallat’s works for a thorough study of multiscale edge detection through wavelet theory (Mallat and Zhong, 1992). The orientation of the feature point was determined through a line-fitting method rather than estimated using the result of the wavelet transform (which is sensitive to noise): it essentially considered a neighbourhood of a detected feature and estimated the orientation of the edge line passing through it and neighbouring edge points. Braumann et al. (2005) used Fourier-Mellin invariant (FMI) descriptors of images (Casasent and Psaltis, 1976). They were obtained by Fourier-Mellin transform of the image in a polar coordinate system, which decoupled translation, rotation and scaling (respectively for rotation and scale invariance). Note that Ghorbel (1994) later showed that using instead the analytical Fourier-Mellin transform allows getting a complete set of similarity-invariant features.

**Blob-like features:** Scale-invariant feature transform (SIFT) is ubiquitous in the computer vision literature. It is based on local extrema (or blob) detection (Lowe, 1999). The detector relies on difference of Gaussians (DoG), which is an approximation of the scale-normalised Laplacian of Gaussian (related to each other through the heat equation) and thus contains no directional information. Keypoints are local optima in the DoG scale space of the image. Candidate keypoints that are unstable i.e., low contrasted extrema or those lying on edges (since they are invariant to translations along their direction) are discarded. Location, scale and orientation (estimated as the main gradient orientation over a keypoint neighbourhood) are encoded in the descriptor of every keypoint. The interested reader may refer to Toews and Wells (2009) for efficient encoding of that vector. An in-depth analysis of the SIFT method is available in Rey Otero and Delbracio (2014).

SIFT was used in Koshevoy et al. (2006) as well as in Saalfeld et al. (2012), based on previous work (Saalfeld et al., 2010) for the registration of tiled serial TEM sections<sup>7</sup>. Wang and Chen (2013) used colour deconvolution (see Section 3) to separate hematoxylin and eosin stain contributions from individual histopathological images. Eosinophilic structures were used as object-level features for image registration, from which points of interest were detected using DoG detector. This was reused in Wang et al. (2014, 2015).

Lobachev et al. (2017) used another popular feature detector and descriptor, SURF (Bay et al., 2006). The keypoint detector is based on the determinant of the Hessian matrix operator and relies on integral images for fast computation. As far as SIFT is concerned, DoG is basically a Laplacian-based detector and the Laplacian operator is defined as the trace of the Hessian matrix. Using its determinant (instead of the trace) as it is the case with SURF, discourages the detection of elongated, ill-localised structures.

Ulrich et al. (2014) used Binary Robust Invariant Scalable Keypoints, BRISK (Leutenegger et al., 2011), based on the AGAST corner detector (Mair et al., 2010). Note that an evaluation of binary feature descriptors performance can be found in Heinly et al. (2012).

**Object-level (or high-level) features:** Another school of thought recommends the use of structures such as vessels, nuclei etc., (Ruiz et al., 2009). The rationale is that traditional feature detection schemes generate a great amount that are regular in appearance, thereby making matching unrealistic. Such features are also described in Gurcan et al. (2009). For example, Schwier et al. (2013) extracted vessel-like structures in greyscale images using thresholding and mathematical morphology in every slice. The sets of structures were then refined using eccentricity, ellipticity and size criteria. Prescott et al. (2006) extracted specific regions in cochlear images using Otsu’s thresholding, mathematical morphology and only kept the largest connected components. For each stain type, colour segmentation followed

<sup>7</sup>Saalfeld and Tomancák (2008) developed plug-ins for ImageJ to extract SIFT and Multi-Scale Oriented Patches, MOPS (Brown et al., 2005) correspondences in two images: [http://imagej.net/Feature\\_Extraction](http://imagej.net/Feature_Extraction)

by mathematical morphology allowed Cooper et al. (2009) to segment significant structures such as blood vessels, other ductal structures or small voids within the tissue area.

Other methods, although relying on the same type of features, address the matching step by comparing informative patches (also referred to as windows, blocks, boxes or tiles) centred around those keypoints. In other words, features are described by the intensities of pixels around them, which comes down to a block-matching strategy to infer correspondences. We thus explain the matching step for such approaches (referred to as tile-based methods) in Section 4.2. As such, Xu et al. (2015) extracted relevant structures from the images based on colour and size. Arganda-Carreras et al. (2010) extracted structures of interest by combining fast marching algorithm and level-sets. Ruiz et al. (2009) selected tiles that have rich content i.e., which variance is above a certain threshold.

The registration of differently stained histological sections also relies on those high-level features but the literature on that problem is sparse (Braumann et al., 2006; Song et al., 2013, 2014). It is a multimodal problem in that every section varies in appearance: images exhibit different colour distributions and different structures due to different staining. This is solved by identifying common structures and grouping them into comparable clusters. The problem thus becomes monomodal using labeled images or probability maps. Braumann et al. (2006) assigned every pixel a “segmentation vector” containing, for successive Gaussian smoothed versions of the image, its RGB value and the colour mean of a neighbourhood around the pixel. The clustering of the image into different numbered classes was based on Pernkopf and Bouchaffra (2005), who selected the number of components that best modeled the distributions in order to represent the characteristics of the images adequately. A similar idea was proposed in Song et al. (2014) except that the segmentation vectors for each pixel, called “appearance feature vectors”, also included information about texture. The clustering of the appearance feature vectors was carried out using a principal eigenvector binary tree clustering algorithm.

One last type of methods makes use of the tissue boundary. After extraction, it is used for contour matching. Extracted curves may also be sampled to perform point matching (those points are also referred to as nodes). Tissue edge points sampled along boundaries have the advantage of being less vulnerable to e.g., tearing—when sampled appropriately—from which intensity-based methods would suffer. However, their detection relies on accurate segmentations, which in turn may be affected by intensity inhomogeneities if for example a simple global threshold is to be used for all the slices. Tissue edges may be obtained through Otsu’s thresholding, such as in Shojaii et al. (2014); Shojaii and Martel (2009).

Tan et al. (2007) extracted the sharpest curvatures from the contours of the tissue, which yielded three feature points at consistent locations in every section. The tractability across slices allowed for the computation of “trajectories”.

Krinidis et al. (2003b) obtained each slice contours using a 2D elastic physics-based deformable model. The model consisted of a set of nodes, initially distributed over a circle. In its fully deformable configuration, the model allowed each node to move

independently, without affecting adjacent ones.

Guest and Baldock (1995) extracted two types of nodes with the aim of creating a mesh: *object nodes* were automatically selected, ideally along the boundary of the structure i.e., with large gradient, and a minimum distance criterion to prevent them from being too close. *Background nodes* were sought in the background region with larger minimum distance. Delaunay triangulation from the obtained nodes provided a mesh with higher density over the domain of the tissue.

Rangarajan et al. (1997) extracted the locations of high confidence edges (including tissue boundaries) by thresholding edge images obtained from Canny edge detection (Canny, 1986).

Cohen et al. (1998) used thresholding to define a contour and it was manually edited if necessary in order to obtain satisfactory boundaries. Contours were then modeled using B-splines and the inverse chord length method was used to estimate knot points that best described a given curve data. This method regulates their number based on the amount of shape variation a region subjected to (fewer knots when the variation is small).

#### 4.1.2. Correspondences and spatial transformations

Correspondences between landmarks may be straightforward, as it is the case when extracted manually (although labour intensive and time-consuming) or using segmented needle track holes. For example, Gaffling et al. (2011) computed the trajectories of landmarks tracked across the slices through a fourth order polynomial fit. Note that polynomial transformations are usually advised to be computed using a low-degree polynomial due to noise and numerical instabilities (Ali and Cohen, 1998). Those landmarks were placed at identifiable locations along the tissue outer and inner boundaries.

Needle track holes allow for the computation of a (linear) transformation by least-squares minimisation. Colchester et al. (2000) used a set of photographs of both anterior and posterior faces of every tissue sections. “Within-slice co-registration” was achieved by minimising the sum of squared distances between centres of labelled needles tracks for every pair of faces. Then, “between-slice co-registration” consisted of registering the posterior face of one section with the anterior face of the next using block-matching (Ourselin et al., 2001b). Other examples of use of fiducial markers include works from Goldszal et al. (1995); Humm et al. (1995). Although they may increase the reliability of the registration process because their locations are easy to track in the images, needles also damage the tissues and introduce bias if the cutting plane is not orthogonal to the needles’ axes. This protocol was however improved in Gibson et al. (2012); Hughes et al. (2013).

In contrast, automatically extracted features require a dedicated step that seeks for correct matching pairs in order to derive the correct transformation. Automatically discarding false matches is critical; otherwise the latter methods would suffer from the same problems that hamper intensity correlation (Rangarajan et al., 1997).

Hsu (2011) used an analytic robust point matching method for global registration. The alignment was refined using a feature-based modified Levenberg-Marquardt algorithm (Moré,

1978). Braumann et al. (2005) matched FMI descriptors between a reference and a target image using a symmetric phase-only matched filtering (Chen et al., 1994). The parameters of rigid transformations were derived from it.

As for blob-like features like SIFT, SURF etc., matching pairs are usually found by minimising the Frobenius norm in the descriptor space. Random sample consensus, RANSAC (Fischler and Bolles, 1981) is then used to discard wrong correspondences and solve for the transformation.

Koshevoy et al. (2006) assumed that serial section transmission electron microscopy (ssTEM) images were taken at the same scale, and suffered from minor deformation on the global scale, which made the scale-invariance requirement unnecessary. Only SIFT descriptors belonging to the same octave and scale of the DoG scale space thus needed to be compared against each other. To this end, they used an optimised *kd*-tree with a best-bin-first nearest neighbour search algorithm (Beis and Lowe, 1997). Wrong correspondences were filtered out using a criterion based on Euclidean distances, similar to that introduced in Hsieh et al. (1997).

Solving for the transformations parameters was achieved using RANSAC in Koshevoy et al. (2006); Wang and Chen (2013); Wang et al. (2014, 2015). It essentially estimates the set of feature points that behave consistently with respect to a linear transformation. Saalfeld et al. (2010) estimated simultaneously the rigid arrangement of tiles within and across sections using SIFT features and RANSAC registration. The methods are available online<sup>8</sup>. It was extended in Saalfeld et al. (2012) by refining the alignment using intensity-based registration (a block-matching strategy detailed in Section 4.2). The combination of both strategies was used to initialise an elastic registration, for which each image was tessellated into a mesh of regular triangles. Like in Guest and Baldock (1995), the the system of equations representing the whole stack of slices was an elastic spring finite element model. The entire system stabilised when the sum of the forces of all springs was close to zero.

Lobachev et al. (2017) used SURF keypoints. Descriptors were matched using a bi-directional brute-force matcher and the rigid transformation was computed using RANSAC. Then, a non-rigid transformation was computed at multiple resolutions using feature pairs in adjacent sections to constrain control points of B-splines. At every iteration, the feature size decreased while the resolution of the grid of control points increased. No reference section was taken and all the images were deformed towards a minimum energy function.

Ulrich et al. (2014) used BRISK feature detector which is faster than SURF. RANSAC-based rigid registration was also performed and the non-rigid registration step consisted of the alignment of all feature pairs by least-squares deformations. This process was repeated if the pairs after transformation were not stable. The methodology was reused in Lobachev et al.

(2017) and incorporated into a multi-resolution framework.

The Euclidean distance in combination with other criteria, such as size, is also used to assess the similarity between pairs of object-level features. As such, Schwier et al. (2013) tried all possible combinations of pairs in adjacent sections. The transformation that gave the best similarity was kept. The matching cost took into account a distance range, within which matching pairs should lie, as well as the closeness in terms of object size (area). This was robust to cases where no valid correspondence was found. Pairwise non-rigid registrations (Modersitzki, 2004) were performed and implemented as part of a software (Boehler et al., 2011).

Prescott et al. (2006) paired features using the area only. Mismatches were identified using a distance-based criterion, similar to that presented in Koshevoy et al. (2006). The linear transformation was derived from a matching graph, in which every node is a matching pair and is associated with a transformation. An edge exists between two nodes if the two transformations are *sufficiently* similar. The global transformation is the average of those constituting the maximal cyclic structure from the graph. It served as an initialisation for subsequent registration based on maximisation of mutual information and gradient information (Pluim et al., 2000).

Cooper et al. (2009) paired features based on both size (area) and eccentricity. Mismatches were filtered out in a way similar to Prescott et al. (2006) and rigid transformation parameters were associated with every correct pair. The correct rigid transformation was then estimated through a voting scheme. Non-rigid registration was performed using second-order polynomials, which coefficients were calculated using correct feature pairs.

In the context of the registration of differently stained histological sections, the problem is that of matching labelled classes corresponding to common structures in the images. Braumann et al. (2006) used a methodology that was partly based on Braumann et al. (2005) and reused in Wentzensen et al. (2007). After clustering the images into different numbered classes, class label adjustment was performed in cases where the assignment was not consistent. The problem of having more and/or different classes—because sections may exhibit different structures—was tackled by merging classes so as to have the same regions segmented in both images. Every labelled image pair was finally aligned by computing the displacement vector field using non-linear, non-parametric curvature-based registration. Song et al. (2014) solved the correspondence problem by grouping clusters into three superclusters (called “content classes”) in each image according to various partition schemes. The pair of partitions that maximised mutual information provided the optimal content classes in each image. These classes were then refined using spatial features. Then, each image was transformed into a multichannel probability map, where each channel corresponded to one content class. Block-matching registration was performed between pairs of probability maps for each channel independently. This provided a displacement field, from which a non-rigid transformation

<sup>8</sup>Two stand-alone plugins were implemented: Elastic Montage, for mosaicing, and Elastic Stack Alignment, for the alignment of images from serially sectioned volumes. They are incorporated in the TrakEM2 software and available at [http://imagej.net/Elastic\\_Alignment\\_and\\_Montage](http://imagej.net/Elastic_Alignment_and_Montage)

was estimated using a regularised least squares difference minimising method.

When sets of points sampled along the boundary of the tissues are to be matched, one popular method is the Iterative Closest Point (ICP) method (Besl and McKay, 1992). Shojaii and Martel (2009) used ICP to register every histological slice with its corresponding blockface photograph. Points were uniformly distributed along every smoothed boundary of the tissue by excluding high curvatures using a rolling-ball filter. They argued that “high-curvature boundaries might lead ICP to converge to local minima and deteriorate its robustness”. Deformable registration was then performed using TPS.

Rangarajan et al. (1997) simultaneously optimised the affine transformation parameters and the one-to-one correspondences between two sets of edge points in adjacent sections. This method is referred to as robust point matching.

Krinidis et al. (2003b) found correspondences between contour nodes of adjacent slices using an affinity matrix. Corresponding nodes between adjacent slices were couples which relative distance was lower than a certain threshold. False matching were filtered out by global affinities, which ensured that correct correspondences also exist in slices further away. Translation and rotation parameters were computed by minimising the mean square error between pairs of matching nodes.

Gaffling et al. (2011) used the offsets of every landmark to a smooth curve representing the trajectory of that landmark across slices, and computed a sparse displacement field for every slice; the vector fields were then densified (Fischer and Modersitzki, 2003). Every image was finally deformed such that its landmarks lied on the trajectories, and every following slice was then registered to it. A similar strategy was followed earlier by Tan et al. (2007), where three edge points in every slice were used as control points of three non-uniform rational B-spline curves (trajectories).

Curve matching was proposed in Cohen et al. (1998). They matched contours from adjacent sections (modeled as B-splines) based on comparing their knot points. The major drawback associated with B-spline representations is the non-uniqueness of the set of control points, which hampers the comparison of curves. This was solved in Ali and Cohen (1998) (see Section 5.1.2) using the intrinsic features of curves, which properties derived from the Frenet frames (Millman and Parker, 1977). Zhao et al. (1993) affinely registered slices of autoradiographs by minimising displacement of manually segmented contours (using SSD) by analysis of point-to-point disparities in two images: a boundary point in one section differs from its corresponding point in the adjacent section by a disparity vector. Trahearn et al. (2014) used Curvature Scale Space (Mokhtarian and Mackworth, 1986) to represent shape (the tissue boundary) at various scales and register whole-slide images of histological sections.

#### 4.2. Iconic methods (intensity/voxel-based)

Histological reconstruction can also be achieved by use of intensity-based registration. The main difference with geometric

methods described in Section 4.1 is that iconic methods are based on voxel intensities instead of features. This means the distance-optimisation framework (where the distance can be a similarity measure) is applied to the entire image domain. In that sense, they can potentially be better at estimating a dense deformation field—feature-based methods require interpolation, which makes them less accurate when the set of landmarks is sparse. However, their efficacy comes at a computational cost.

Some authors have relied on linear registrations to address the task. Andreasen et al. (1992) optimised the parameters of every rigid transformation by minimising a weighted SSD between the intensities of two adjacent slices. Weights were defined as the ratio of intensities of both images. More recently, methods more robust to intensity variations across slices have been proposed.

Ourselin et al. (2001b) used block-matching (Ourselin et al., 2000), in which correspondences between blocks of two images were found by maximisation of a certain similarity locally. This provided a displacement field and a global rigid transformation was obtained through least trimmed squares (LTS) (Rousseeuw, 1984) in order to filter out mismatches.

Nikou et al. (2003) defined a local energy function that was optimised sequentially in order to bring into rigid alignment every unvisited slice with a group of neighbouring slices. This was repeated until convergence. They used M-estimators as cost functions, which aimed to reduce the effect of outliers in the regression process by replacing the square function of the residual in the standard least square minimisation by the German-McClure  $\rho$ -function.

Dubois et al. (2007) opted for a robust way of jointly reconstructing histological and autoradiographic volumes. After stacking sections using their centre of mass, pairwise rigid registration was carried out using block-matching between adjacent sections for each stack. The histological volume was then used as a reference for the refinement of the reconstructed autoradiographic volume (2D-2D registration between autoradiographs and histology), due to the fact that inner anatomical structures of the brain are more visible in histology.

Other authors employed non-linear transformations (Gefen et al., 2003) for reconstruction. Such methods are usually initialised with a linear registration. One should note that initialisation is a non-trivial and non-negligible step, and this statement holds for Section 5 too. Incidentally, non-linearly deforming slices has been criticised in Lee et al. (2005) and Dubois et al. (2007); in particular, Lee *et al.* stated that they preferred to preserve the shape of the tissue rather than arbitrarily and possibly wrongly compensate for distortions. As no external information about the shape is available, bias is introduced by choosing one slice as the reference shape.

Cifor et al. (2011) ensured smoothness of the reconstructed volume in three steps: the volume was initially reconstructed using pairwise rigid registrations. Next, boundaries of interesting structures were extracted (by thresholding) in every 2D section and smoothed using a min-max curvature flow constrained to 2D (out-of-plane)—and using a mean curvature flow in (Cifor et al., 2009). This provided a sparse displacement field computed over

pixels along the initial boundary of the extracted surface, then extrapolated to the entire slices.

Smoothness was also used as a criterion for histological reconstruction in Casero *et al.* (2017), where the refined alignment of the stack was a solution of the heat diffusion equation. The algorithm alternated between the updates of slices' transformations and their neighbours' transformations until convergence. Finally, accumulated transformations updates were applied to each slice.

Following the same purpose, Gaffling *et al.* (2015) formulated the reconstruction of a stack of histological slices as an iterative Gauss-Seidel update scheme applied to images, using by definition two adjacent slices (above and below) and modified to also include information from the image itself (Gaffling *et al.*, 2009)—thereby, they also showed that a small neighbourhood is sufficient to restore smoothness. That scheme allowed for smoothing high-frequency perturbations more than lower frequencies associated with the progression of anatomical structures along the stack (as it is assumed to vary slowly enough by nature of the histological process). A similar strategy was followed earlier in Krinidis *et al.* (2003a), using iterated conditional modes (Besag, 1986) for the optimisation of a global energy function that quantified similarity between slices.

Gaffling *et al.* (2009) are, to the best of our knowledge, the only work addressing the problem of histological reconstruction with missing slices by interpolating them. Images adjacent to a missing slice were non-rigidly registered using the variational approach of the problem defined in Modersitzki (2003). The interpolated deformation field, which is a fraction of the resulting deformation field depending on the gap between the two registered images, is applied to the template image to approximate the missing intermediate slice.

Ju *et al.* (2006) represented deformations by independent single valued functions in horizontal and vertical directions: they considered that every 2D warp can be decomposed into 1D piecewise linear deformations with elastic constraint in  $x$  and  $y$ . The minimisation of the error function for registration was achieved by means of an extension of the dynamic time warping in 1D (Sakoe and Chiba, 1978) to 2D problems.

Wirtz *et al.* (2004) first rigidly registering slices using principal axis transformation, and then performed multi-scale non-linear registration with a regularisation based on elastic potentials. The system of Navier-Lamé equations was linearised by means of a non-linear Gauss-Seidel iteration method and approximated by finite differences. This was extended in Wirtz *et al.* (2005) by replacing the SSD similarity measure in the variational formulation with a weighted combination of two derivative-based (respectively gradient and Laplacian of the image) SSD measures. The error function was thereby less sensitive to intensity inhomogeneities.

Braumann *et al.* (2005) performed non-rigid registration on rigidly pre-aligned slices in two steps. First, they used polynomial warping on luminance-transformed images: correspondences between control points of adjacent slices were used to estimate the polynomial coefficients through the minimisation of a least-square error. This provided a sparse displacement field. Then, a curvature-based registration (Fischer and Modersitzki,

2003) was performed on staining-based tumour probability maps. Such maps reduced artefacts around the tumour and thus eased the registration. Braumann *et al.* also suggested to skip the intermediate polynomial registration as improved performance is expected using a multi-grid scheme for the curvature-based registration.

Pitiot *et al.* (2006) developed a method that computed a global non-linear transformation by elastically interpolating between linear transforms defined on pairs of sub-images (hence the name of “piecewise affine registration”). These sub-images represented geometrically, and often anatomically, coherent components. They were automatically extracted through clustering of an initial displacement field (Ourselin *et al.*, 2000) computed between the images to be registered.

Feuerstein *et al.* (2011) formulated the problem of optimising transformation parameters for every slice relative to, simultaneously, a reference image and the two neighbouring sections, as Markov random fields (MRF). The MRF energy is composed of unary potentials, which account for the registration to the reference images and pairwise potentials, which encode the registration to neighbouring slices and the regularisation of the displacement field. This formulation served as basis for the deformation field model in Müller *et al.* (2014).

Brandt *et al.* (2005) performed an initial affine registration followed by non-rigid registration, both by maximisation of the NMI. The latter transformation was modeled as a cubic B-spline free-form deformation (Sederberg and Parry, 1986).

Schmitt *et al.* (2007) initialised the reconstruction by registering slices affinely using a variant of principal axes transformation (PAT, Alpert *et al.*, 1990). They adopted the stochastic interpretation of PAT presented in Modersitzki (2004) (p.45), in which the images are represented as Gaussian density functions. The problem was formulated as the estimation of a density that best fits a set of reference densities in the sense that the Kullback-Leibler distance is minimised. Due to the lack of robustness of Gaussian distributions to perturbations, such as tears, wrinkles, torn out pieces, artefacts etc., Schmitt *et al.* used Cauchy density functions instead, on which robust PAT relies. Standard PAT was used in Cooper *et al.* (2006). This was followed by two partial optimisations of the SSD with respect to the shear first, and then to rotation, shearing and translation. Finally, elastic deformation was performed, similar to that used in Saalfeld *et al.* (2012).

Tile-based methods introduced in Section 4.1.1 use patches of the image as features and are therefore similar to block-matching when establishing correspondences. Ruiz *et al.* (2009) found the translation and rotation parameters relating a block with its corresponding block within a sufficiently large area in the adjacent slice by maximisation of normalised cross-correlation. This provided a sparse displacement field and a second-order polynomial transformation was computed, which coefficients were obtained using least squares. Xu *et al.* (2015) explicitly based their method on block-matching (Ourselin *et al.*, 2000). Arganda-Carreras *et al.* (2010) proposed a shape-based rigid registration method. After an initial rigid-body registration between adjacent sections, correspondences between structures of interest

were sought for by means of bounding boxes around them. Overlapping boxes in adjacent sections were assigned the same group label. Two bounding boxes overlapping in the same section were grouped into a supergroup. Remaining ungrouped structures were assigned the number of the closest group/supergroup in the adjacent section. Registration of every grouped structures was performed using the phase correlation method. Correction of remaining misalignments was achieved by elastic registration using B-splines in a multiresolution framework. Auer et al. (2005) also kept meaningful tiles (called “subimages”) that satisfied a variance criterion. Their centres were used as control points for TPS registration. TPS was preferred for its physical properties but Auer and colleagues outline that it highly depends on the control points, as opposed to e.g., B-spline interpolation.

## 5. Histological reconstruction using medical images

In this section, we survey pipelines that seek for correspondences between histology and 3D medical imaging. This process reconstructs a histological volume from a set of 2D sections using structural information from the medical image volume. Different approaches exist and some of them require an initial histological reconstruction, prior to using 3D information from medical imaging.

Combining histology and medical imaging dates back to the late 1980s. Early attempts include Sze et al. (1986), who aimed to provide histological explanation for high intensities detected routinely in MR. Nesbit et al. (1991) studied the pathogenesis of multiple sclerosis using MR, computed tomography (CT) and a biopsy.

The process of combination benefits from the heterogeneity and multiple resolutions of the images. In the end, it serves to increase the specificity of medical imaging analysis with baseline information about the actual properties of [brain] tissues (Annese, 2012): since medical imaging provides only indirect information, it is essential to show that resultant findings correlate with pathological findings.

Multi-modal works treat their different images as separate entities: the terms (co-)registration, (co-)alignment, matching, mapping or warping are used interchangeably in the covered literature. They all provide additional, combined information in the form of overlays for diagnostics, treatments, quantification etc. The term “fusion” is also commonly used but it should be distinguished from “data fusion” in the sense of creating a single composite image from different sources via numerical fusion operators, extensively reviewed in Bloch (1996) and more recently in James and Dasarthy (2014) for medical images.

The section is structured according to the modalities involved in the registration process: (i) registration of histology with *ex* and/or *in vivo* 3D medical imaging (Section 5.1). This includes cases where *ex vivo* is used as an intermediate modality; (ii) registration of histology with *ex* and/or *in vivo* 3D medical imaging using blockface photographs as an intermediate modality (Section 5.2). This also includes cases where both blockface photographs and *ex vivo* are used as intermediate modalities.

### 5.1. Histology ↔ 3D medical imaging

Multi-modal registration between histological slices and 3D medical imaging can be addressed in three ways:

- *Slice-based approaches* (Sections 5.1.1 and 5.1.2) They consider every histological slice as an individual object. Those may be preferred over volume-based approaches in cases where e.g., the histological dataset is too sparse or has too few slices. The alignment between histology and medical imaging is then carried out using either (i) slice-to-volume (2D-3D) registration or (ii) slice-to-slice (2D-2D) registration, which is a simplification of the former point and requires careful identification of the “corresponding” plane in the medical image volume.
- *Volume-based approaches* (Section 5.1.3) They consider the set of histological slices as a whole and therefore rely on an initial histological volume. The main goal of initial reconstruction is to correct for the various orientations that the tissues may have across slices (when mounted on glass slides) in order to facilitate subsequent registration with 3D medical imaging. It provides better “support”—as opposed to simply stacking slices—and aids the optimisation of the similarity measure. More complex initialisations have also been developed, which intended to be more robust to registration failures. Both the alignment and the reconstruction are then refined in various ways.
- *Hybrid approaches* (Section 5.1.4) They also rely on initial histological reconstructions and alternate between volume- and slice-based approaches so as to get the best out of the two worlds: a more accurate histological reconstruction for a refined alignment with clinical imaging and *vice versa*. They repeat until the histological reconstruction has converged.

#### 5.1.1. Slice-to-slice approaches (2D-2D)

These methods assume that the cutting planes of histological slices and the acquisition planes of the 3D medical image are parallel and that there always exists a histological section that has a counterpart in the set of MR slices. The problem therefore simplifies to a 2D-2D registration between every histological slice and its corresponding slice in the 3D medical image.

Slice Correspondences can be achieved visually (Gangolli et al., 2017; Chappelow et al., 2011a; Mazaheri et al., 2010), in which case an expert radiologist is most commonly asked to identify the MRI slice corresponding to a histological slice on the basis of anatomical landmarks. Chappelow et al. took advantage of all the data to drive image registration using a multivariate formulation of mutual information, while Mazaheri et al. performed rigid alignment of the images’ centres of mass, followed by 2D affine registration and finally 2D non-rigid registration using free-form deformations (FFD) (Rueckert et al., 1999). Li et al. (2006) used TPS transformation to register the *in vivo* MR plane with its visually corresponding histological slice. It was a smooth registration based on specified corresponding landmarks. The optimal number of landmarks was evaluated as a minimiser of the non-rigid registration error. Gangolli et al. (2017) used manually extracted landmarks at visually matching locations along the tissue edges, within and at the boundary



**Figure 3:** Strategies to register histology with volumetric medical imaging (*ex* or *in vivo* alone). The three main approaches (slice-based, volume-based and iterative) are presented. (\*) In cases where *ex vivo* imaging is used as an intermediate modality, correspondences between *ex vivo* and histology are achieved through steps 2 and 3, and the mapping between histology and *in vivo* is completed via registration between *ex* and *in vivo* scans (extra step).

between grey and white matter. Then, a forward non-linear moving least squares transformation (Goshtasby, 1988) was applied to register the histological section with the MRI slice.

Automated selection of corresponding slices can be achieved via the optimisation of a similarity measure between each histological slice and every slice of the 3D medical image. This assumes that the maximum similarity is obtained when *actual* corresponding slices are compared. However, Xiao *et al.* (2011) showed that both visual and automated approaches failed to reliably determine slice correspondences mostly due to the alteration of the tissue during the histology preparation i.e., direct comparison of images from different modalities is a non-trivial task which is prone to errors. Xiao *et al.* proposed to compare the set of histological slices with all possible subsets of equal number of *in vivo* MR slices using mutual information. These subsets were ranked based on cumulated similarity. A group of top-ranked MRI subsets was retained and their lists of correspondences were averaged. The final list was used for 2D affine registrations between slices from both modalities followed by 3D affine registration.

Slice-to-slice approaches seem to be favoured in the clinical literature for the visual control they allow but many works address the problem only partly (Harkins *et al.*, 2015; Kilsdonk *et al.*, 2016; Hammelrath *et al.*, 2016). Lopez Gonzalez *et al.* (2016) performed linear registrations between *ex vivo* MR slices and histological images and these were then visually matched to the closest (*in vivo*) 3T MR slice. Hartevelde *et al.* (2016) and Van Der Kolk *et al.* (2015) manually matched histological

sections to their corresponding MR planes using the marked locations with the fiducials in the MR images, the ink markings in the histologic sections, and gross morphologic features. Nakagawa *et al.* (2016) identified the histological sections that were morphologically close to the  $T_{1\rho}$  mapping image and only stained those. Koh *et al.* (2016) performed side-by-side comparison between the tissue sections of the largest cut surface of the tumour and MR imaging.

State of the art data analyses therefore rely on loose assumptions: (i) the histological cutting plane is not necessarily consistently parallel to the scan acquisition plane and (ii) the sampling is different within and across modalities, all the more due to uneven cutting. In addition, the accuracy of the registration highly depends on the MR slice thickness. On that matter, apparatus have been developed to help cutting the specimen at the *same* interval and orientation as the MR images, as proposed by Drew *et al.* (2010); Trivedi *et al.* (2012) in the context of prostatectomy, or by means of 3D-printed brain holders (Absinta *et al.*, 2014; Guy *et al.*, 2016). The error made when selecting the *closest* MR slice was considered in Steenbergen *et al.* (2015), and the consequences of differences in sampling were noted in Martel *et al.* (2016) in the specific case of vascular trees from the femoral trochlea. By disregarding such approximations, one needs to be aware that wrong correspondences are very likely to be established and this directly affects, for example, statistical analyses. Similarly, Meyer *et al.* (2013) described these challenges and listed numerous erroneous assumptions made during the process of alignment in the case of prostate cancer.

### 5.1.2. Slice-to-volume approaches (2D-3D)

They extend those presented in Section 5.1.1 by considering that nothing ensures that the cutting plane of histological slices is parallel to the 3D medical image acquisition plane. Likewise, there is no guarantee that the histological slices are parallel to each other. This means that structures belonging to a tissue slice may extend over several 3D medical image slices, or in other words, a histological slice may lie obliquely in the medical image volume. This in turn suggests that the corresponding 3D medical image slice can only be found through a slice-to-volume (2D-3D) registration. Reviews on slice-to-volume registration can be found in [Markelj et al. \(2012\)](#) and [Ferrante and Paragios \(2017\)](#).

[Khimchenko et al. \(2016\)](#) rigidly registered a histological section with a  $\mu$ CT volume using a density-driven RANSAC for plane fitting ([Chicherova et al., 2014](#)). The landmarks were SURF points detected in both histological and each  $\mu$ CT slices. The resulting 3D point cloud had an increased density of matches at the correct location of the histology section, and this was used as a criterion to filter out incorrect pairs. The random sampling of RANSAC plane fitting was thereby biased towards those points that were close to the  $\mu$ CT plane of interest. The alignment between the interpolated plane and histology was further refined using 2D Demon registration tool<sup>9</sup> ([Kroon and Slump, 2009](#)).

[Nir et al. \(2014\)](#) formulated the problem as finding the poses of all the histological slices such that the transformed segmented histology slices optimally matched the corresponding re-sliced images of the 3D medical image. They made use of particle filtering to model pose uncertainty, where each particle represents a combination of histological slices in various 3D poses, and derived optimal affine registration parameters in a Bayesian approach. The admissible space of 3D poses was constrained such that the transformed slices do not intersect.

[Osechinskiy and Kruggel \(2010\)](#) computed a geometric transformation that combined a rigid alignment with a 3D deformation field parametrised by various classes of spline functions, various similarity measures, different optimisation algorithms and different optimisation strategies.

[Gibson et al. \(2012\)](#) utilised well-arranged strand-shaped fiducial markers that allowed for the determination of the location and orientation of each section. First, a 2D-3D affine transformation that mapped a fiducial histological slice to its corresponding points on the MR image was found by minimisation of the residuals. Then, a 2D-2D affine transformation mapping each histology slice to its counterpart in the MR was computed using spatial information from all fiducial markers. Finally, the fiducial correspondences were refined using a local optimisation and one last affine transformation was computed initialised with the affine transformation computed at the previous step. Using non-anatomical fiducials was argued to provide robustness to variations in the appearance of the prostate on MR and histology images.

[Gefen et al. \(2008\)](#) proposed a non-linear registration method to align histological brain sections with a volumetric brain atlas. They started with an image to planar surface matching,

during which sections were linearly matched with an oblique slice automatically extracted from the atlas. An image-to-curved surface matching was then performed, during which each section was matched with its corresponding image overlaid on a curved-surface within the atlas. Specifically, a PDE-based registration technique was developed that was driven by a local NMI similarity.

[Kim et al. \(2000\)](#) used polynomial transformations to warp an initial *in vivo* MRI slice that produced minimum error (when compared with all the histological slices). The parameters of a low-order polynomial transformation between the MRI slice and the histological section were optimised by minimisation of the SSD and the correlation coefficient. This method was reused in [Zarow et al. \(2004\)](#); [Singh et al. \(2008\)](#).

[Ali and Cohen \(1998\)](#) approached registration as a contour matching problem. This means representing images in their most elementary form: a line (describing the *shape* of the main object). Most importantly, the multimodal registration problem thereby becomes monomodal. The contour curves were described by means of sets of affine invariants constructed from the sequence of area patches bounded by the contour and the line connecting two consecutive inflections. The affine transformation was estimated from matching vertices using least square error estimation method.

### 5.1.3. Volume-based approaches (3D-3D)

The main drawback of slice-based (2D-3D) approaches is their sensitivity to initialisation as the landscape of any cost function is full of local minima. Other challenges involve the cost function selection, the convergence behaviour and the optimisation strategy ([Osechinskiy and Kruggel, 2010](#)). The information from a single histological slice is used alone and its content may be hard to handle by itself (see Sections 2 and 3) in a multi-modal registration problem: the performance of slice-to-volume registration shows greater dependence on the input images than 3D-3D registration ([Osechinskiy and Kruggel, 2010](#)). Considering histological slices altogether i.e., the histological dataset as a whole, allows overcoming such issue. Volume-based approaches follow Procedure 1.

---

#### Procedure 1 Volume-based approaches (3D-3D)

---

**Input:**  $M$ , *ex or in vivo* 3D MRI and  $\{H_i\}$ , a set of 2D histological slices.

**Output:** histological volume  $H^f$  aligned with  $M$ .

- 1:  $H^0 \leftarrow$  Reconstruct histological volume from  $\{H_i\}$  ▷ Step 1
  - 2:  $H^1 \leftarrow$  Linearly register  $M$  and  $H$  ▷ Step 2
  - 3:  $H^f \leftarrow$  Non-linearly register  $M$  and  $H^1$  ▷ opt. Step 3
- 

Initial histological reconstruction (Step 1) can be achieved in several ways and the reader is referred to Section 4 for a more complete list of methods dedicated to that purpose. Simple stacking by alignment of centres of mass was used in [Goubran et al. \(2013\)](#). The most common way however consists of serial pairwise linear registrations and provides roughly aligned though satisfactory enough initial volumes ([Delzescaux et al., 2003](#);

<sup>9</sup>Code is available on MathWorks File Exchange.

Malandain et al., 2004; Li et al., 2009; Ou and Davatzikos, 2009; Ceritoglu et al., 2010; Alic et al., 2011; Yang et al., 2012; Stille et al., 2013). In particular, Ceritoglu et al. (2010) registered every slice to its successor starting from the bottom of the stack and repeated the process starting from the top of the resultant stack. In contrast, Stille et al. (2013) started from the middle of the stack (they manually selected the most central slice with minimum artefacts) and performed registration between pairs of adjacent slices after aligning the centres of mass of masked images. Maximisation of mutual information was used in Ou and Davatzikos (2009), and block-matching in Malandain et al. (2004) and Yang et al. (2012). Initial reconstruction may also be achieved by use of fiducial rods, such as in Humm et al. (2003), for which the Euclidean distance between corresponding segmented holes from pairs of adjacent slices was minimised.

Other reconstruction methods consider neighbourhoods of slices (as opposed to a single neighbouring slice) in order to improve the consistency of the resulting volume. Chakravarty et al. (2006) registered every slice with both its successor and its predecessor and applied the average transformation to the original slice so that the transformed slices match both their neighbours simultaneously. A similar strategy was used in Rusu et al. (2015). Yushkevich et al. (2006) extended the size of the neighbouring up to five slices away. A weighted graph was built, with slices as vertices, edges symbolised registrations, and weights were given by an information- and distance-based measure. The shortest path from every vertex in the graph to a specific reference slice was found using Dijkstra’s algorithm, and incidentally favoured slices that registered well (hence bypassing those that registered poorly). The concatenation of rigid transformations yielded a reconstructed histological volume. Such reconstruction method was reused in Adler et al. (2014) with different edge weights. Later, however, Yushkevich et al. (2016) and Adler et al. (2016) relied on manual histological reconstructions using HistoloZee. While much more labor-intensive, they found that manual reconstructions led to better histological reconstructions especially when slices were torn or poorly stained.

Once an initial histological volume is available, a coarse, linear alignment of the geometries of both medical image and histological volumes is performed (Step 2), which may then be refined by non-linear registration (Step 3). This can be achieved using standard inter-modality registration techniques implemented in packages such as AIR (Woods et al., 1998a) followed by Diffeomap (LDDMM) (Li and Mori, 2001) in Ceritoglu et al. (2010), landmark-based registration followed by ANIMAL (Collins and Evans, 1997) in Chakravarty et al. (2006), or maximisation of mutual information (Wells et al., 1996) followed by free-form deformations (Rueckert et al., 1999) and a pyramidal approach with gradually increasing number of control points in Delzescaux et al. (2003). Only global linear registration was performed in Stille et al. (2013).

A variation of Procedure 1 consists of complementing Step 2 with the registration of every slice from the globally aligned histological volume with its 2D counterpart in the medical image

volume. Such variation is the cornerstone of hybrid approaches described in Section 5.1.4. Li et al. (2009) aligned the centres of mass of each histological slice and its corresponding *in vivo* MR plane (although this is not a registration *per se*) after 3D rigid registration between both volumes. This was refined by 3D non-rigid registration using the adaptive bases algorithm (ABA) Rohde et al. (2003). Yushkevich et al. (2006) deformed each histological slice of the 3D aligned histological volume towards the average of its immediate neighbours (predecessor and successor) and the corresponding MR slice. Some of their methods have been included in the framework developed by Majka and Wójcik (2015)<sup>10</sup>. In Humm et al. (2003), only linear registration between every histological slice and its 2D counterpart in the MR was performed.

*Ex vivo* correspondences can be further carried to *in vivo* space by an extra registration between both image volumes. Given the registration between histology and *ex vivo*, concatenating transformations relates histology and *in vivo* medical imaging. As such, Alic et al. (2011) performed 3D linear (rigid, affine) and elastic registration between histological and *ex vivo* MR volumes, followed by 3D rigid, affine and elastic registration between *ex vivo* and *in vivo* MR volumes. All registrations were performed using Elastix (Klein et al., 2010). Rusu et al. (2015) performed affine registration, also using Elastix, between the reconstructed histological and *ex vivo* volumes. *Ex vivo* and *in vivo* medical images were affinely registered, yielding linear alignment between histology and *in vivo*. Finally, non-rigid registration between histological and *in vivo* volumes refined the alignment of both modalities using free-form deformations in a multiscale setting.

#### 5.1.4. Hybrid methods

We call hybrid methods those similar to Procedure 1 except both the serial arrangement of the histological volume (its reconstruction) and its alignment relative to the medical image volume are jointly refined (Procedure 2). Both processes hence benefit from each other as changing one affects the other.

Initial histological reconstruction follows methods presented in Section 5.1.3.

Step 2 consists of iterating over two registrations: (i) a 3D-3D registration, which updates the global alignment between the current estimate of the histological volume and the 3D medical image, and (ii) 2D-2D registrations, which affect the serial arrangement of slices relative to each other by aligning them with their (current) corresponding slice in the medical image volume used. This in turn provides a new histological volume which is used at the next iteration. This process is repeated until convergence. In general linear registrations are used in the iterative process to avoid creating wrong correspondences through non-rigid registration. In particular, Malandain et al. (2004) used block-matching, Adler et al. (2014) used the ANTs

<sup>10</sup><http://www.3dbar.org/wiki/barPosSupp>. The source code is available for download at <https://github.com/pmajka/poSSum>.

---

**Procedure 2** Hybrid methods

---

**Input:**  $M$ , *ex vivo* 3D MRI and  $\{H_i\}$ , a set of 2D histological slices

**Parameter:**  $N$ , number of iterations after convergence

**Output:** histological volume  $H^f$  aligned with  $M$

- 1:  $H^0 \leftarrow$  Reconstruct histological volume from  $\{H_i\}$  ▷ Step 1
  - 2:  $k = 0$
  - 3: **repeat** ▷ Step 2
  - 4:   Linearly register  $H^k$  and  $M$
  - 5:   **for all** slices **do**
  - 6:      $H_i^k \leftarrow$  Linearly register  $H_i^k$  and  $M_i$
  - 7:   **end for**
  - 8:    $H^{k+1} \leftarrow \{H_i^k\}$
  - 9:    $k = k + 1$
  - 10: **until** convergence
  - 11:  $H^f \leftarrow$  Non-linearly register  $H^N$  and  $M$  ▷ opt. Step 3
- 

toolkit with NMI and Yang *et al.* (2012) used maximisation of MI. The latter addressed the specific case of separate pieces of tissue by using 2D piecewise local registration. They also addressed the challenging case of automatically initialising the location of a tissue block that is a sub-volume of the tissue MR. Yang *et al.* identified the locations of the first and last slices of the histological block in the MR as those maximising NMI after 2D rigid registrations.

Once the iterative process has converged, a final step may consist of a non-rigid registration to refine the matching (Step 3). Adler *et al.* reused the 2D diffeomorphic registration from Yushkevich *et al.* (2006), while Yang *et al.* used cubic B-spline parametrisation for 3D non-rigid registration and NCC similarity measure.

A variation of Step 2 of procedure 2 was proposed by Ou and Davatzikos (2009). They iterated over: (i) a 3D affine registration between the current histological and MR volumes, by maximisation of the correlation coefficient and (ii) a 2D rigid registration between every histological slice and the central histological slice. Subsequent steps jointly addressed the segmentation and the refinement of the registration of prostate cancer images and also consisted of an iterative process.

Another variation was proposed by Goubran *et al.* (2013), who embedded the non-rigid registration of Step 3 in the iterative process of Step 2. The pipeline thus consisted of iterating over: (i) a 3D rigid registration of the current estimate between the current histological volume with the MR, (ii) 2D rigid registrations between every histological slice and its currently corresponding MR plane, and (iii) 2D non-rigid registrations between every histological slice and its currently corresponding MR plane using FFD.

Correspondences between histology and *ex vivo* can be further carried to *in vivo* space similarly to Section 5.1.3. As such, Goubran *et al.* (2015a) extended previous work (Goubran *et al.*, 2013) in order to relate histology and *in vivo* scans. They started with translating the *ex vivo* MR to match the *in vivo* MR space

in order to facilitate the placement of landmarks in subsequent steps. Then, they performed 3D linear (rigid+scaling) landmark-based registration *in vivo* and *ex vivo* MRs using manually picked landmarks. This was refined by 3D non-rigid registration between both 3D MRIs using landmark-based registration and a symmetric implementation of FFD, respectively for hippocampal and neocortical specimen.

### 5.2. Histology $\leftrightarrow$ 3D medical imaging using blockface photographs

Blockface photographs provide structural information of the tissue face prior to cutting and therefore allow correcting for subsequent tissue deformations (mainly induced by cutting, floating and mounting).

In theory, blockface photographs should be inherently aligned by virtue of the set-up: it consists of a camera on e.g., a tripod—or mounted on the microtome itself—oriented towards the face of the tissue block secured on the microtome, and which imaging plane is parallel to the block face. Though, it is common to affinely register them with each other in order to account for small displacements (Annese *et al.*, 2006; Yelnik *et al.*, 2007; Groen *et al.*, 2010) but this is not robust to perspective distortions (the camera imaging plane is never and can not remain truly parallel to the block face). Eiben *et al.* (2010) considered that each time the microtome cuts a section out of the tissue block, its face lies in a slightly different plane (due to small mechanical imprecisions or due to the expansion of the tissue when a new face is exposed). This leads to a perspective error, which may hinder the consistency of the reconstructed volume. Their method provided a way to correct for scaling variations and displacements of the sample that may occur from one acquisition to the next. However, they did not take into account the camera motion (as small as it may be). Breen *et al.* (2005b) assessed the camera lens for image distortion by ensuring that lines from manually selected points (including edges of the image) remained straight. They also ensured those lines were not blurred in any region of the image. Casero *et al.* (2017) corrected the perspective error of the blockface photograph acquisition by computing a projective transformation using manually extracted landmarks. Casero *et al.* also corrected “scratched” photographs (which occur when using a poor quality knife blade during microtomy). They first rotated the images to make the scratches horizontal/vertical using the wax block sides. The image rows/columns intensities were then scaled so that their median values equaled the wax median value.

There are three main types of pipelines that relate histology to volumetric medical imaging according to how they exploit blockface photographs as an intermediate modality (Figure 4), namely for histological reconstruction or for alignment with medical imaging (Section 5.2.1: resp. BF for histoRec, and BF for MedIm alignment) and for both (Section 5.2.2: BF<sup>2</sup>).

#### 5.2.1. Unary use of blockface photographs

These pipelines follow Procedure 3.

In Step 1, Alegro *et al.* (2016) affinely registered each histological image to its corresponding blockface photograph

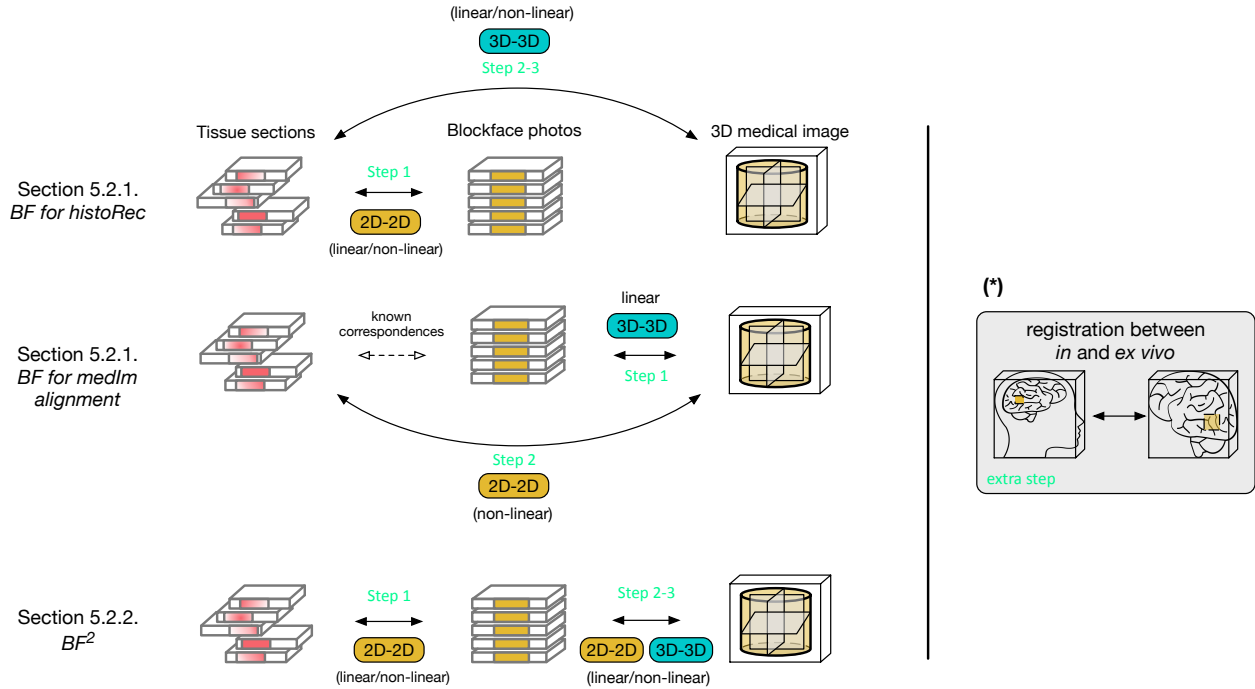


**Figure 4:** Strategies to register histology with volumetric medical images using blockface photographs as intermediate modality; (\*) see Figure 3.

### Procedure 3 BF for histoRec

**Input:**  $M$ , *ex or in vivo* 3D MRI,  $\{H_i\}$ , a set of 2D histological slices,  $B = \{B_i\}$ , a set of 2D blockface photographs.

**Output:** histological volume  $H$  aligned with  $M$

- 1: **for all** slices  $\mathbf{do}$  ▷ Step 1
- 2:    $H_i^0 \leftarrow$  Register  $H_i$  and  $B_i$
- 3: **end for**
- 4:  $H^0 \leftarrow \{H_i^0\}$
- 5:  $H^1 \leftarrow$  Register  $H^0$  and  $M$  ▷ Step 2
- 6:  $H^f \leftarrow$  Non-linearly register  $H^1$  and  $M$  ▷ opt. Step 3

by optimisation of mutual information as defined by Mattes et al. (2003). Schormann and Zilles (1998) first reconstructed the blockface volume by least square minimisation between corresponding pairs of landmarks in adjacent photographs (Schormann et al., 1995) and then registered each histological section with its corresponding blockface photographs using an extension of principal axes theory generalised to affine transformations (in order to be able to account for shearing artefacts introduced during the tissue preparation). Johnson et al. (2010) used 2D moments-based rigid alignment for some brains, refined using AIR software. For other brains, Johnson and colleagues used the method from Thevenaz et al. (1998) between corresponding images with manual refinement. This protocol was reused in (Johnson et al., 2012).

In Step 2, Alegro et al. (2016) used symmetric diffeomorphic 3D registration, SyN (Avants et al., 2008) to align the reconstructed histological and the MRI volumes. Johnson et al. (2010) first linearly aligned the reconstructed histological and MR vol-

umes using a quaternion transform followed by an affine transform. Then, they refined the alignment using a multi-resolution diffeomorphic registration algorithm (Avants et al., 2008). Schormann and Zilles (1998) started with a 3D affine registration between the histological and the MR volume, followed by a 2D non-linear registration between every histological sections and its corresponding MR plane using a 3D elastic full-multigrid technique (Stüben and Trottenberg, 1982) restricted to 2D (Rohr et al., 1996). It was initialised with a 2D linear registration driven by the analysis of Rayleigh-Bessel statistics, which describe the probability density of local non-linear deformations in histological sections (Schormann et al., 1995).

A variation of Step 2 consists of considering slices instead of volumes: after reconstructing the histological volume, Bürgel et al. (1999), based on the methodology developed in Schormann et al. (1993, 1995) warped every histological slice to its corresponding *ex vivo* MR plane.

A variation of Procedure 3, BF for MedIm alignment, was proposed in Amunts et al. (2013) and relied on the registration between the blockface volume and the 3D medical image. Then, using the direct, known 2D correspondences between histology and blockface, every histological slice was registered with its corresponding MR plane.

#### 5.2.2. Binary use of blockface photographs

Such works use blockface photographs for both histological reconstruction and matching with 3D medical images. They are to be the most frequent way to address the problem and follow Procedure 4.

The choice of aligning every histological slice to its corresponding blockface photograph (Step 1) using linear registration

---

**Procedure 4** BF<sup>2</sup>

---

**Input:**  $M$ , *ex or in vivo* 3D MRI,  $\{H_i\}$ , a set of 2D histological slices,  $B = \{B_i\}$ , a set of 2D blockface photographs.

**Output:** histological volume  $H^f$  aligned with  $M$

- 1: **for all** slices **do** ▷ Step 1
  - 2:      $H_i^0 \leftarrow$  Register  $H_i$  and  $B_i$
  - 3: **end for**
  - 4:  $H^0 \leftarrow \{H_i^0\}$
  - 5: Register  $B$  and  $M$  ▷ Step 2
  - 6: Non-linearly register  $B$  and  $M$  ▷ opt. Step 3
- 

(as opposed to non-linear) may stem from the poor content that the unstained tissue face exhibits. Blockface photographs provide little structural information apart from the tissue borders (higher contrast with the surrounding embedding medium), which could lead to erroneous deformations of the inside of the tissue. Linearly registering every pair of corresponding images may suffice to restore a globally consistent arrangement of histological slices, which will be refined locally when matched with the medical image volume. [Lebenberg et al. \(2010\)](#) rigidly aligned every histological section with its corresponding blockface photograph and every autoradiograph (see “Cerebral function” in Section 6 for a brief definition) was then rigidly registered with its histological slice counterpart, both using block-matching ([Ourselin et al., 2000](#)). This was reused in [Vandenberghe et al. \(2016\)](#). [Yelnik et al. \(2007\)](#) started with reconstructing the blockface volumes using iterative closest point ([Besl and McKay, 1992](#)) i.e., by registering every photograph to its immediate neighbour (binary images of segmented rivets) and then performed 2D rigid registration between every histological section and its cryo-blockface counterpart. In order to refine the histological volume, 3D regions of interest centred around the basal ganglia were extracted using Yav++ software ([Delingette et al., 2001](#)) in both histological and blockface volumes and 2D hierarchical registration (rigid, homothetic and affine) was performed between corresponding 2D images. [Dauguet et al. \(2007b\)](#) aligned every histological section with its corresponding blockface photograph using a “hemi-rigid” method, which accounted for the independent spreading of the hemispheres on the glass slides.

Other authors have chosen to refine this step with a non-rigid registration. For instance, [Choe et al. \(2011\)](#) performed 2D linear followed by 2D non-linear registration between light micrographs and corresponding blockface photographs using respectively maximisation of MI and ABA ([Rohde et al., 2003](#)). [Breen et al. \(2005b\)](#) performed 2D non-rigid registration of a histological section with its corresponding blockface photograph using TPS and corresponding landmarks: interior ink fiducials and anatomical landmarks, such as blood vessels, and corresponding points along the external tissue boundary using “live-wire” semi-automated algorithm ([Falcão et al., 1998](#); [Mortensen et al., 1992](#)). [Meyer et al. \(2006\)](#) also used TPS with 7 control points; six control points were used in [Piert et al. \(2009\)](#) and [Park et al. \(2008\)](#). [Groen et al. \(2010\)](#) performed

2D rigid, followed by 2D non-rigid FFD-based registrations ([Rueckert et al., 1999](#)).

In [Steps 2](#) and [3](#)—consisting of registering blockface and medical imaging—pipelines start with 3D linear registration ([Groen et al., 2010](#)). [Dauguet et al. \(2007b\)](#) performed 3D rigid registration between the blockface volume and the *in vivo* T1 MRI by maximisation of mutual information ([Viola and Wells III, 1997](#)). 3D non-rigid registration between the blockface volume and the MRI was performed using free form deformations ([Rueckert et al., 1999](#)), as in [Groen et al. \(2010\)](#), and the composition of the two previous transformations was applied to the “hemi-rigid” transformed histological volume. The same sequence was applied in [Lebenberg et al. \(2010\)](#). This was also found in [Choe et al. \(2011\)](#) except that the last non-rigid registration between blockface and *ex vivo* T2w MR volumes made use of ABA. The composition of the transformations between blockface and the medical image volume, and between histology and blockface volume was applied to the T2w image in order to resample it in the histological space. The 3D non-rigid registration between blockface and *ex vivo* MR volumes was performed using TPS with 6 control points in [Meyer et al. \(2006\)](#); 18 control points were used in [Piert et al. \(2009\)](#) and [Park et al. \(2008\)](#).

Other applications of Procedure 4—without the non-rigid refinement of [Step 3](#)—include [Yelnik et al. \(2007\)](#), who performed 3D rigid registration between blockface and *ex vivo* T1w MR volumes one hemisphere at a time ([Prima et al., 2002](#)). The alignment was refined by a 3D hierarchical registration between 3D regions of interest centred around the basal ganglia and propagated to the full volumes. [Breen et al. \(2005b\)](#) performed 3D linear (rigid+scaling) registration between the blockface volume (stack of 3mm-thick slice faces) and the MR volume, in which the centres of the needle paths were manually segmented. The global transformation was optimised using the iterative closest point algorithm ([Besl and McKay, 1992](#)). Non-rigid refinement was not performed and the method was validated in [Lazebnik et al. \(2003\)](#).

A variation of Procedure 4 was proposed by [Uberti et al. \(2009\)](#) and consists, as in Section 5.2.1, of considering slices instead of volumes. After reconstructing the histological volume according to [Step 1](#), they performed 2D non-registration between every blockface photograph and the corresponding *in vivo* MR planes. Registrations were based on moving landmarks sampled on curves generated from the contours of corresponding anatomical features. Once landmarks locations were optimised for matching through minimisation of a cost function based on the local curvature of the curves and limited to small displacements, TPS interpolation ([Bookstein, 1989](#)) for point-based registration was performed.

As in Sections 5.1.3 and 5.1.4, *ex vivo* correspondences can be further carried to *in vivo* space through an extra registration between *ex* and *in vivo* medical image volumes in order to relate histology to *in vivo* imaging. As such, in [Groen et al. \(2010\)](#) the *ex vivo*  $\mu$ CT and the *in vivo* CTA were rigidly (point-based) registered using manually selected landmarks (e.g., calcium

spots, lumen, bifurcation position are clearly visible in both medical imaging modalities). Meyer et al. (2006) performed a 3D non-rigid registration between the *ex vivo* and *in vivo* MRs using 3D TPS with 14 control points, and it was used as an initialisation for a last non-rigid registration between *in vivo* volume and the blockface image by optimising the position of 7 control points and using mutual information as the objective function. Piert et al. (2009) used the methodology presented in Park et al. (2008) and non-rigidly registered the *ex vivo* MR and *in vivo* T2 MR volumes using TPS with 7 control points. The T2 MRI was chosen as the reference space. Additionally, *in vivo* T2 and CT volumes were non-rigidly registered using TPS with 7 control points and PET and CT volumes were rigidly registered.

## 6. Validation methods

We hereafter detail the ways authors have validated the accuracy and the precision of image registration, as defined by Maintz and Viergever (1998), in the context of mono- or multimodal histological reconstruction (with or without medical imaging).

*Visual assessment.* It may be the most intuitive way of validating the registration accuracy but must be carried out by experts and does not provide with any quantitative measure. In the case of histological volume reconstruction, criteria used to tell whether registrations are successful encompass improved representations of small structures (subcortical nuclei, cortical areas) and smooth inner and outer borders (Wirtz et al., 2004). Wirtz and colleagues used three classes of neuroanatomical structures that are recognisable after registration when examining whole rat brains: subcortical nuclei, ventricles, certain cerebral and cerebellar cytoarchitectonic layers. Smoothness was explicitly used a criterion for reconstruction in Cifor et al. (2011). Ju et al. (2006) compared the reconstructed volume to real histology sections from Paxinos Atlas (Paxinos et al., 2000) at similar sagittal and horizontal locations.

Visual assessment can also be used when comparing one method against others (assuming that the same data have been used). Gaffling et al. (2011) compared the reconstruction against that obtained through standard non-registration scheme (without landmarks) using histological data from Ju et al. (2006) and artificial data. Ju et al. (2006) compared their reconstruction against that obtained from the method described in Guest and Baldock (1995).

In the case of multi-modal alignment, visual assessment can be performed by (i) cross-section comparison. Malandain et al. (2004) used two synchronised 3D viewers to display the two volumes in the same geometry. This allowed showing same cross-sections (axial, sagittal and coronal) as well as a cursor at corresponding positions. In Alic et al. (2011), the alignment between 3D *in vivo* T2 and histological volumes was qualitatively evaluated by two observers using visual inspection with a moving quadrant view; or by (ii) superposition of adjacent sections (Li et al., 2009; Choe et al., 2011). Dauguet et al. (2007b) superimposed the external and internal borders of the

MRI brain—extracted using Deriche filter (Deriche, 1987)—registered onto the blockface volume. A similar methodology was used in Lebenberg et al. (2010). Malandain et al. (2004) superimposed both volumes while adjusting colour maps and transparency. This can also be used when assessing the quality of the histological reconstruction (Colchester et al., 2000).

*Landmark-based validation.* It is the most widespread method, used for example in Nir et al. (2014); Gibson et al. (2012); Liu et al. (2012); Ward et al. (2012); Yang et al. (2012); Ou and Davatzikos (2009). It consists of computing the Euclidean norm between corresponding tie points extracted in two images (also referred to as target registration error, TRE). This measure might not be not appropriate for the validation of histological reconstruction from 2D sections only (Ju et al., 2006): a minimum distance does not mean the true shape has been recovered. It is however very relevant in the case of multi-modal registration. Those landmarks can be (i) *needle tracks*, such as in Colchester et al. (2000); Lazebnik et al. (2003); Breen et al. (2003); or (ii) *manually identified anatomical landmarks*, that are visually tractable across modalities. Kim et al. (2000) used the anterior commissure, the pillars of fornix, perivascular spaces and optic chiasm. Osechinskiy and Kruggel (2010) used sulcal lines of maximal depth (sulcal fundi or sulcal bottom lines), which were automatically extracted in 3D by the procedure described in Lohmann (1998). Nir et al. (2014) included the urethra, nodules, scars (from previous biopsies), calcifications, and “other general distinguished anatomical features” with the help of a radiologist. Goubran et al. (2013, 2015a) computed the target registration error based on 128 manually identified corresponding intrinsic landmarks on MR images and histological slices. Adler et al. (2014) calculated the boundary displacement error between two manually drawn boundary curves in the MRI and the histology. When such (manually extracted) landmarks are used for registration, reliability of their locations is usually assessed by looking at intra- and inter-user variability. For example, Gaggoli et al. (2017) dealt with the former by asking a user to perform landmark selection twice, five days apart, and compared registered voxels shifts. The latter was dealt with by asking two different users to perform the previous procedure. In addition, artificial perturbation of an established set of landmarks in histology was performed in order to test the robustness of the registration method to such changes. Landmark points may also be (iii) *anatomical artefacts*. Singh et al. (2008) used the centroids of manually segmented lesions to evaluate and validate the registration accuracy. Alic et al. (2011) used characteristic features in the tumour and on its contour. (iv) Ink marks were used for example in Breen et al. (2005b).

*Measures of overlap.* They rely on regions of interest (RoIs) manually delineated by an expert in two images. The Dice score or the Jaccard index are two measures that can be computed to quantify the amount of overlap between the two regions. Dice score was used for instance in Alegro et al. (2016); Li et al. (2009); Beare et al. (2008); Hess et al. (1998); Baheerathan et al. (1998). Specifically, Lebenberg et al. (2010) manually delineated the hippocampus, cortex, and striatum, as well as the

corpus callosum and substantia nigra, for comparison between different reconstructed histological volumes. The hippocampus was also manually delineated in every histological atlas in [Palm et al. \(2010\)](#). In [Mazaheeri et al. \(2010\)](#), the whole prostate, the peripheral zone, and the transition zone were outlined by an experienced radiologist in MR and histology images. [Nir et al. \(2014\)](#) compared the registered histological slices with the corresponding re-sliced images of the MR volume. For each slice, its histological segmentation was compared with the corresponding cross-section of the prostate surface, as obtained from a manual segmentation of the volumetric image by a radiologist. The Dice score was shown to be a reliable indicator of registration accuracy only for small and localised RoIs (which approximate point landmarks) in several locations in the image space ([Rohlfing, 2012](#)).

*Texture-based methods.* Grey-level co-occurrence matrices (GLCM) were presented in [Haralick \(1979\)](#) and were used to assess the alignment quality of the histological reconstruction in [Baheerathan et al. \(1998\)](#) and [Cifor et al. \(2011\)](#). Such matrices were computed by calculating how often the pair made of a pixel of interest with a certain intensity and its immediate neighbour in the direction going across slices (orthogonal to the cutting plane) occurs. [Cifor et al. \(2011\)](#) computed GLCMs in the neighbourhood around the boundaries of the tissue rather than the whole volume in order to quantify the smoothness of the reconstruction.

*Artificial perturbation of a ground truth.* Artificially perturbing a ground truth allows having access to the original alignment, against which the resulting alignment is compared. It is done by taking a volumetric image which original alignment is known (e.g., a 3D medical image) and applying random, smooth transformations to each of its slice independently (as well as e.g., including artefacts that simulate holes/tears, ignoring some slices etc.). The error made after reconstruction is then computed. It was used in [Cifor et al. \(2011\)](#); [Nikou et al. \(2003\)](#); [Ju et al. \(2006\)](#); [Braumann et al. \(2005\)](#); [Majka and Wójcik \(2015\)](#); [Bagci and Bai \(2010\)](#). Synthetic datasets (e.g., phantom models) were used in [Schwier et al. \(2013\)](#); [Ou and Davatzikos \(2009\)](#); [Arganda-Carreras et al. \(2010\)](#). Comparison against manually realigned stack (by an expert physician researcher) was done in [Krinidis et al. \(2003a\)](#); [Groen et al. \(2010\)](#). Robustness to holes and tears was tested in [Cifor et al. \(2011\)](#), and the effect of missing sections was assessed in [Arganda-Carreras et al. \(2010\)](#). Both were addressed in [Nikou et al. \(2003\)](#).

## 7. Applications

We underline three main areas of applications within which the covered literature falls into: (i) examining structures with respect to their environment in 3D (Section 7.1) with or without the help of 3D medical imaging; (ii) the correlation of data (Section 7.2), which benefits from the access to the underlying microbiology to improve the characterisation/discrimination of signals in non-invasive imaging; and (iii) the creation of digital

atlases (Section 7.3), which allows for easy 2D and 3D visualisations as well as quantitative measures of anatomy when independent data from different subjects are included.

### 7.1. Examining functions and relationships in 3D

This section includes works for histological reconstruction with or without the help of 3D medical imaging.

Mice brains were reconstructed in [Gaffling et al. \(2011, 2015\)](#) and [Müller et al. \(2014\)](#). [Gaffling et al.](#) reconstructed Nissl-stained cryosections of an adult mouse brain, available from [Ju et al. \(2006\)](#). Other organs, such as rat liver tissue were studied in [Schwier et al. \(2013\)](#), who proposed a registration method for the reconstruction of histological whole slide images that exhibit vessel structures. Human liver tissues were studied in [Song et al. \(2013\)](#) and [Roberts et al. \(2012\)](#). [Chen et al. \(2003\)](#) described the 3D configuration of extravascular matrix patterns in archival human uveal melanoma tissue. Mice lungs was studied in [Rusu et al. \(2015\)](#), and the heart, in [Magee et al. \(2015\)](#) and [Mansoori et al. \(2007\)](#).

Tumours were studied in [Braumann et al. \(2005\)](#) and [Wentzensen et al. \(2007\)](#). [Braumann et al.](#) analysed the 3D structure of tumoural invasion fronts of carcinoma of the uterine cervix to understand their architectural-functional relationship, while [Wentzensen et al.](#) analysed the spatial organisation of a cervical cancer.

Vasculature was investigated in [Xu et al. \(2015\)](#), who studied the microvascular structure of the mouse hind-limb. Due to the 3D rearrangement of the microvessel networks during pathology, a reconstruction is critical in understanding the dysfunction of organs during disease. [Ulrich et al. \(2014\)](#) reconstructed the 3D vascular network from immunostained sections of the human spleen.

Cerebral function is dependant on neurological organisation and metabolic activity ([Hibbard et al., 1987](#)). Autoradiography allows looking in great details at, among others, the cerebral metabolic rate of glucose utilisation in response to physiologic activation of the visual, auditory, somatosensory, and motor systems, and in pathologic conditions. Rat brains were looked at in [Hibbard and Hawkins \(1984, 1988\)](#); [Zhao et al. \(1993\)](#); [Kim et al. \(1997, 1995\)](#); [Bronchti et al. \(2002\)](#); [Nikou et al. \(2003\)](#); [Lee et al. \(2005\)](#); [Dubois et al. \(2007\)](#). [Bronchti et al. \(2002\)](#) studied the auditory activation of visual cortical areas in the blind mole rat. [Lee et al. \(2005\)](#) looked into the cerebral glucose metabolism in the rat cortical deafness model using 3D voxel-based statistical analysis of autoradiographic data. They observed a significant decrease in the glucose metabolism in the bilateral auditory cortices. [Dubois et al. \(2007\)](#) combined histology and autoradiography and studied interhemispheric differences through voxel-wise statistical analyses. [Hess et al. \(1998\)](#) studied the metabolism and function of gerbil brains. Autoradiographic volumes from 2-DG autoradiographs of primates were reconstructed using 3D MRI in [Rangarajan et al. \(1997\)](#) and [Malandain et al. \(2004\)](#).

### 7.2. Characterising 3D medical imaging signals

In the context of neurological diseases, [Colchester et al. \(2000\)](#) proposed a method for 3D reconstruction from 2D histological

sections using fiducial markers with the aim of registering these *post mortem* volumes with MR images. This provides a 3D mapping of pathological changes throughout the brain, with application to Creutzfeld-Jacob disease. [Goubran et al. \(2013, 2015a\)](#) addressed the identification and delineation of lesions in MRI to improve the surgical treatment of epilepsy. [Lockwood-Estrin et al. \(2012\)](#) investigated whether specific semi-quantitative 3T MRI parameters are associated with particular histological features in temporal lobe specimens in epilepsy surgery patients whose conventional MRI scan appeared normal.

Stroke was studied in [Li et al. \(2006\)](#), who correlated signal changes observed in T1-weighted images acquired during brain ischemia in small animal models to molecular features obtained from histology. A similar effort was followed in [Stille et al. \(2013\)](#), who registered “abnormal” images from a rat model of stroke with 3D *in vivo* T2w MR images to study neurobiological correlates of the variations in MRI signal intensities.

Another important application relates to cancer, for which histopathologic examination can be related to *in vivo*—or *ex vivo* ([Gibson et al., 2012](#)), MR imaging with the aim of improving prostate cancer detection rate ([Nir et al., 2014](#); [Ward et al., 2012](#); [Alic et al., 2011](#); [Chappelow et al., 2011a](#); [Samavati et al., 2011](#); [Xiao et al., 2011](#); [Mazaheri et al., 2010](#); [Ou and Davatzikos, 2009](#); [Zhan et al., 2007](#)). [Le Nobin et al. \(2015\)](#) compared prostate tumour boundaries on MRI and histology in order to define an optimal treatment margin for achieving complete tumour destruction during image guided focal ablation. [Edwards et al. \(2005\)](#) used histology to identify the tumour boundaries in oral cancer patients with better accuracy in order to enable precise PET-guided resection. [Jiang et al. \(2013\)](#) combined *in vivo* MRI/MRSI, *ex vivo* brightfield/fluorescence microscopic imaging, and histology to study human breast cancer. [Seeley et al. \(2014\)](#) studied secondary breast cancer in the bone. They used diffusion weighted MRI, Matrix-Assisted Laser Desorption/Ionisation Imaging Mass Spectrometry and histology to observe changes caused by tumour cells in the bone at the protein level. The mapping between histology and 3D whole specimen imaging along with whole mastectomy volume reconstruction from radiographs were studied in [Mertzanidou et al. \(2017\)](#) and [Mertzanidou et al. \(2016\)](#). [Breen et al. \(2005b\)](#) correlated *in vivo* MR thermal lesion images in rabbit thighs with histological tissue damage. [Humm et al. \(2003\)](#) developed a stereotactic fiducial marker system for hypopharyngeal tumour xenografts in rodents to co-register MRI, PET, histology, autoradiography, and measurements from physiologic probes.

Vascular lesions can be seen in human MRI but are only detected reliably in histology. [Singh et al. \(2008\)](#) registered lesions microscopical features with their corresponding locations in the *in vivo* MR images in order to understand better their MRI signatures. [Coombs et al. \(2001\)](#) correlated MR signal characteristics with carotid atherosclerosis plaque components to define resolution and other requirements for future clinical carotid MRI. [Groen et al. \(2010\)](#) studied the relationship between biomechanical parameters and atherosclerotic tissue components in the carotid using histology, *in vivo* CT angiography and *ex vivo* MRI and CT imaging.

### 7.3. Combined MRI-histology atlases

Atlases provide detailed segmentations and classifications of certain regions and sub-regions in a common anatomical reference framework. They stem from the need for accurate maps of architectonic areas with reference to MRI images. The main rationale is to help understanding the localisation of functional activity in different regions ([Brett et al., 2002](#)) but they are also of great importance in segmentation ([Aljabar et al., 2009](#)) or can be used to improve preoperative planning ([Goerres et al. \(2017\)](#)) and post-operative follow-up.

There exist three types of atlases: (i) *MRI-based atlases* ([Kovačević et al., 2005](#); [Dorr et al., 2008](#)). They are useful for measuring volumes and analysing large morphological features but suffer from imprecise delineations due to low resolutions. (ii) *Histology-based atlases* ([Ju et al., 2006](#)). Most of them derive from rodent brains but are limited: [Ma et al. \(2005\)](#) reported that distortions during tissue preparation and the lack of structural ground-truth in 3D make it hard to extract spatial cues or to derive quantitative group variations. [Annese et al. \(2006\)](#) proposed a high-resolution 3D reconstruction of blockface-imaged, Methylene blue perfused primate brain tissue as the basis for detailed stereotaxic anatomical atlases. The use of blockface images bypasses the tedious correction and alignment of histological sections without external information. (iii) *Combined MRI and histology atlases* ([Saleem and Logothetis, 2012](#)). They combine accurate anatomical delineations in histology for propagation in the 3D medical image, with ground truth 3D shape for improved histological reconstructions. We emphasize the last type of atlases as it involves multimodal image registration.

In human brain, [Ourselin et al. \(2001a\)](#) worked on the creation of a brain atlas of the human basal ganglia based on histological images and MR images. [Chakravarty et al. \(2006\)](#) proposed another brain atlas of the basal ganglia and the thalamus derived from serial histological data. Then, [Yelnik et al. \(2007\)](#)—and [Bardinet et al. \(2009\)](#) later—both described the construction of new atlases of the human basal ganglia based on immunohistochemical and MRI data.

In the context of animal studies, [Johnson et al. \(2007, 2010\)](#) presented an atlas of the C57BL/6 mouse brain based on MRI and conventional Nissl histology. [Lebenberg et al. \(2010\)](#) proposed to match an MRI-based 3D digital atlas derived from C57Bi/6J mouse brain with 3D reconstructed post-mortem data to automatically in order to evaluate morphology and function in mouse brain structures in the context of Alzheimer’s disease. [Mailly et al. \(2010\)](#) reported a procedure for the construction of a 3D digital model of the primate and rodent basal ganglia. [Yushkevich et al. \(2006\)](#) used an average MRI of 30 *in vivo* scans of 10 mice in order to build a 3D reference histological atlas of the mouse brain from Nissl-stained sections. [Ali and Cohen \(1998\)](#) contributed to brain mapping by combining histological sections of rat brain with a 3D brain atlas. [Gefen et al. \(2008\)](#) followed the same effort and aligned Nissl-stained histological sections with a volumetric mouse brain atlas for the segmentation of hippocampal complex. [Dauguet et al. \(2007b\)](#) proposed a pipeline for the reconstruction of a histological volume from whole baboon brain Nissl-stained sections using *in vivo* MRI.

Amunts et al. (2013) created an ultrahigh-resolution 3D model of a human brain at nearly cellular resolution of 20 micrometers.

Finally, histology-MRI atlases have also been used by Burton et al. (2006), who combined MRI and Trichrome-stained histological sections in order to construct histo-anatomically detailed models of cardiac 3D structure and function at a high resolution.

## 8. Discussion and perspectives

This section covers four topics: (i) some methodological comments on pipelines (Section 8.1), their differences, advantages and drawbacks; (ii) some of the remaining challenges (Section 8.2); and (iii) concluding remarks on the importance of cross-disciplinary knowledge in solving the biological question associated with histology-MRI registration (Section 8.3).

### 8.1. Methodological comments

*On hybrid pipelines.* To start with, volume-based approaches (Section 5.1.3) rely on a single round of registration between histology and medical image volumes. In that respect, changing the input (another reconstructed histological volume) results in a different global alignment and thereby establishes different correspondences between both modalities. In contrary, hybrid pipelines (Section 5.1.4) rely on the principle that global alignment between both volumes is optimal only when the arrangement of histological slices relative to each other is optimal, and *vice versa*. In other words, should it be 3D-3D or 2D-2D registration, one conditions the performance of the other. This strategy offers a robust way to achieving accurate reconstructions (Adler et al., 2014; Goubran et al., 2015b). While Adler et al. performed 2D non-rigid registrations between histology and medical imaging only after an iterative process had converged—consisting of 2D and 3D multimodal linear registrations, Goubran et al. proposed to include 2D non-rigid registrations of every histological slice with its corresponding MR slice into the above-mentioned iterative process. Non-rigidly deforming histological slices iteratively may however create wrong correspondences and thus potentially lead to erroneous global alignment with medical imaging if the initialisation is not already good.

In view of Figure 9 in Adler et al. (2014), the gain from complex methods for initial histological reconstructions is also, in general, unclear in multimodal registration pipelines (compared to pairwise registrations or simple stacking). Furthermore, whereas consistency and accuracy of the initial reconstruction would matter in the case of volume-based approaches, hybrid pipelines allow to relax that constraint as they account for it by design. Manual reconstructions using open-source softwares represent another attractive solution (Yushkevich et al., 2016; Adler et al., 2016).

*On the use of intermediate modalities.* Mapping histology with medical imaging is challenging due to the alteration of the tissue between the starting (*in* or *ex vivo*) and the end (histological images) points of its handling. Not using any proxy may complicate the path to solution.



**Figure 5:** Working with blockface photographs. Left: camera fixed on a tripod, standing behind the histopathologist collecting tissue sections from an automated microtome (bottom right). Top right: one blockface photograph is shown.

Similarly to longitudinal image analysis, the more snapshots during tissue preparation, the easier it is to track and correct deformations between *in vivo* imaging and sectioned histology (of the same specimen). This is where blockface photographs are of great value (Figure 5). Using in addition fixed *ex vivo* medical images allows accounting for the non-uniform shrinkage that happens when extracting the sample. Besides, the main rationale for also using fresh *ex vivo* scans may be the study of the influence of fixation on tissues magnetic properties (see Section 8.3). The right balance should however be found when using intermediate modalities as this not only calls for more resources (time, space, study goals etc.), but also impacts the accuracy of the histological reconstruction: (i) none (Adler et al., 2014); (ii) *ex vivo* medical images (Goubran et al., 2013); (iii) fresh + fixed *ex vivo* and blockface photographs (Samavati et al., 2011).

Another advantage of intermediate modalities lies in that they offer additional levels of resolutions between that of *in vivo* and histology. This naturally results in pyramidal schemes, in which the optimisation of the transformation parameters is less likely to get trapped in local optima.

### 8.2. Remaining challenges in histological reconstruction

*Preprocessing.* Tears and folds may be the most challenging artefacts to account for and frequently result in discarding the damaged section. The correction of tears requires to ascertain that no tissue material has been lost. Assuming this is possible to tell automatically, the problem is to recover in-plane continuity between separated structures. The problem of tears can be extended to purposeful cuts when for example, whole mount histology is to be studied and the tissue slice needs to be cut into several pieces. Mosaicing/stitching is extensively studied in the general computer vision literature (Brown and Lowe, 2007) and may also be approached as Jigsaw puzzle solving (Gallagher, 2012; Noroozi and Favaro, 2016). So far, detection of folds has relied on rather simplistic assumptions about the colour brightness properties of an image and could benefit from the addition of geometrical considerations. It is challenging to know how many layers a single fold is made of. Assuming it is possible to know that number, the correction of a fold still requires the

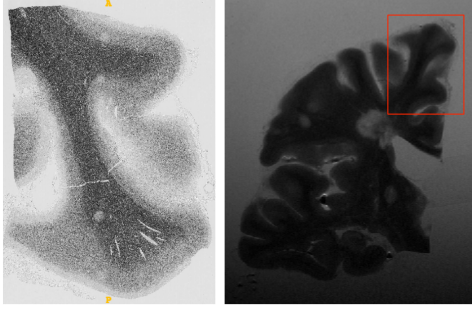


**Figure 6:** Part-to-whole registration. One T2 slice from a slab of a whole brain is shown in the image on the right. It was then cut into blocks, each of which was put in separate cassettes and processed for histology. A GFAP-stained section from one of these blocks (delineated in red) is shown in the image on the left.

separation of structures belonging to each of the layers that compose it. It also necessitates the rearrangement of the entire piece of tissue according to its configuration prior to folding (i.e., unfolding), which may be approximated from adjacent sections.

Other fields are involved in similar problems and give potential to exciting parallels. They include computational geometry (Demaine and O’Rourke, 2005) and computer vision with e.g., the simulation and visualisation of realistic tearing and cracking of thin sheets (Pfaff et al., 2014); material science with e.g., the study of mechanical instabilities of certain materials during compression (Kim et al., 2011; Pociavsek et al., 2008); statistical physics with e.g., the modeling of folding of thin sheets (Deboeuf et al., 2013; Adda-Bedia et al., 2010); or even geology with e.g. the study of orogeny (Ramsay, 1962). As a matter of fact, Dempster (1942) gave extensive information about the nature of tissue distortions during microtomy.

*Image analysis.* The extraction and manipulation of meaningful information from histology and medical images is a very complicated task. Thus, attention has been directed towards simplifying them, that is classically, using the *shape* and the *edges*.

Such simplification is not trivial (Marr, 1982) and it cannot be achieved by only looking at intensity changes (Guichard et al., 2004): many unwanted edges are produced in the process, and not only texture and noise are responsible for it (e.g., tears and cuts in histological images). The reduction of images to their main features thus relies on smoothing, which has become a commonplace to separate “true edges” from noise. However, what smoothing to use in multi-scale approaches—as in how to actually build a scale space? (Morel and Yu, 2011), remains an important matter to guarantee reliable and tractable detections.

In the monomodal case, feature-based methods were successfully applied to the registration of histological slices but investigations such as the study of factors that influence keypoint stability in scale space (Rey-Otero et al., 2015), or the derivation of criteria for detectors comparison (Rey-Otero and Delbracio, 2015) may be of great benefit to the field: in general, little details are given about the consistency and reliability of detections. Besides, a common drawback in their use for histopathological image analysis is the large amount of features that may be gener-

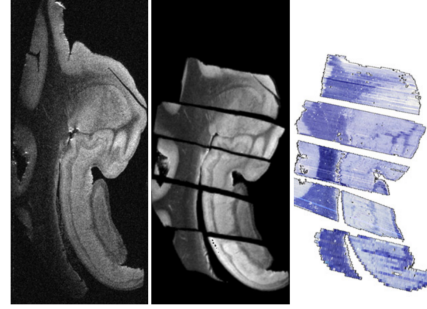


**Figure 7:** The block of tissue (left) being too thick for histology processing, was cut into sub-blocks, re-scanned (middle) and individually processed. Nissl-stained reconstructed and rearranged histological sub-blocks are shown (right). Image reproduced with permission from Adler et al. (2014).

ated; this is due to the rich content of images, which can quickly turn into “biological noise”.

In the multimodal case, histology and medical imaging have, by nature, their own contrast and there does not always exist a mapping between their constituents—incidentally, the latter is one reason why intensity-based methods tend to get trapped in local optima. As a matter of fact, classical feature description methods, such as SIFT (Lowe, 1999), will also fail to match features (Toews et al., 2013) especially due to non-linear local intensity mappings (letting aside the lack of counterpart, which could be handled with suitable descriptions). Alternative methods are necessary and rethinking descriptions may be required (Heinrich et al., 2012). Note that manual extraction of anatomical landmarks in histology and medical imaging still remains a safe way to establish correspondences (Gangolli et al., 2017).

Lastly, shape—as defined by Attneave (1954), can become a valuable asset (see Figure 6), and multimodal registration may be obtained as a result of shape recognition (Lisani et al., 2003).

Gutiérrez-Becker et al. (2016) tackled the aforementioned limitations about description in a multimodal setting by learning correspondences between context-aware Haar-like features from intravascular ultrasound and histology, and inferring displacements by means of a regression forest. Such approach naturally brings the promising tracks related to convolutional neural networks (Greenspan et al., 2016) in the medical domain. The alignment problem could directly benefit from the computational power of such methods for learning correspondences between two different modalities. For example, Miao et al. (2016) developed a method for real-time 2D-3D registration of tools images with 3D CT. A survey on deep learning in medical image analysis can be found in Litjens et al. (2017).

*Part-to-whole.* It is not uncommon for histopathology laboratories to receive tissue samples that are (P1) too wide (Figure 6) or (P2) too thick (Figure 7) to be processed as they are. The sample is therefore cut into separate sub-blocks, each of which is processed individually. If no scan of each sub-block is available, one has to keep track on which part of the sample each sub-block corresponds to and use that knowledge to initialise the registration of histological slices with the clinical image, or

manually align them. As for problem (P2), attempts at using similarity measures have been made to initialise registrations, but those are ambiguous and rely on absolute measures rather than relative ones (Yang et al., 2012). On that matter, Xiao et al. (2011) showed that direct comparison of images from different modalities is non-trivial, and fails to reliably determine slice correspondences. To the best of our knowledge, no automatic method to address (P1) has been proposed in the literature.

*Fusion.* To the best of our knowledge, Van de Plas et al. (2015) made the first true attempt at drawing mutual enrichment from separate modalities (mass spectrometry and microscopy). This seems reasonable to think that one goal of combining information could also be to actually do so through fusion (as opposed to only overlay images), and thereby for example, increase the spatial resolution as well as augment the informative power of 3D medical imaging.

### 8.3. Concluding remarks

The problem of histological reconstruction using medical imaging involves at least four experts: a histopathologist, a physicist, a computer scientist and a physician in order to answer a single biological question. Interdisciplinary collaborations are essential and communication on the object to be delivered/handled at every stage, time constraints and resources is critical (what?, how?, when?). This allows avoiding compromises, thinking backward and instead appropriately (re)defining a problem (Cristancho et al., 2017). For the sake of illustration, such a timeline is presented in Figure 2 of the Supplementary Methods 1 from Hawrylycz et al. (2012). Cross-field awareness is crucial as data analyses rely on the assumption that the object remains similar enough through time and stages to be reliably compared across modalities. Improvements are consistently being made to minimise alterations of tissue and towards understanding the causes and effects of such variations.

Let us consider the case of *ex vivo* MRI, which is commonly applied in neuroscience for a better understanding of the contrast mechanisms of disease-induced tissue changes. Its use supposes that the tissue has been preserved (fixed/frozen). As a matter of fact, the effect of time and storage conditions on the magnetic properties of *post mortem* tissue is important for correct interpretation of *in vivo* clinical results based upon *ex vivo* measurements.

According to Fischer et al. (1989) and more recently to Kaye et al. (2010), quick deep freezing is a satisfactory method of storage for tissue samples (e.g. brain, heart) which does not affect T1 or T2 significantly. However, this method is not applicable to liver and muscle tissues (Duck, 2013).

In contrast, chemical fixation (aldehydes, and commonly formalin) causes reduction in tissue T1 and increase in T2 relaxation times for human tissue (Duck, 2013), as well as a significant decrease of mean water diffusivity in e.g. nervous tissue. Little is known about how fixative solutions alter the tissue microstructures responsible for its MRI properties: while some effects may be reversible, others may be irreversible (Porea and Webb, 2006; Shepherd et al., 2009). Conducting such investigations may require the imaging of the fresh specimen (fixative-free) as

well as examinations of the effects of different fixation protocols (Shepherd et al., 2009).

Lastly, detailing data acquisition protocols goes beyond the scope of this review but it still seems relevant to stress out the importance of generating standard data. As far as image registration is concerned, it is simply a tool designed to achieve accurate and reproducible correspondences between separate images. However, improving it becomes vain if similar attention is not also directed towards ensuring consistent, quality input data within and across institutions (Lin and Shi, 2015; Milidoni et al., 2015; Traboulsee et al., 2016). Standardising protocols is not easy and immediate, and although the importance of such undertaking is acknowledged by many, so is the amount of work that remains to be done. At the other end, since quantitative measurements are to be extracted from those images and interpreted by clinicians/physicians, a comparable amount awaits computational imaging scientists dealing with such variations (Madabhushi and Lee, 2016).

### Acknowledgements

The authors would like to thank Dr. Smriti Patodia, from UCL Institute of Neurology (Department of Neuropathology), for her comments on Section 2 and the images used in Figures 2 and 5, as well as Dr. Steven Van de Pavert, Mr. Marcello Moccia, and Prof. Olga Ciccarelli from UCL Institute of Neurology (Queen Square MS Centre), for the images used in Figure 6.

This research was supported by the European Research Council (Starting Grant 677697, project BUNGEE-TOOLS), the EP-SRC (EP/H046410/1, EP/J020990/1, EP/K005278), the MRC (MR/J01107X/1), the EU-FP7 project VPH-DARE@IT (FP7-ICT-2011-9-601055), the NIHR Biomedical Research Unit (Dementia) at UCL, the National Institute for Health Research University College London Hospitals Biomedical Research Centre (NIHR BRC UCLH/UCL High Impact Initiative), the UCL Leonard Wolfson Experimental Neurology Centre and the Alzheimer's Society.

### References

- Absinta, M., Nair, G., Filippi, M., Ray-Chaudhury, A., Reyes-Mantilla, M. I., Pardo, C. A., Reich, D. S., 2014. Postmortem magnetic resonance imaging to guide the pathologic cut. *Journal of Neuropathology & Experimental Neurology* 73 (8), 780–788. 17
- Adda-Bedia, M., Boudaoud, A., Boué, L., Deboeuf, S., 2010. Statistical distributions in the folding of elastic structures. *Journal of Statistical Mechanics: Theory and Experiment* 2010 (11), P11027. 27
- Adler, D. H., Ittyerah, R., Pluta, J., Pickup, S., Liu, W., Wolk, D. A., Yushkevich, P. A., 2016. Probabilistic atlas of the human hippocampus combining *ex vivo* mri and histology. In: *International Conference on Medical Image Computing and Computer-Assisted Intervention*. Springer, pp. 63–71. 19, 26
- Adler, D. H., Pluta, J., Kadivar, S., Craige, C., Gee, J. C., Avants, B. B., Yushkevich, P. A., 2014. Histology-derived volumetric annotation of the human hippocampal subfields in postmortem mri. *Neuroimage* 84, 505–523. 4, 7, 8, 10, 11, 19, 23, 26, 27
- Alegro, M., Amaro-Jr, E., Loring, B., Heinsen, H., Alho, E., Zollei, L., Ushizima, D., Grinberg, L. T., 2016. Multimodal whole brain registration: Mri and high resolution histology. In: *Proceedings of the IEEE Conference on Computer Vision and Pattern Recognition Workshops*. pp. 194–202. 7, 20, 21, 23

- Ali, W. S. I., Cohen, F. S., 1998. Registering coronal histological 2-d sections of a rat brain with coronal sections of a 3-d brain atlas using geometric curve invariants and b-spline representation. *IEEE Transactions on Medical Imaging* 17 (6), 957–966. [4](#), [12](#), [14](#), [18](#), [25](#)
- Alic, L., Haeck, J. C., Bol, K., Klein, S., van Tiel, S. T., Wielepolski, P. A., de Jong, M., Niessen, W. J., Bernsen, M., Veenland, J. F., 2011. Facilitating tumor functional assessment by spatially relating 3d tumor histology and in vivo mri: image registration approach. *PLoS One* 6 (8), e22835. [4](#), [11](#), [19](#), [23](#), [25](#)
- Aljabar, P., Heckemann, R. A., Hammers, A., Hajnal, J. V., Rueckert, D., 2009. Multi-atlas based segmentation of brain images: atlas selection and its effect on accuracy. *Neuroimage* 46 (3), 726–738. [25](#)
- Alpert, N., Bradshaw, J., Kennedy, D., Correia, J., 1990. The principal axes transformation—a method for image registration. *J Nucl Med* 31, 1717–1723. [15](#)
- Amunts, K., Lepage, C., Borgeat, L., Mohlberg, H., Dickscheid, T., Rousseau, M.-É., Bludau, S., Bazin, P.-L., Lewis, L. B., Oros-Peusquens, A.-M., et al., 2013. Bigbrain: an ultrahigh-resolution 3d human brain model. *Science* 340 (6139), 1472–1475. [2](#), [21](#), [26](#)
- Amunts, K., Zilles, K., 2015. Architectonic mapping of the human brain beyond brodmann. *Neuron* 88 (6), 1086–1107. [2](#)
- Andersson, M., Groseclose, M. R., Deutch, A. Y., Caprioli, R. M., 2008. Imaging mass spectrometry of proteins and peptides: 3d volume reconstruction. *Nature Methods* 5 (1), 101–108. [10](#)
- Andreasen, A., Drewes, A., Assentoft, J., Larsen, N., 1992. Computer-assisted alignment of standard serial sections without use of artificial landmarks. a practical approach to the utilization of incomplete information in 3-d reconstruction of the hippocampal region. *Journal of neuroscience methods* 45 (3), 199–207. [14](#)
- Andrey, P., Maurin, Y., 2005. Free-d: an integrated environment for three-dimensional reconstruction from serial sections. *Journal of neuroscience methods* 145 (1), 233–244. [10](#)
- Annese, J., 2012. The importance of combining mri and large-scale digital histology in neuroimaging studies of brain connectivity. Mapping the connectome: Multi-level analysis of brain connectivity. [2](#), [4](#), [16](#)
- Annese, J., Schenker-Ahmed, N. M., Bartsch, H., Maechler, P., Sheh, C., Thomas, N., Kayano, J., Ghatan, A., Bresler, N., Frosch, M. P., et al., 2014. Postmortem examination of patient hms brain based on histological sectioning and digital 3d reconstruction. *Nature communications* 5. [4](#)
- Annese, J., Sforza, D., Dubach, M., Bowden, D., Toga, A., 2006. Postmortem high-resolution 3-dimensional imaging of the primate brain: blockface imaging of perfusion stained tissue. *Neuroimage* 30 (1), 61–69. [4](#), [20](#), [25](#)
- Arganda-Carreras, I., Fernández-González, R., Muñoz-Barrutia, A., Ortiz-De-Solorzano, C., 2010. 3d reconstruction of histological sections: Application to mammary gland tissue. *Microscopy research and technique* 73 (11), 1019–1029. [4](#), [8](#), [12](#), [15](#), [24](#)
- Arganda-Carreras, I., Sorzano, C. O., Kybic, J., Ortiz-de Solorzano, C., 2008. bunwarj: Consistent and elastic registration in imagej, methods and applications. In: *Second ImageJ User & Developer Conference*. [11](#)
- Atit, K., Shipley, T. F., Tikoff, B., 2013. Twisting space: are rigid and non-rigid mental transformations separate spatial skills? *Cognitive processing* 14 (2), 163–173. [1](#)
- Attneave, F., 1954. Some informational aspects of visual perception. *Psychological review* 61 (3), 183. [27](#)
- Auer, M., Regitnig, P., Holzzapfel, G. A., 2005. An automatic nonrigid registration for stained histological sections. *IEEE Transactions on Image Processing* 14 (4), 475–486. [16](#)
- Avants, B. B., Epstein, C. L., Grossman, M., Gee, J. C., 2008. Symmetric diffeomorphic image registration with cross-correlation: evaluating automated labeling of elderly and neurodegenerative brain. *Medical image analysis* 12 (1), 26–41. [21](#)
- Avants, B. B., Tustison, N., Song, G., 2009. Advanced normalization tools (ants). *Insight J* 2, 1–35. [11](#)
- Avants, B. B., Tustison, N. J., Wu, J., Cook, P. A., Gee, J. C., 2011. An open source multivariate framework for n-tissue segmentation with evaluation on public data. *Neuroinformatics* 9 (4), 381–400. [8](#)
- Axer, M., Amunts, K., Grässel, D., Palm, C., Dammers, J., Axer, H., Pietrzyk, U., Zilles, K., 2011. A novel approach to the human connectome: ultra-high resolution mapping of fiber tracts in the brain. *Neuroimage* 54 (2), 1091–1101. [4](#)
- Badano, A., Revie, C., Casertano, A., Cheng, W.-C., Green, P., Kimpe, T., Krupinski, E., Sisson, C., Skråvseth, S., Treanor, D., et al., 2015. Consistency and standardization of color in medical imaging: a consensus report. *Journal of digital imaging* 28 (1), 41–52. [7](#)
- Bagci, U., Bai, L., 2010. Automatic best reference slice selection for smooth volume reconstruction of a mouse brain from histological images. *IEEE Transactions on Medical imaging* 29 (9), 1688–1696. [7](#), [9](#), [24](#)
- Baheerathan, S., Albrechtsen, F., Danielsen, H., 1998. Registration of serial sections of mouse liver cell nuclei. *Journal of microscopy* 192 (1), 37–53. [3](#), [23](#), [24](#)
- Bajcsy, P., LEE, S.-C., Lin, A., Folberg, R., 2006. Three-dimensional volume reconstruction of extracellular matrix proteins in uveal melanoma from fluorescent confocal laser scanning microscope images. *Journal of microscopy* 221 (1), 30–45. [4](#)
- Bancroft, J. D., Gamble, M., 2008. *Theory and practice of histological techniques*. Elsevier Health Sciences. [3](#)
- Bardinet, E., Bhattacharjee, M., Dormont, D., Pidoux, B., Malandain, G., Schüpbach, M., Ayache, N., Cornu, P., Agid, Y., Yelnik, J., 2009. A three-dimensional histological atlas of the human basal ganglia. ii. atlas deformation strategy and evaluation in deep brain stimulation for parkinson disease: Clinical article. *Journal of neurosurgery* 110 (2), 208–219. [25](#)
- Barthel, L. K., Raymond, P. A., 1990. Improved method for obtaining 3-microns cryosections for immunocytochemistry. *Journal of Histochemistry & Cytochemistry* 38 (9), 1383–1388. [4](#)
- Bautista, P. A., Hashimoto, N., Yagi, Y., et al., 2014. Color standardization in whole slide imaging using a color calibration slide. *Journal of pathology informatics* 5 (1), 4. [7](#)
- Bautista, P. A., Yagi, Y., 2015. Staining correction in digital pathology by utilizing a dye amount table. *Journal of digital imaging* 28 (3), 283–294. [7](#)
- Bautista, P. A., Yagi, Y., et al., 2010. Improving the visualization and detection of tissue folds in whole slide images through color enhancement. *Journal of pathology informatics* 1 (1), 25. [7](#)
- Bay, H., Tuytelaars, T., Van Gool, L., 2006. Surf: Speeded up robust features. In: *European conference on computer vision*. Springer, pp. 404–417. [11](#)
- Beare, R., Richards, K., Murphy, S., Petrou, S., Reutens, D., 2008. An assessment of methods for aligning two-dimensional microscope sections to create image volumes. *Journal of neuroscience methods* 170 (2), 332–344. [4](#), [11](#), [23](#)
- Beis, J. S., Lowe, D. G., 1997. Shape indexing using approximate nearest-neighbour search in high-dimensional spaces. In: *Computer Vision and Pattern Recognition, 1997. Proceedings., 1997 IEEE Computer Society Conference on*. IEEE, pp. 1000–1006. [13](#)
- Bejnordi, B. E., Litjens, G., Timofeeva, N., Otte-Höller, I., Homeyer, A., Karssemeijer, N., van der Laak, J. A., 2016. Stain specific standardization of whole-slide histopathological images. *IEEE transactions on medical imaging* 35 (2), 404–415. [7](#)
- Belanger, L. F., LeBlond, C. P., 1946. A method for locating radioactive elements in tissues by covering histological sections with a photographic emulsion. *Endocrinology* 39 (1), 8–13. [5](#)
- Benetazzo, L., Bizzego, A., De Caro, R., Frigo, G., Guidolin, D., Stecco, C., 2011. 3d reconstruction of the crural and thoracolumbar fasciae. *Surgical and radiologic anatomy* 33 (10), 855–862. [11](#)
- Besag, J., 1986. On the statistical analysis of dirty pictures. *Journal of the Royal Statistical Society. Series B (Methodological)*, 259–302. [15](#)
- Besl, P. J., McKay, N. D., 1992. Method for registration of 3-d shapes. In: *Robotics-DL tentative*. International Society for Optics and Photonics, pp. 586–606. [14](#), [22](#)
- Bloch, I., 1996. Information combination operators for data fusion: a comparative review with classification. *Systems, Man and Cybernetics, Part A: Systems and Humans*, IEEE Transactions on 26 (1), 52–67. [16](#)
- Boehler, T., van Straaten, D., Wirtz, S., Peitgen, H.-O., 2011. A robust and extendible framework for medical image registration focused on rapid clinical application deployment. *Computers in biology and medicine* 41 (6), 340–349. [11](#), [13](#)
- Bonnet, M., Djelloul, M., Tillement, V., Tardivel, C., Mounien, L., Trouslard, J., Troade, J.-D., Dallaporta, M., 2013. Central ncb2/nesfatin-1-expressing neurones belong to the hypothalamic-brainstem circuitry activated by hypoglycaemia. *Journal of neuroendocrinology* 25 (1), 1–13. [10](#)
- Bookstein, F. L., 1989. Principal warps: Thin-plate splines and the decomposition of deformations. *IEEE Transactions on Pattern Analysis & Machine Intelligence* (6), 567–585. [8](#), [22](#)
- Brandt, R., Rohlfing, T., Rybak, J., Krofczik, S., Maye, A., Westerhoff, M., Hege, H.-C., Menzel, R., 2005. Three-dimensional average-shape atlas of

the honeybee brain and its applications. *Journal of Comparative Neurology* 492 (1), 1–19. [15](#)

Braumann, U.-D., Eienkel, J., Horn, L.-C., Kuska, J.-P., Löffler, M., Scherf, N., Wentzensen, N., 2006. Registration of histologic colour images of different staining. In: *Bildverarbeitung für die Medizin 2006*. Springer, pp. 231–235. [12](#), [13](#)

Braumann, U.-D., Kuska, J.-P., Eienkel, J., Horn, L.-C., Löffler, M., Höckel, M., 2005. Three-dimensional reconstruction and quantification of cervical carcinoma invasion fronts from histological serial sections. *Medical Imaging, IEEE Transactions on* 24 (10), 1286–1307. [7](#), [11](#), [13](#), [15](#), [24](#)

Breen, M. S., Lancaster, T. L., Lazebnik, R. S., Nour, S. G., Lewin, J. S., Wilson, D. L., 2003. Three-dimensional method for comparing in vivo interventional mr images of thermally ablated tissue with tissue response. *Journal of Magnetic Resonance Imaging* 18 (1), 90–102. [23](#)

Breen, M. S., Lancaster, T. L., Wilson, D. L., 2005a. Correcting spatial distortion in histological images. *Computerized Medical Imaging and Graphics* 29 (6), 405–417. [8](#)

Breen, M. S., Lazebnik, R. S., Wilson, D. L., 2005b. Three-dimensional registration of magnetic resonance image data to histological sections with model-based evaluation. *Annals of biomedical engineering* 33 (8), 1100–1112. [4](#), [8](#), [20](#), [22](#), [23](#), [25](#)

Brett, M., Johnsrude, I. S., Owen, A. M., 2002. The problem of functional localization in the human brain. *Nature reviews neuroscience* 3 (3), 243–249. [25](#)

Brey, E. M., King, T. W., Johnston, C., McIntire, L. V., Reece, G. P., Patrick, C. W., 2002. A technique for quantitative three-dimensional analysis of microvascular structure. *Microvascular research* 63 (3), 279–294. [11](#)

Bronchti, G., Heil, P., Sadka, R., Hess, A., Scheich, H., Wollberg, Z., 2002. Auditory activation of visualcortical areas in the blind mole rat (spalax ehrenbergi). *European Journal of Neuroscience* 16 (2), 311–329. [24](#)

Brown, M., Lowe, D. G., 2007. Automatic panoramic image stitching using invariant features. *International journal of computer vision* 74 (1), 59–73. [9](#), [26](#)

Brown, M., Szelski, R., Winder, S., 2005. Multi-image matching using multi-scale oriented patches. In: *Computer Vision and Pattern Recognition, 2005. CVPR 2005*. IEEE Computer Society Conference on. Vol. 1. IEEE, pp. 510–517. [11](#)

Buesa, R. J., 2007. Histology safety: now and then. *Annals of diagnostic pathology* 11 (5), 334–339. [3](#)

Bürigel, U., Schormann, T., Schleicher, A., Zilles, K., 1999. Mapping of histologically identified long fiber tracts in human cerebral hemispheres to the mri volume of a reference brain: position and spatial variability of the optic radiation. *Neuroimage* 10 (5), 489–499. [3](#), [8](#), [21](#)

Burton, R. A., Plank, G., Schneider, J. E., Grau, V., Ahammer, H., Keeling, S. L., Lee, J., Smith, N. P., Gavaghan, D., Trayanova, N., et al., 2006. Three-dimensional models of individual cardiac histology: Tools and challenges. *Annals of the New York Academy of Sciences* 1080 (1), 301–319. [4](#), [26](#)

Canny, J., 1986. A computational approach to edge detection. *IEEE Transactions on pattern analysis and machine intelligence* (6), 679–698. [12](#)

Capek, M., Bruza, P., Janacek, J., Karen, P., Kubinova, L., Vagnerova, R., 2009. Volume reconstruction of large tissue specimens from serial physical sections using confocal microscopy and correction of cutting deformations by elastic registration. *Microscopy research and technique* 72 (2), 110–119. [4](#), [8](#), [9](#)

Čapek, M., Janáček, J., Kubínová, L., 2006. Methods for compensation of the light attenuation with depth of images captured by a confocal microscope. *Microscopy research and technique* 69 (8), 624–635. [8](#)

Cardona, A., Saalfeld, S., Schindelin, J., Arganda-Carreras, I., Preibisch, S., Longair, M., Tomancak, P., Hartenstein, V., Douglas, R. J., 2012. Trakem2 software for neural circuit reconstruction. *PloS one* 7 (6), e38011. [10](#)

Casasent, D., Psaltis, D., 1976. Position, rotation, and scale invariant optical correlation. *Applied optics* 15 (7), 1795–1799. [11](#)

Casero, R., Siedlecka, U., Jones, E. S., Gruscheski, L., Gibb, M., Schneider, J. E., Kohl, P., Grau, V., 2017. Transformation diffusion reconstruction of three-dimensional histology volumes from two-dimensional image stacks. *Medical image analysis* 38, 184–204. [7](#), [15](#), [20](#)

Ceritoglu, C., Wang, L., Selemo, L. D., Csernansky, J. G., Miller, M. I., Ratnanather, J. T., 2010. Large deformation diffeomorphic metric mapping registration of reconstructed 3d histological section images and in vivo mr images. *Frontiers in human neuroscience* 4, 43. [7](#), [19](#)

Chakravarty, M. M., Bertrand, G., Descoteaux, M., Sadikot, A. F., Collins, D. L., 2003. The creation of a brain atlas for image guided neurosurgery using serial histological data. In: *International Conference on Medical Image Computing and Computer-Assisted Intervention*. Springer, pp. 343–350. [7](#)

Chakravarty, M. M., Bertrand, G., Hodge, C. P., Sadikot, A. F., Collins, D. L., 2006. The creation of a brain atlas for image guided neurosurgery using serial histological data. *Neuroimage* 30 (2), 359–376. [4](#), [7](#), [11](#), [19](#), [25](#)

Chappelow, J., Bloch, B. N., Rofsky, N., Genega, E., Lenkinski, R., DeWolf, W., Madabhushi, A., 2011a. Elastic registration of multimodal prostate mri and histology via multiattribute combined mutual information. *Medical Physics* 38 (4), 2005–2018. [16](#), [25](#)

Chappelow, J., Tomaszewski, J. E., Feldman, M., Shih, N., Madabhushi, A., 2011b. Histostitcher©: An interactive program for accurate and rapid reconstruction of digitized whole histological sections from tissue fragments. *Computerized Medical Imaging and Graphics* 35 (7), 557–567. [8](#), [9](#)

Chen, Q.-s., Defrise, M., Deconinck, F., 1994. Symmetric phase-only matched filtering of fourier-mellin transforms for image registration and recognition. *IEEE Transactions on pattern analysis and machine intelligence* 16 (12), 1156–1168. [13](#)

Chen, X., Ai, Z., Rasmussen, M., Bajcsy, P., Auvil, L., Welge, M., Leach, L., Vangveeravong, S., Maniotis, A. J., Folberg, R., 2003. Three-dimensional reconstruction of extravascular matrix patterns and blood vessels in human uveal melanoma tissue: techniques and preliminary findings. *Investigative ophthalmology & visual science* 44 (7), 2834–2840. [3](#), [9](#), [24](#)

Chicherova, N., Fundana, K., Müller, B., Cattin, P. C., 2014. Histology to  $\mu$ ct data matching using landmarks and a density biased ransac. In: *International Conference on Medical Image Computing and Computer-Assisted Intervention*. Springer, pp. 243–250. [18](#)

Chklovskii, D. B., Vitaladevuni, S., Scheffer, L. K., 2010. Semi-automated reconstruction of neural circuits using electron microscopy. *Current opinion in neurobiology* 20 (5), 667–675. [10](#)

Choe, A. S., Gao, Y., Li, X., Compton, K. B., Stepniwska, I., Anderson, A. W., 2011. Accuracy of image registration between mri and light microscopy in the ex vivo brain. *Magnetic resonance imaging* 29 (5), 683–692. [4](#), [8](#), [22](#), [23](#)

Chow, S. K., Hakozaki, H., Price, D. L., MacLean, N. A., Deerinck, T. J., Bouwer, J. C., Martone, M. E., Peltier, S. T., Ellisman, M. H., 2006. Automated microscopy system for mosaic acquisition and processing. *Journal of Microscopy* 222 (2), 76–84. [9](#)

Cifor, A., Bai, L., Pitiot, A., 2011. Smoothness-guided 3-d reconstruction of 2-d histological images. *Neuroimage* 56 (1), 197–211. [9](#), [14](#), [23](#), [24](#)

Cifor, A., Pridmore, T., Pitiot, A., 2009. Smooth 3-d reconstruction for 2-d histological images. In: *Information Processing in Medical Imaging*. Springer, pp. 350–361. [14](#)

Cohen, F. S., Yang, Z., Huang, Z., Nianov, J., 1998. Automatic matching of homologous histological sections. *IEEE transactions on biomedical engineering* 45 (5), 642–649. [12](#), [14](#)

Cointepas, Y., Mangin, J.-F., Garnero, L., Poline, J.-B., Benali, H., 2001. Brainvisa: software platform for visualization and analysis of multi-modality brain data. *Neuroimage* 13 (6), 98. [10](#)

Colchester, A., Ourselin, S., Zhu, Y., Bardin, E., He, Y., Roche, A., Al-Sarraj, S., Nailon, B., Ironside, J., Ayache, N., 2000. 3-d reconstruction of macroscopic optical brain slice images. In: *Medical Image Computing and Computer-Assisted Intervention—MICCAI 2000*. Springer, pp. 95–105. [9](#), [10](#), [12](#), [23](#), [24](#)

Collins, D. L., Evans, A. C., 1997. Animal: validation and applications of nonlinear registration-based segmentation. *International journal of pattern recognition and artificial intelligence* 11 (08), 1271–1294. [19](#)

Collins, D. L., Holmes, C. J., Peters, T. M., Evans, A. C., 1995. Automatic 3-d model-based neuroanatomical segmentation. *Human brain mapping* 3 (3), 190–208. [11](#)

Collins, D. L., Neelin, P., Peters, T. M., Evans, A. C., 1994. Automatic 3d intersubject registration of mr volumetric data in standardized talairach space. *Journal of computer assisted tomography* 18 (2), 192–205. [11](#)

Coombs, B. D., Rapp, J. H., Ursell, P. C., Reilly, L. M., Saloner, D., 2001. Structure of plaque at carotid bifurcation high-resolution mri with histological correlation. *Stroke* 32 (11), 2516–2521. [25](#)

Cooper, L., Huang, K., Sharma, A., Mosaliganti, K., Pan, T., 2006. Registration vs. reconstruction: Building 3-d models from 2-d microscopy images. In: *Proceedings of the workshop on multiscale biological imaging, data mining and informatics*. pp. 57–58. [15](#)

Cooper, L., Sertel, O., Kong, J., Lozanski, G., Huang, K., Gurcan, M., 2009. Feature-based registration of histopathology images with different stains: an application for computerized follicular lymphoma prognosis. *Computer*

methods and programs in biomedicine 96 (3), 182–192. [12](#), [13](#)

Cornillie, P., Van Den Broeck, W., Simoens, P., 2008. Three-dimensional reconstruction of the remodeling of the systemic vasculature in early pig embryos. *Microscopy research and technique* 71 (2), 105–111. [10](#)

Cristancho, S., Lingard, L., Forbes, T., Ott, M., Novick, R., 2017. Putting the puzzle together: the role of “problem definition” in complex clinical judgement. *Medical education* 51 (2), 207–214. [28](#)

Culling, C. F. A., 2013. *Handbook of histopathological and histochemical techniques: including museum techniques*. Butterworth-Heinemann. [1](#)

Dauguet, J., Bock, D., Reid, R. C., Warfield, S. K., 2007a. Alignment of large image series using cubic b-splines tessellation: Application to transmission electron microscopy data. In: *International Conference on Medical Image Computing and Computer-Assisted Intervention*. Springer, pp. 710–717. [5](#)

Dauguet, J., Delzescaux, T., Condé, F., Mangin, J.-F., Ayache, N., Hantraye, P., Frouin, V., 2007b. Three-dimensional reconstruction of stained histological slices and 3d non-linear registration with in-vivo mri for whole baboon brain. *Journal of neuroscience methods* 164 (1), 191–204. [8](#), [22](#), [23](#), [25](#)

Dauguet, J., Mangin, J.-F., Delzescaux, T., Frouin, V., 2004. Robust inter-slice intensity normalization using histogram scale-space analysis. In: *International Conference on Medical Image Computing and Computer-Assisted Intervention*. Springer, pp. 242–249. [7](#)

Dauguet, J., Peled, S., Berezovskii, V., Delzescaux, T., Warfield, S. K., Born, R., Westin, C.-F., 2007c. Comparison of fiber tracts derived from in-vivo dti tractography with 3d histological neural tract reconstruction on a macaque brain. *Neuroimage* 37 (2), 530–538. [4](#), [5](#)

Deboeuf, S., Katzav, E., Boudaoud, A., Bonn, D., Adda-Bedia, M., 2013. Comparative study of crumpling and folding of thin sheets. *Physical review letters* 110 (10), 104301. [27](#)

Delingette, H., Bardinet, E., Rey, D., Lemarechal, J., Montagnat, J., Ourselin, S., Roche, A., Dormont, D., Yelnik, J., Ayache, N., 2001. Yav++: a software platform for medical image processing and visualization. In: *Workshop on Interactive Medical Image Visualization and Analysis satellite symposia of MICCAI, IMIVA'01*. [22](#)

Delzescaux, T., Dauguet, J., Condé, F., Maroy, R., Frouin, V., 2003. Using 3d non rigid ffd-based method to register post mortem 3d histological data and in vivo mri of a baboon brain. In: *Medical Image Computing and Computer-Assisted Intervention-MICCAI 2003*. Springer, pp. 965–966. [18](#), [19](#)

Demaine, E. D., O’Rourke, J., 2005. A survey of folding and unfolding in computational geometry. *Combinatorial and computational geometry* 52, 167–211. [27](#)

Dempster, W. T., 1942. The mechanics of paraffin sectioning by the microtome. *The Anatomical Record* 84 (3), 241–267. [27](#)

Denk, W., Horstmann, H., 2004. Serial block-face scanning electron microscopy to reconstruct three-dimensional tissue nanostructure. *PLoS Biol* 2 (11), e329. [5](#)

Deriche, R., 1987. Using canny’s criteria to derive a recursively implemented optimal edge detector. *International journal of computer vision* 1 (2), 167–187. [23](#)

Dezso, K., Papp, V., Bugyik, E., Hegyesi, H., Sáfrány, G., Bödör, C., Nagy, P., Paku, S., 2012. Structural analysis of oval-cell-mediated liver regeneration in rats. *Hepatology* 56 (4), 1457–1467. [10](#)

Ding, S.-L., Royall, J. J., Sunkin, S. M., Ng, L., Facer, B. A., Lesnar, P., Guillozet-Bongaarts, A., McMurray, B., Szafer, A., Dolbeare, T. A., et al., 2016. *Comprehensive cellular-resolution atlas of the adult human brain*. *Journal of Comparative Neurology* 524 (16), 3127–3481. [2](#)

Dorr, A., Lerch, J. P., Spring, S., Kabani, N., Henkelman, R. M., 2008. High resolution three-dimensional brain atlas using an average magnetic resonance image of 40 adult c57bl/6j mice. *Neuroimage* 42 (1), 60–69. [25](#)

Drew, B., Jones, E. C., Reinsberg, S., Yung, A. C., Goldenberg, S. L., Kozlowski, P., 2010. Device for sectioning prostatectomy specimens to facilitate comparison between histology and in vivo mri. *Journal of Magnetic Resonance Imaging* 32 (4), 992–996. [17](#)

Dubois, A., Dauguet, J., Herard, A.-S., Besret, L., Duchesnay, E., Frouin, V., Hantraye, P., Bonvento, G., Delzescaux, T., 2007. Automated three-dimensional analysis of histological and autoradiographic rat brain sections: application to an activation study. *Journal of Cerebral Blood Flow & Metabolism* 27 (10), 1742–1755. [3](#), [5](#), [8](#), [10](#), [14](#), [24](#)

Duck, F. A., 2013. *Physical properties of tissues: a comprehensive reference book*. Academic press. [28](#)

Edwards, P. J., Nijmeh, A. D., McGurk, M., Odell, E., Fenlon, M. R., Marsden, P. K., Hawkes, D. J., 2005. Validation of pet imaging by alignment to histology slices. In: *Medical Image Computing and Computer-Assisted Intervention-MICCAI 2005*. Springer, pp. 968–975. [25](#)

Eiben, B., Palm, C., Pietrzyk, U., Amunts, K., Davatzikos, C., 2010. Perspective error correction using registration for blockface volume reconstruction of serial histological sections of the human brain. In: *Bildverarbeitung für die Medizin*. Citeseer, pp. 301–305. [20](#)

Emmenlauer, M., Ronneberger, O., Ponti, A., Schwarb, P., Griffa, A., Filippi, A., Nitschke, R., Driever, W., Burkhardt, H., 2009. Xuvtools: free, fast and reliable stitching of large 3d datasets. *Journal of microscopy* 233 (1), 42–60. [9](#)

Falcão, A. X., Udupa, J. K., Samarasekera, S., Sharma, S., Hirsch, B. E., Lotufo, R. d. A., 1998. User-steered image segmentation paradigms: Live wire and live lane. *Graphical models and image processing* 60 (4), 233–260. [8](#), [22](#)

Fernandez-Gonzalez, R., Deschamps, T., Idica, A., Malladi, R., de Solorzano, C. O., 2004. Automatic segmentation of histological structures in mammary gland tissue sections. *Journal of biomedical optics* 9 (3), 444–453. [8](#)

Ferrante, E., Paragios, N., 2017. Slice-to-volume medical image registration: A survey. *Medical Image Analysis* 39, 101–123. [18](#)

Feuerstein, M., Heibel, H., Gardiazabal, J., Navab, N., Groher, M., 2011. Reconstruction of 3-d histology images by simultaneous deformable registration. In: *Medical Image Computing and Computer-Assisted Intervention-MICCAI 2011*. Springer, pp. 582–589. [10](#), [15](#)

Fiala, J. C., 2005. Reconstruct: a free editor for serial section microscopy. *Journal of microscopy* 218 (1), 52–61. [10](#)

Filippi, M., Rocca, M. A., Barkhof, F., Brück, W., Chen, J. T., Comi, G., DeLuca, G., De Stefano, N., Erickson, B. J., Evangelou, N., et al., 2012. Association between pathological and mri findings in multiple sclerosis. *The Lancet Neurology* 11 (4), 349–360. [2](#)

Fischer, B., Modersitzki, J., 2003. Curvature based image registration. *Journal of Mathematical Imaging and Vision* 18 (1), 81–85. [14](#), [15](#)

Fischer, H. W., Van Haverbeke, Y., Rinck, P. A., Schmitz-Feuerhake, I., Muller, R. N., 1989. The effect of aging and storage conditions on excised tissues as monitored by longitudinal relaxation dispersion profiles. *Magnetic resonance in medicine* 9 (3), 315–324. [28](#)

Fischl, B., 2013. Estimating the location of brodmann areas from cortical folding patterns using histology and ex vivo mri. In: *Microstructural Parcellation of the Human Cerebral Cortex*. Springer, pp. 129–156. [2](#)

Fischler, M. A., Bolles, R. C., 1981. Random sample consensus: a paradigm for model fitting with applications to image analysis and automated cartography. *Communications of the ACM* 24 (6), 381–395. [13](#)

Fónyad, L., Shinoda, K., Farkash, E. A., Groher, M., Sebastian, D. P., Szász, A. M., Colvin, R. B., Yagi, Y., 2015. 3-dimensional digital reconstruction of the murine coronary system for the evaluation of chronic allograft vasculopathy. *Diagnostic pathology* 10 (1), 16. [10](#)

Frick, A., Möhring, W., Newcombe, N. S., 2014. Development of mental transformation abilities. *Trends in cognitive sciences* 18 (10), 536–542. [1](#)

Friedrich, F., Beutel, R. G., 2010. The thoracic morphology of nannochorista (nannochoristidae) and its implications for the phylogeny of mecoptera and antliophora. *Journal of Zoological systematics and evolutionary Research* 48 (1), 50–74. [10](#)

Gaffling, S., Daum, V., Hornegger, J., 2011. Landmark-constrained 3-d histological imaging: A morphology-preserving approach. In: *VMV*. pp. 309–316. [10](#), [12](#), [14](#), [23](#), [24](#)

Gaffling, S., Daum, V., Steidl, S., Maier, A., Köstler, H., Hornegger, J., 2015. A gauss-seidel iteration scheme for reference-free 3-d histological image reconstruction. *IEEE transactions on medical imaging* 34 (2), 514–530. [15](#), [24](#)

Gaffling, S., Jäger, F., Daum, V., Tauchi, M., Lütjen-Drecoll, E., 2009. Interpolation of histological slices by means of non-rigid registration. In: *Bildverarbeitung für die Medizin 2009*. Springer, pp. 267–271. [7](#), [15](#)

Gagnier, K. M., Shipley, T. F., 2013. Completion in the wild: Perception of 3d forms from cross-sections. In: *Proceedings of the 35th Annual Meeting of the Cognitive Science Society, Austin, TX*. Vol. 31. pp. 2350–2355. [1](#)

Gallagher, A. C., 2012. Jigsaw puzzles with pieces of unknown orientation. In: *Computer Vision and Pattern Recognition (CVPR), 2012 IEEE Conference on*. IEEE, pp. 382–389. [26](#)

Gangolli, M., Holleran, L., Kim, J. H., Stein, T. D., Alvarez, V., McKee, A. C., Brody, D. L., 2017. Quantitative validation of a nonlinear histology-mri coregistration method using generalized q-sampling imaging in complex human cortical white matter. *NeuroImage* 153, 152–167. [16](#), [23](#), [27](#)

Gareau, D. S., Li, Y., Huang, B., Eastman, Z., Nehal, K. S., Rajadhyaksha, M.,

2008. Confocal mosaicing microscopy in mohs skin excisions: feasibility of rapid surgical pathology. *Journal of biomedical optics* 13 (5), 054001–054001. 9
- Gefen, S., Kiryati, N., Nissanov, J., 2008. Atlas-based indexing of brain sections via 2-d to 3-d image registration. *Biomedical Engineering, IEEE Transactions on* 55 (1), 147–156. 4, 18, 25
- Gefen, S., Tretiak, O., Nissanov, J., 2003. Elastic 3-d alignment of rat brain histological images. *IEEE transactions on medical imaging* 22 (11), 1480–1489. 14
- Ghaznavi, F., Evans, A., Madabhushi, A., Feldman, M., 2013. Digital imaging in pathology: whole-slide imaging and beyond. *Annual Review of Pathology: Mechanisms of Disease* 8, 331–359. 5
- Ghorbel, F., 1994. A complete invariant description for gray-level images by the harmonic analysis approach. *Pattern recognition letters* 15 (10), 1043–1051. 11
- Gibson, E., Crukley, C., Gaed, M., Gómez, J. A., Moussa, M., Chin, J. L., Bauman, G. S., Fenster, A., Ward, A. D., 2012. Registration of prostate histology images to ex vivo mr images via strand-shaped fiducials. *Journal of Magnetic Resonance Imaging* 36 (6), 1402–1412. 4, 12, 18, 23, 25
- Gijtenbeek, J. M., Wesseling, P., Maass, C., Burgers, L., van der Laak, J. A., 2006. Three-dimensional reconstruction of tumor microvasculature: simultaneous visualization of multiple components in paraffin-embedded tissue. *Angiogenesis* 8 (4), 297–305. 11
- Goerres, J., Uneri, A., De Silva, T., Ketcha, M., Reangamornrat, S., Jacobson, M., Vogt, S., Kleinszig, G., Osgood, G., Wolinsky, J.-P., et al., 2017. Spinal pedicle screw planning using deformable atlas registration. *Physics in Medicine and Biology* 62 (7), 2871. 25
- Goldszal, A. F., Tretiak, J., Hand, P. J., Bhasin, S., McEachron, D. L., 1995. Three-dimensional reconstruction of activated columns from 2-[14 c] deoxy-d-glucose data. *Neuroimage* 2 (1), 9–20. 12
- Gonzalez, R. C., 1987. *P. wintz digital image processing*. Addison-Wesley Publishing Company, 275–281. 8
- Gonzalez, R. C., Woods, R. E., 2002. *Digital image processing*. 7
- Gore, J. C., 2015. Biomedical imaging: current and future trends. *Physics World*. <http://medicalphysicsweb.org/cws/article/opinion/60791>. 2
- Goshtasby, A., 1988. Image registration by local approximation methods. *Image and Vision Computing* 6 (4), 255–261. 17
- Goubran, M., Crukley, C., de Ribaupierre, S., Peters, T. M., Khan, A. R., 2013. Image registration of ex-vivo mri to sparsely sectioned histology of hippocampal and neocortical temporal lobe specimens. *Neuroimage* 83, 770–781. 8, 18, 20, 23, 25, 26
- Goubran, M., de Ribaupierre, S., Hammond, R. R., Currie, C., Burneo, J. G., Parrent, A. G., Peters, T. M., Khan, A. R., 2015a. Registration of in-vivo to ex-vivo mri of surgically resected specimens: A pipeline for histology to in-vivo registration. *Journal of neuroscience methods* 241, 53–65. 20, 23, 25
- Goubran, M., Hammond, R. R., de Ribaupierre, S., Burneo, J. G., Mirsattari, S., Steven, D. A., Parrent, A. G., Peters, T. M., Khan, A. R., 2015b. Magnetic resonance imaging and histology correlation in the neocortex in temporal lobe epilepsy. *Annals of neurology* 77 (2), 237–250. 26
- Graham, L., Orenstein, J. M., 2007. Processing tissue and cells for transmission electron microscopy in diagnostic pathology and research. *Nature protocols* 2 (10), 2439–2450. 5
- Greenspan, H., van Ginneken, B., Summers, R. M., 2016. Guest editorial deep learning in medical imaging: Overview and future promise of an exciting new technique. *IEEE Transactions on Medical Imaging* 35 (5), 1153–1159. 27
- Groen, H. C., Van Walsum, T., Rozie, S., Klein, S., Van Gaalen, K., Gijzen, F. J., Wielopolski, P. A., Van Beusekom, H. M., De Crom, R., Verhagen, H. J., et al., 2010. Three-dimensional registration of histology of human atherosclerotic carotid plaques to in-vivo imaging. *Journal of biomechanics* 43 (11), 2087–2092. 4, 20, 22, 24, 25
- Guest, E., Baldock, R., 1995. Automatic reconstruction of serial sections using the finite element method. *Bioimaging* 3 (4), 154–167. 12, 13, 23
- Guichard, F., Morel, J., Ryan, R., 2004. Contrast invariant image analysis and pdes. preprint. 27
- Gurcan, M. N., Boucheron, L. E., Can, A., Madabhushi, A., Rajpoot, N. M., Yener, B., 2009. Histopathological image analysis: a review. *Biomedical Engineering, IEEE Reviews in* 2, 147–171. 1, 11
- Gutiérrez-Becker, B., Mateus, D., Peter, L., Navab, N., 2016. Learning optimization updates for multimodal registration. In: *International Conference on Medical Image Computing and Computer-Assisted Intervention*. Springer, pp. 19–27. 27
- Guy, J. R., Sati, P., Leibovitch, E., Jacobson, S., Silva, A. C., Reich, D. S., 2016. Custom fit 3d-printed brain holders for comparison of histology with mri in marmosets. *Journal of Neuroscience Methods* 257, 55–63. 17
- Hammelrath, L., Škokić, S., Khmelinskii, A., Hess, A., van der Knaap, N., Starling, M., Lelieveldt, B. P., Wiedermann, D., Hoehn, M., 2016. Morphological maturation of the mouse brain: An in vivo mri and histology investigation. *NeuroImage* 125, 144–152. 17
- Handschuh, S., Schwaha, T., Metscher, B. D., 2010. Showing their true colors: a practical approach to volume rendering from serial sections. *BMC developmental biology* 10 (1), 41. 4
- Haralick, R. M., 1979. Statistical and structural approaches to texture. *Proceedings of the IEEE* 67 (5), 786–804. 24
- Hardy, W. B., 1899. On the structure of cell protoplasm: Part i. the structure produced in a cell by fixative and post-mortem change. the structure of colloidal matter and the mechanism of setting and of coagulation. *The Journal of physiology* 24 (2), 158. 3
- Harkins, K. D., Xu, J., Dula, A. N., Li, K., Valentine, W. M., Gochberg, D. F., Gore, J. C., Does, M. D., 2015. The microstructural correlates of t1 in white matter. *Magnetic resonance in medicine*. 17
- Hartevelde, A., Denswil, N., Siero, J., Zwanenburg, J., Vink, A., Pouran, B., Spliet, W., Klomp, D., Luijten, P., Daemen, M., et al., 2016. Quantitative intracranial atherosclerotic plaque characterization at 7t mri: an ex vivo study with histologic validation. *American Journal of Neuroradiology* 37 (5), 802–810. 17
- Hartkens, T., Rueckert, D., Schnabel, J. A., Hawkes, D. J., Hill, D. L., 2002. Vtk cimg registration toolkit an open source software package for affine and non-rigid registration of single-and multimodal 3d images. In: *Bildverarbeitung für die Medizin 2002*. Springer, pp. 409–412. 11
- Hawrylycz, M. J., Lein, E. S., Guillozet-Bongaarts, A. L., Shen, E. H., Ng, L., Miller, J. A., Van De Lagemaat, L. N., Smith, K. A., Ebbert, A., Riley, Z. L., et al., 2012. An anatomically comprehensive atlas of the adult human brain transcriptome. *Nature* 489 (7416), 391–399. 2, 28
- Heinly, J., Dunn, E., Frahm, J.-M., 2012. Comparative evaluation of binary features. In: *Computer Vision—ECCV 2012*. Springer, pp. 759–773. 11
- Heinrich, M. P., Jenkinson, M., Bhushan, M., Matin, T., Gleeson, F. V., Brady, M., Schnabel, J. A., 2012. Mind: Modality independent neighbourhood descriptor for multi-modal deformable registration. *Medical Image Analysis* 16 (7), 1423–1435. 27
- Hess, A., Lohmann, K., Gundelfinger, E. D., Scheich, H., 1998. A new method for reliable and efficient reconstruction of 3-dimensional images from autoradiographs of brain sections. *Journal of neuroscience methods* 84 (1), 77–86. 23, 24
- Hibbard, L. S., Hawkins, R. A., 1984. Three-dimensional reconstruction of metabolic data from quantitative autoradiography of rat brain. *American Journal of Physiology-Endocrinology and Metabolism* 247 (3), E412–E419. 24
- Hibbard, L. S., Hawkins, R. A., 1988. Objective image alignment for three-dimensional reconstruction of digital autoradiograms. *Journal of neuroscience methods* 26 (1), 55–74. 24
- Hibbard, L. S., McGlone, J. S., Davis, D. W., Hawkins, R. A., 1987. Three-dimensional representation and analysis of brain energy metabolism. *Science* 236 (4809), 1641–1646. 24
- Hill, D. L., Batchelor, P. G., Holden, M., Hawkes, D. J., 2001. Medical image registration. *Physics in medicine and biology* 46 (3), R1. 9
- Holmes, D. P., Crosby, A. J., 2010. Draping films: A wrinkle to fold transition. *Physical review letters* 105 (3), 038303. 8
- Hopwood, N., 1999. "giving body" to embryos: Modeling, mechanism, and the microtome in late nineteenth-century anatomy. *Isis*, 462–496. 1
- Hsieh, J.-W., Liao, H.-Y. M., Fan, K.-C., Ko, M.-T., Hung, Y.-P., 1997. Image registration using a new edge-based approach. *Computer Vision and Image Understanding* 67 (2), 112–130. 11, 13
- Hsu, W.-Y., 2011. Analytic differential approach for robust registration of rat brain histological images. *Microscopy research and technique* 74 (6), 523–530. 11, 12
- Hsu, W.-Y., Poon, W.-F., Sun, Y.-N., 2008. Automatic seamless mosaicing of microscopic images: enhancing appearance with colour degradation compensation and wavelet-based blending. *Journal of Microscopy* 231 (3), 408–418. 8, 9, 11
- Hughes, C., Rouvière, O., Mege-Lechevallier, F., Souchon, R., Prost, R., 2013. Robust alignment of prostate histology slices with quantified accuracy. *IEEE*

- Transactions on Biomedical Engineering 60 (2), 281–291. [10](#), [12](#)
- Humm, J., Ballon, D., Hu, Y., Ruan, S., Chui, C., Tulipano, P., Erdi, A., Koutcher, J., Zakian, K., Urano, M., et al., 2003. A stereotactic method for the three-dimensional registration of multi-modality biologic images in animals: Nmr, pet, histology, and autoradiography. *Medical physics* 30 (9), 2303–2314. [5](#), [19](#), [25](#)
- Humm, J., Macklis, R. M., Lu, X., Yang, Y., Bump, K., Beresford, B., Chin, L., 1995. The spatial accuracy of cellular dose estimates obtained from 3d reconstructed serial tissue autoradiographs. *Physics in medicine and biology* 40 (1), 163. [12](#)
- James, A. P., Dasarathy, B. V., 2014. Medical image fusion: A survey of the state of the art. *Information Fusion* 19, 4–19. [16](#)
- Jia, J., Tang, C.-K., 2008. Image stitching using structure deformation. *IEEE Transactions on Pattern Analysis and Machine Intelligence* 30 (4), 617–631. [9](#)
- Jiang, L., Greenwood, T. R., Hove, E. R. A., Chughtai, K., Raman, V., Winnard, P. T., Heeren, R., Artemov, D., Glunde, K., 2013. Combined mr, fluorescence and histology imaging strategy in a human breast tumor xenograft model. *NMR in Biomedicine* 26 (3), 285–298. [4](#), [25](#)
- Johnson, G. A., Ali-Sharief, A., Badea, A., Brandenburg, J., Cofer, G., Fubara, B., Gewalt, S., Hedlund, L. W., Upchurch, L., 2007. High-throughput morphologic phenotyping of the mouse brain with magnetic resonance histology. *Neuroimage* 37 (1), 82–89. [25](#)
- Johnson, G. A., Badea, A., Brandenburg, J., Cofer, G., Fubara, B., Liu, S., Nisanov, J., 2010. Waxholm space: an image-based reference for coordinating mouse brain research. *Neuroimage* 53 (2), 365–372. [4](#), [21](#), [25](#)
- Johnson, G. A., Calabrese, E., Badea, A., Paxinos, G., Watson, C., 2012. A multidimensional magnetic resonance histology atlas of the wistar rat brain. *Neuroimage* 62 (3), 1848–1856. [21](#)
- Ju, T., Warren, J., Carson, J., Bello, M., Kakadiaris, I., Chiu, W., Thaller, C., Eichele, G., 2006. 3d volume reconstruction of a mouse brain from histological sections using warp filtering. *Journal of Neuroscience Methods* 156 (1), 84–100. [15](#), [23](#), [24](#), [25](#)
- Kakar, S., Torbenson, M., Jain, D., Wu, T.-T., Yeh, M., Ferrell, L. D., 2015. Immunohistochemical pitfalls in the diagnosis of hepatocellular adenomas and focal nodular hyperplasia: accurate understanding of diverse staining patterns is essential for diagnosis and risk assessment. *Modern Pathology* 28 (1), 159–160. [3](#)
- Karen, P., Jirkovská, M., Tomori, Z., Demjénová, E., Janáček, J., Kubinova, L., 2003. Three-dimensional computer reconstruction of large tissue volumes based on composing series of high-resolution confocal images by gluemrc and linkmrc software. *Microscopy research and technique* 62 (5), 415–422. [9](#)
- Kaye, E. A., Josan, S., Lu, A., Rosenberg, J., Daniel, B. L., Pauly, K. B., 2010. Consistency of signal intensity and t2\* in frozen ex vivo heart muscle, kidney, and liver tissue. *Journal of Magnetic Resonance Imaging* 31 (3), 719–724. [28](#)
- Khan, A. M., Rajpoot, N., Treanor, D., Magee, D., 2014. A nonlinear mapping approach to stain normalization in digital histopathology images using image-specific color deconvolution. *IEEE Transactions on Biomedical Engineering* 61 (6), 1729–1738. [7](#)
- Khimchenko, A., Deyhle, H., Schulz, G., Schweighauser, G., Hench, J., Chicherova, N., Bikis, C., Hieber, S. E., Müller, B., 2016. Extending two-dimensional histology into the third dimension through conventional micro computed tomography. *NeuroImage* 139, 26–36. [18](#)
- Kilsdonk, I. D., Jonkman, L. E., Klaver, R., van Veluw, S. J., Zwanenburg, J. J., Kuijper, J. P., Pouwels, P. J., Twisk, J. W., Wattjes, M. P., Luijten, P. R., et al., 2016. Increased cortical grey matter lesion detection in multiple sclerosis with 7 t mri: a post-mortem verification study. *Brain* 139 (5), 1472–1481. [17](#)
- Kim, B., Boes, J. L., Frey, K. A., Meyer, C. R., 1997. Mutual information for automated unwarping of rat brain autoradiographs. *Neuroimage* 5 (1), 31–40. [24](#)
- Kim, B., Frey, K. A., Mukhopadhyay, S., Ross, B. D., Meyer, C. R., 1995. Co-registration of mri and autoradiography of rat brain in three-dimensions following automatic reconstruction of 2d data set. In: *Computer vision, virtual reality and robotics in medicine*. Springer, pp. 262–266. [24](#)
- Kim, P., Abkarian, M., Stone, H. A., 2011. Hierarchical folding of elastic membranes under biaxial compressive stress. *Nature materials* 10 (12), 952–957. [27](#)
- Kim, T.-S., Singh, M., Sungkara, W., Zarow, C., Chui, H., 2000. Automatic registration of postmortem brain slices to mri reference volume. *Nuclear Science, IEEE Transactions on* 47 (4), 1607–1613. [18](#), [23](#)
- Kindle, L., Kakadiaris, I., Ju, T., Carson, J., 2011. A semiautomated approach for artefact removal in serial tissue cryosections. *Journal of microscopy* 241 (2), 200–206. [8](#), [11](#)
- Klein, S., Staring, M., Murphy, K., Viergever, M. A., Pluim, J. P., 2010. Elastix: a toolbox for intensity-based medical image registration. *Medical Imaging, IEEE Transactions on* 29 (1), 196–205. [11](#), [19](#)
- Koh, J., Chung, Y. E., Nahm, J. H., Kim, H. Y., Kim, K.-S., Park, Y. N., Kim, M.-J., Choi, J.-Y., 2016. Intrahepatic mass-forming cholangiocarcinoma: prognostic value of preoperative gadoteric acid-enhanced mri. *European radiology* 26 (2), 407–416. [17](#)
- Kong, W., Kimia, B. B., 2001. On solving 2d and 3d puzzles using curve matching. In: *Computer Vision and Pattern Recognition, 2001. CVPR 2001. Proceedings of the 2001 IEEE Computer Society Conference on*. Vol. 2. IEEE, pp. II–583. [8](#)
- Koshevoy, P., Tasdizen, T., Whitaker, R., 2006. Implementation of an automatic slice-to-slice registration tool. University of Utah, SCI Institute Technical Report UUSCI-2006-018. [11](#), [13](#)
- Kothari, S., Phan, J. H., Wang, M. D., et al., 2013. Eliminating tissue-fold artifacts in histopathological whole-slide images for improved image-based prediction of cancer grade. *Journal of pathology informatics* 4 (1), 22. [7](#), [8](#)
- Kovačević, N., Henderson, J., Chan, E., Lifshitz, N., Bishop, J., Evans, A., Henkelman, R., Chen, X., 2005. A three-dimensional mri atlas of the mouse brain with estimates of the average and variability. *Cerebral cortex* 15 (5), 639–645. [25](#)
- Kremer, J. R., Mastronarde, D. N., McIntosh, J. R., 1996. Computer visualization of three-dimensional image data using imod. *Journal of structural biology* 116 (1), 71–76. [10](#)
- Krinidis, S., Nikou, C., Pitas, I., 2003a. A global energy function for the alignment of serially acquired slices. *Information Technology in Biomedicine, IEEE Transactions on* 7 (2), 108–113. [9](#), [15](#), [24](#)
- Krinidis, S., Nikou, C., Pitas, I., 2003b. Reconstruction of serially acquired slices using physics-based modeling. *IEEE Transactions on Information Technology in Biomedicine* 7 (4), 394–403. [12](#), [14](#)
- Kroon, D.-J., Slump, C. H., 2009. Mri modality transformation in demon registration. In: *Biomedical Imaging: From Nano to Macro, 2009. ISBI'09. IEEE International Symposium on*. IEEE, pp. 963–966. [18](#)
- Laissue, P., Reiter, C., Hiesinger, P., Halter, S., Fischbach, K., Stocker, R., 1999. Three-dimensional reconstruction of the antennal lobe in drosophila melanogaster. *Journal of Comparative Neurology* 405 (4), 543–552. [10](#)
- Lazebnik, R. S., Lancaster, T. L., Breen, M. S., Lewin, J. S., Wilson, D. L., 2003. Volume registration using needle paths and point landmarks for evaluation of interventional mri treatments. *IEEE transactions on medical imaging* 22 (5), 653–660. [22](#), [23](#)
- Le Nobin, J., Rosenkrantz, A. B., Villers, A., Orczyk, C., Deng, F.-M., Melamed, J., Mikheev, A., Rusinek, H., Taneja, S. S., 2015. Image guided focal therapy for magnetic resonance imaging visible prostate cancer: defining a 3-dimensional treatment margin based on magnetic resonance imaging histology co-registration analysis. *The Journal of urology* 194 (2), 364–370. [4](#), [10](#), [25](#)
- Lebenberg, J., Hérard, A.-S., Dubois, A., Dauguet, J., Frouin, V., Dhenain, M., Hantraye, P., Delzescaux, T., 2010. Validation of mri-based 3d digital atlas registration with histological and autoradiographic volumes: an anatomofunctional transgenic mouse brain imaging study. *Neuroimage* 51 (3), 1037–1046. [5](#), [22](#), [23](#), [25](#)
- Lee, J. S., Ahn, S.-H., Lee, D. S., Oh, S. H., Kim, C. S., Jeong, J. M., Park, K. S., Chung, J.-K., Lee, M. C., 2005. Voxel-based statistical analysis of cerebral glucose metabolism in the rat cortical deafness model by 3d reconstruction of brain from autoradiographic images. *European journal of nuclear medicine and molecular imaging* 32 (6), 696–701. [8](#), [9](#), [14](#), [24](#)
- Leong, F. W., Brady, M., McGee, J. O., 2003. Correction of uneven illumination (vignetting) in digital microscopy images. *Journal of clinical pathology* 56 (8), 619–621. [8](#)
- Leutenegger, S., Chli, M., Siegwart, R. Y., 2011. Brisk: Binary robust invariant scalable keypoints. In: *2011 International conference on computer vision*. IEEE, pp. 2548–2555. [11](#)
- Levinthal, C., Ware, R., 1972. Three dimensional reconstruction from serial sections. [9](#)
- Li, C., Xu, C., Gui, C., Fox, M. D., 2005. Level set evolution without re-initialization: a new variational formulation. In: *2005 IEEE Computer Society Conference on Computer Vision and Pattern Recognition (CVPR'05)*. Vol. 1. IEEE, pp. 430–436. [8](#)
- Li, G., Nikolova, S., Bartha, R., 2006. Registration of in vivo magnetic resonance

- t 1-weighted brain images to triphenyltetrazolium chloride stained sections in small animals. *Journal of neuroscience methods* 156 (1), 368–375. **16, 25**
- Li, X., J. H., Mori, S., 2001. Diffreomap. Kennedy Krieger Insitute & Johns Hopkins University, <https://www.mristudio.org/>. **19**
- Li, X., Yankeelov, T. E., Rosen, G. D., Gore, J. C., Dawant, B. M., 2009. Enhancement of histological volumes through averaging and their use for the analysis of magnetic resonance images. *Magnetic resonance imaging* 27 (3), 401–416. **4, 7, 8, 19, 23**
- Lin, F., Shi, J., 2015. Standardization of diagnostic immunohistochemistry. In: *Handbook of Practical Immunohistochemistry*. Springer, pp. 17–30. **28**
- Lisani, J. L., Moisan, L., Monasse, P., Morel, J.-M., 2003. On the theory of planar shape. *Multiscale Modeling & Simulation* 1 (1), 1–24. **27**
- Litjens, G., Kooi, T., Bejnordi, B. E., Setio, A. A. A., Ciompi, F., Ghafoorian, M., van der Laak, J. A., van Ginneken, B., Sánchez, C. I., 2017. A survey on deep learning in medical image analysis. arXiv preprint arXiv:1702.05747. **27**
- Liu, Y., Sajja, B. R., Uberti, M. G., Gendelman, H. E., Kielian, T., Boska, M. D., 2012. Landmark optimization using local curvature for point-based nonlinear rodent brain image registration. *Journal of Biomedical Imaging* 2012, 1. **23**
- Lobachev, O., Ulrich, C., Steiniger, B. S., Wilhelmi, V., Stachniss, V., Guthe, M., 2017. Feature-based multi-resolution registration of immunostained serial sections. *Medical Image Analysis* 35, 288–302. **11, 13**
- Lockwood-Estrin, G., Thom, M., Focke, N. K., Symms, M. R., Martinian, L., Sisodiya, S. M., Duncan, J. S., Eriksson, S. H., 2012. Correlating 3t mri and histopathology in patients undergoing epilepsy surgery. *Journal of neuroscience methods* 205 (1), 182–189. **5, 25**
- Lohmann, G., 1998. Extracting line representations of sulcal and gyral patterns in mr images of the human brain. *IEEE Transactions on Medical Imaging* 17 (6), 1040–1048. **23**
- Lohmann, K., Gundelfinger, E. D., Scheich, H., Grimm, R., Tischmeyer, W., Richter, K., Hess, A., 1998. Brainview: a computer program for reconstruction and interactive visualization of 3d data sets. *Journal of neuroscience methods* 84 (1), 143–154. **10**
- Lopez, X. M., D’Andrea, E., Barbot, P., Bridoux, A.-S., Rorive, S., Salmon, I., Debeir, O., Decaestecker, C., 2013. An automated blur detection method for histological whole slide imaging. *PLoS one* 8 (12), e82710. **6**
- Lopez Gonzalez, M., Foo, S., Holmes, W., Stewart, W., Muir, K., Condon, B., Welch, G., Forbes, K., 2016. Atherosclerotic carotid plaque composition: A 3t and 7t mri-histology correlation study. *Journal of Neuroimaging*. **17**
- Lopresti, V., Macagno, E., Levinthal, C., 1973. Structure and development of neuronal connections in isogenic organisms: cellular interactions in the development of the optic lamina of daphnia. *Proceedings of the National Academy of Sciences* 70 (2), 433–437. **9**
- Lowe, D. G., 1999. Object recognition from local scale-invariant features. In: *Computer vision, 1999. The proceedings of the seventh IEEE international conference on*. Vol. 2. Ieee, pp. 1150–1157. **11, 27**
- Ma, B., Zimmermann, T., Rohde, M., Winkelbach, S., He, F., Lindenmaier, W., Dittmar, K. E., 2007. Use of autostitch for automatic stitching of microscope images. *Micron* 38 (5), 492–499. **9**
- Ma, Y., Hof, P., Grant, S., Blackband, S., Bennett, R., Slatest, L., McGuigan, M., Benveniste, H., 2005. A three-dimensional digital atlas database of the adult c57bl/6j mouse brain by magnetic resonance microscopy. *Neuroscience* 135 (4), 1203–1215. **25**
- Macenko, M., Niethammer, M., Marron, J. S., Borland, D., Woosley, J. T., Guan, X., Schmitt, C., Thomas, N. E., 2009. A method for normalizing histology slides for quantitative analysis. In: *ISBI*. Vol. 9. pp. 1107–1110. **7**
- Madabhushi, A., Lee, G., 2016. Image analysis and machine learning in digital pathology: challenges and opportunities. **1, 2, 28**
- Magee, D., Song, Y., Gilbert, S., Roberts, N., Wijayathunga, N., Wilcox, R., Bulpiatt, A., Treanor, D., 2015. Histopathology in 3d: From three-dimensional reconstruction to multi-stain and multi-modal analysis. *Journal of pathology informatics* 6. **4, 24**
- Magee, D., Treanor, D., Crellin, D., Shires, M., Smith, K., Mohee, K., Quirke, P., 2009. Colour normalisation in digital histopathology images. In: *Proc Optical Tissue Image analysis in Microscopy, Histopathology and Endoscopy (MICCAI Workshop)*. Vol. 100. Citeseer. **7**
- Mailly, P., Haber, S. N., Groenewegen, H. J., Deniau, J.-M., 2010. A 3d multi-modal and multi-dimensional digital brain model as a framework for data sharing. *Journal of neuroscience methods* 194 (1), 56–63. **4, 25**
- Maintz, J. A., Viergever, M. A., 1998. A survey of medical image registration. *Medical image analysis* 2 (1), 1–36. **9, 23**
- Mair, E., Hager, G. D., Burschka, D., Suppa, M., Hirzinger, G., 2010. Adaptive and generic corner detection based on the accelerated segment test. In: *European conference on Computer vision*. Springer, pp. 183–196. **11**
- Majka, P., Wójcik, D. K., 2015. Possum—a framework for three-dimensional reconstruction of brain images from serial sections. *Neuroinformatics*, 1–14. **10, 19, 24**
- Malandain, G., Bardinet, E., 2003. Intensity compensation within series of images. In: *International Conference on Medical Image Computing and Computer-Assisted Intervention*. Springer, pp. 41–49. **7, 8**
- Malandain, G., Bardinet, É., Nelissen, K., Vanduffel, W., 2004. Fusion of autoradiographs with an mr volume using 2-d and 3-d linear transformations. *NeuroImage* 23 (1), 111–127. **2, 5, 8, 10, 19, 23, 24**
- Mallat, S., Zhong, S., 1992. Characterization of signals from multiscale edges. *IEEE Transactions on pattern analysis and machine intelligence* 14 (7), 710–732. **11**
- Mangin, J.-F., Coulon, O., Frouin, V., 1998. Robust brain segmentation using histogram scale-space analysis and mathematical morphology. In: *International Conference on Medical Image Computing and Computer-Assisted Intervention*. Springer, pp. 1230–1241. **8**
- Mansoori, T., Plank, G., Burton, R., Schneider, J., Kohl, P., Gavaghan, D., Grau, V., 2007. An iterative method for registration of high-resolution cardiac histoanatomical and mri images. In: *Biomedical Imaging: From Nano to Macro, 2007. ISBI 2007. 4th IEEE International Symposium on*. IEEE, pp. 572–575. **24**
- Markelj, P., Tomaževič, D., Likar, B., Pernuš, F., 2012. A review of 3d/2d registration methods for image-guided interventions. *Medical image analysis* 16 (3), 642–661. **18**
- Marr, D., 1982. *Vision: A computational investigation into the human representation and processing of visual information*, henry holt and co. Inc., New York, NY 2, 4–2. **27**
- Martel, G., Kiss, S., Gilbert, G., Anne-Archard, N., Richard, H., Moser, T., Laverty, S., 2016. Differences in the vascular tree of the femoral trochlear growth cartilage at osteochondrosis-susceptible sites in foals revealed by swi 3t mri. *Journal of Orthopaedic Research*. **17**
- Mathiisen, T. M., Lehre, K. P., Danbolt, N. C., Ottersen, O. P., 2010. The perivascular astroglial sheath provides a complete covering of the brain microvessels: an electron microscopic 3d reconstruction. *Glia* 58 (9), 1094–1103. **10**
- Mattes, D., Haynor, D. R., Vesselle, H., Lewellen, T. K., Eubank, W., 2003. Pet-ct image registration in the chest using free-form deformations. *IEEE transactions on medical imaging* 22 (1), 120–128. **21**
- Mazaheri, Y., Bokacheva, L., Kroon, D.-J., Akin, O., Hricak, H., Chamudot, D., Fine, S., Koutcher, J. A., 2010. Semi-automatic deformable registration of prostate mr images to pathological slices. *Journal of Magnetic Resonance Imaging* 32 (5), 1149–1157. **4, 16, 24, 25**
- Mazziotta, J. C., Toga, A. W., Evans, A., Fox, P., Lancaster, J., 1995. A probabilistic atlas of the human brain: theory and rationale for its development the international consortium for brain mapping (icbm). *Neuroimage* 2 (2PA), 89–101. **2**
- McCann, M. T., Ozolek, J. A., Castro, C. A., Parvin, B., Kovacevic, J., 2015. Automated histology analysis: Opportunities for signal processing. *IEEE Signal Processing Magazine* 32 (1), 78. **9**
- Mertzanidou, T., Hipwell, J. H., Reis, S., Bejnordi, B. E., Hermsen, M., Dalmis, M., Vreemann, S., Platel, B., van der Laak, J., Karssemeijer, N., et al., 2016. Whole mastectomy volume reconstruction from 2d radiographs and its mapping to histology. In: *International Workshop on Digital Mammography*. Springer, pp. 367–374. **10, 25**
- Mertzanidou, T., Hipwell, J. H., Reis, S., Hawkes, D. J., Bejnordi, B. E., Dalmis, M., Vreemann, S., Platel, B., der Laak, J., Karssemeijer, N., et al., 2017. 3d volume reconstruction from serial breast specimen radiographs for mapping between histology and 3d whole specimen imaging. *Medical Physics*. **25**
- Meyer, C., Ma, B., Kunju, L. P., Davenport, M., Piert, M., 2013. Challenges in accurate registration of 3-d medical imaging and histopathology in primary prostate cancer. *European journal of nuclear medicine and molecular imaging* 40 (1), 72–78. **17**
- Meyer, C. R., Moffat, B. A., Kuszpit, K., Bland, P. L., Chenevert, T., Rehemtulla, A., Ross, B., 2006. A methodology for registration of a histological slide and in vivo mri volume based on optimizing mutual information. *Molecular imaging* 5 (1), 16. **4, 22, 23**
- Miao, S., Wang, Z. J., Liao, R., 2016. A cnn regression approach for real-time 2d/3d registration. *IEEE transactions on medical imaging* 35 (5), 1352–1363.

- Micheva, K. D., Smith, S. J., 2007. Array tomography: a new tool for imaging the molecular architecture and ultrastructure of neural circuits. *Neuron* 55 (1), 25–36. [10](#)
- Mikula, S., Denk, W., 2015. High-resolution whole-brain staining for electron microscopic circuit reconstruction. *Nature methods* 12 (6), 541–546. [5](#)
- Milidonis, X., Marshall, I., Macleod, M. R., Sena, E. S., 2015. Magnetic resonance imaging in experimental stroke and comparison with histology systematic review and meta-analysis. *Stroke* 46 (3), 843–851. [28](#)
- Millman, R. S., Parker, G. D., 1977. Elements of differential geometry. [14](#)
- Mishchenko, Y., 2009. Automation of 3d reconstruction of neural tissue from large volume of conventional serial section transmission electron micrographs. *Journal of neuroscience methods* 176 (2), 276–289. [10](#)
- Modat, M., Cash, D. M., Daga, P., Winston, G. P., Duncan, J. S., Ourselin, S., 2014. Global image registration using a symmetric block-matching approach. *Journal of Medical Imaging* 1 (2), 024003–024003. [11](#)
- Modat, M., Ridgway, G. R., Taylor, Z. A., Lehmann, M., Barnes, J., Hawkes, D. J., Fox, N. C., Ourselin, S., 2010. Fast free-form deformation using graphics processing units. *Computer methods and programs in biomedicine* 98 (3), 278–284. [11](#)
- Modersitzki, J., 2003. Numerical methods for image registration. Oxford university press. [15](#)
- Modersitzki, J., 2004. Numerical methods for image registration. Oxford University Press on Demand. [13, 15](#)
- Mokhtarian, F., Mackworth, A., 1986. Scale-based description and recognition of planar curves and two-dimensional shapes. *IEEE transactions on pattern analysis and machine intelligence* (1), 34–43. [14](#)
- Moré, J. J., 1978. The levenberg-marquardt algorithm: implementation and theory. In: *Numerical analysis*. Springer, pp. 105–116. [12](#)
- Morel, J.-M., Yu, G., 2011. Is sift scale invariant? *Inverse Problems and Imaging* 5 (1), 115–136. [27](#)
- Mori, K., 2016. From macro-scale to micro-scale computational anatomy: a perspective on the next 20 years. [2](#)
- Mortensen, E., Morse, B., Barrett, W., Udupa, J., 1992. Adaptive boundary detection using 'live-wire' two-dimensional dynamic programming. *IEEE*. [8, 22](#)
- Mosaliganti, K., Pan, T., Sharp, R., Ridgway, R., Iyengar, S., Gulacy, A., Wenzel, P., de Bruin, A., Machiraju, R., Huang, K., et al., 2006. Registration and 3d visualization of large microscopy images. In: *Medical imaging. International Society for Optics and Photonics*, pp. 61442V–61442V. [11](#)
- Müller, M., Yigitsoy, M., Heibel, H., Navab, N., 2014. Deformable reconstruction of histology sections using structural probability maps. In: *Medical Image Computing and Computer-Assisted Intervention–MICCAI 2014*. Springer, pp. 122–129. [15, 24](#)
- Nakagawa, Y., Sekiya, I., Kondo, S., Tabuchi, T., Ichinose, S., Koga, H., Tsuji, K., Muneta, T., 2016. Relationship between mri T1rho value and histological findings of intact and radially incised menisci in microminipigs. *Journal of Magnetic Resonance Imaging* 43 (2), 434–445. [17](#)
- Nesbit, G. M., Forbes, G. S., Scheithauer, B. W., Okazaki, H., Rodriguez, M., 1991. Multiple sclerosis: histopathologic and mr and/or ct correlation in 37 cases at biopsy and three cases at autopsy. *Radiology* 180 (2), 467–474. [16](#)
- Nikou, C., Heitz, F., Nehlig, A., Namer, I. J., Armspach, J.-P., 2003. A robust statistics-based global energy function for the alignment of serially acquired autoradiographic sections. *Journal of neuroscience methods* 124 (1), 93–102. [8, 10, 14, 24](#)
- Nir, G., Sahebjavaher, R. S., Kozlowski, P., Chang, S. D., Jones, E. C., Goldenberg, S. L., Salcudean, S. E., 2014. Registration of whole-mount histology and volumetric imaging of the prostate using particle filtering. *Medical Imaging, IEEE Transactions on* 33 (8), 1601–1613. [4, 18, 23, 24, 25](#)
- Noroozi, M., Favaro, P., 2016. Unsupervised learning of visual representations by solving jigsaw puzzles. In: *European Conference on Computer Vision*. Springer, pp. 69–84. [26](#)
- Nyul, L. G., Udupa, J. K., 1999. On standardizing the mr image intensity scale. *image* 1081. [7](#)
- Oh, S. W., Harris, J. A., Ng, L., Winslow, B., Cain, N., Mihalas, S., Wang, Q., Lau, C., Kuan, L., Henry, A. M., et al., 2014. A mesoscale connectome of the mouse brain. *Nature* 508 (7495), 207–214. [2](#)
- Onozato, M. L., Hammond, S., Merren, M., Yagi, Y., 2013. Evaluation of a completely automated tissue-sectioning machine for paraffin blocks. *Journal of clinical pathology* 66 (2), 151–154. [10](#)
- Osechinskiy, S., Kruggel, F., 2010. Slice-to-volume nonrigid registration of histological sections to mr images of the human brain. *Anatomy Research International* 2011. [4, 18, 23](#)
- Ou, Y., Davatzikos, C., 2009. Dramms: deformable registration via attribute matching and mutual-saliency weighting. In: *Information Processing in Medical Imaging*. Springer, pp. 50–62. [4, 9, 11, 19, 20, 23, 24, 25](#)
- Ourselin, S., Bardin, E., Dormont, D., Malandain, G., Roche, A., Ayache, N., Tande, D., Parain, K., Yelnik, J., 2001a. Fusion of histological sections and mr images: towards the construction of an atlas of the human basal ganglia. In: *Medical Image Computing and Computer-Assisted Intervention–MICCAI 2001*. Springer, pp. 743–751. [25](#)
- Ourselin, S., Roche, A., Prima, S., Ayache, N., 2000. Block matching: A general framework to improve robustness of rigid registration of medical images. In: *International Conference on Medical Image Computing And Computer-Assisted Intervention*. Springer, pp. 557–566. [14, 15, 22](#)
- Ourselin, S., Roche, A., Subsol, G., Pennec, X., Ayache, N., 2001b. Reconstructing a 3d structure from serial histological sections. *Image and vision computing* 19 (1), 25–31. [9, 12, 14](#)
- Paikin, G., Tal, A., 2015. Solving multiple square jigsaw puzzles with missing pieces. In: *2015 IEEE Conference on Computer Vision and Pattern Recognition (CVPR)*. IEEE, pp. 4832–4839. [8](#)
- Palm, C., Axer, M., Gräbel, D., Dammers, J., Lindemeyer, J., Zilles, K., Pietrzyk, U., Amunts, K., 2010. Towards ultra-high resolution fibre tract mapping of the human brain—registration of polarised light images and reorientation of fibre vectors. *Frontiers in human neuroscience* 4, 9. [4, 5, 8, 24](#)
- Palm, C., Penney, G. P., Crum, W. R., Schnabel, J. A., Pietrzyk, U., Hawkes, D. J., 2008. Fusion of rat brain histology and mri using weighted multi-image mutual information. In: *Medical Imaging. International Society for Optics and Photonics*, pp. 69140M–69140M. [4](#)
- Palokangas, S., Selinummi, J., Yli-Harja, O., 2007. Segmentation of folds in tissue section images. In: *2007 29th Annual International Conference of the IEEE Engineering in Medicine and Biology Society. IEEE*, pp. 5641–5644. [7, 8](#)
- Park, H., Piert, M. R., Khan, A., Shah, R., Hussain, H., Siddiqui, J., Chenevert, T. L., Meyer, C. R., 2008. Registration methodology for histological sections and in vivo imaging of human prostate. *Academic radiology* 15 (8), 1027–1039. [22, 23](#)
- Paxinos, G., Huang, X.-F., Toga, A. W., 2000. The rhesus monkey brain in stereotaxic coordinates. [23](#)
- Peng, T., Wang, L., Bayer, C., Conjeti, S., Baust, M., Navab, N., 2014. Shading correction for whole slide image using low rank and sparse decomposition. In: *International Conference on Medical Image Computing and Computer-Assisted Intervention*. Springer, pp. 33–40. [8](#)
- Penzias, G., Janowczyk, A., Singanamalli, A., Rusu, M., Shih, N., Feldman, M., Stricker, P. D., Delprado, W., Tiwari, S., Böhm, M., et al., 2016. Autostitcher: An automated program for efficient and robust reconstruction of digitized whole histological sections from tissue fragments. *Scientific Reports* 6, 29906. [9](#)
- Pernkopf, F., Bouchaffra, D., 2005. Genetic-based em algorithm for learning gaussian mixture models. *IEEE Transactions on Pattern Analysis and Machine Intelligence* 27 (8), 1344–1348. [12](#)
- Peters, S. R., 2003. The art of embedding tissue for frozen section. part i: a system for precision face down cryoembedding of tissues using freezing temperature-embedding wells. *Journal of histotechnology* 26 (1), 11–19. [4](#)
- Peters, S. R., 2010. A practical guide to frozen section technique. Springer. [4, 6](#)
- Pfaff, T., Narain, R., de Joya, J. M., O'Brien, J. F., 2014. Adaptive tearing and cracking of thin sheets. *ACM Transactions on Graphics (TOG)* 33 (4), 110. [8, 27](#)
- Piccinini, F., Bevilacqua, A., Lucarelli, E., 2013a. Automated image mosaics by non-automated light microscopes: the micromos software tool. *Journal of microscopy* 252 (3), 226–250. [9](#)
- Piccinini, F., Bevilacqua, A., Smith, K., Horvath, P., 2013b. Vignetting and photo-bleaching correction in automated fluorescence microscopy from an array of overlapping images. In: *2013 IEEE 10th International Symposium on Biomedical Imaging*. IEEE, pp. 464–467. [8](#)
- Pichat, J., Modat, M., Yousry, T., Ourselin, S., 2015. A multi-path approach to histology volume reconstruction. In: *Biomedical Imaging (ISBI), 2015 IEEE 12th International Symposium on*. IEEE, pp. 1280–1283. [7, 10, 11](#)
- Piert, M., Park, H., Khan, A., Siddiqui, J., Hussain, H., Chenevert, T., Wood, D., Johnson, T., Shah, R. B., Meyer, C., 2009. Detection of aggressive primary prostate cancer with 11c-choline pet/ct using multimodality fusion techniques. *Journal of Nuclear Medicine* 50 (10), 1585–1593. [22, 23](#)

- Pitiot, A., Bardinet, E., Thompson, P. M., Malandain, G., 2006. Piecewise affine registration of biological images for volume reconstruction. *Medical image analysis* 10 (3), 465–483. **9, 15**
- Plum, J. P., Maintz, J. A., Viergever, M. A., 2000. Image registration by maximization of combined mutual information and gradient information. In: *International Conference on Medical Image Computing and Computer-Assisted Intervention*. Springer, pp. 452–461. **13**
- Pocivavsek, L., Dellsy, R., Kern, A., Johnson, S., Lin, B., Lee, K. Y. C., Cerda, E., 2008. Stress and fold localization in thin elastic membranes. *Science* 320 (5878), 912–916. **27**
- Preibisch, S., Saalfeld, S., Tomancak, P., 2009. Globally optimal stitching of tiled 3d microscopic image acquisitions. *Bioinformatics* 25 (11), 1463–1465. **9**
- Prescott, J., Clary, M., Wiet, G., Pan, T., Huang, K., 2006. Automatic registration of large set of microscopic images using high-level features. In: *3rd IEEE International Symposium on Biomedical Imaging: Nano to Macro, 2006. IEEE*, pp. 1284–1287. **11, 13**
- Priester, A., Natarajan, S., Khoshnoodi, P., Margolis, D. J., Raman, S. S., Reiter, R. E., Huang, J., Grundfest, W., Marks, L. S., 2016. Mri underestimation of prostate cancer geometry: Use of patient-specific molds to correlate images with whole-mount pathology. *The Journal of Urology*. **2**
- Prima, S., Ourselin, S., Ayache, N., 2002. Computation of the mid-sagittal plane in 3-d brain images. *Medical Imaging, IEEE Transactions on* 21 (2), 122–138. **22**
- Purea, A., Webb, A. G., 2006. Reversible and irreversible effects of chemical fixation on the nmr properties of single cells. *Magnetic resonance in medicine* 56 (4), 927–931. **28**
- Qiu, X., Pridmore, T., Pitiot, A., 2009. Correcting distorted histology slices for 3d reconstruction. *Med Image Underst Anal*. **8**
- Ramsay, J. G., 1962. Interference patterns produced by the superposition of folds of similar type. *The Journal of Geology*, 466–481. **27**
- Rangarajan, A., Chui, H., Mjolsness, E., Pappu, S., Davachi, L., Goldman-Rakic, P., Duncan, J., 1997. A robust point-matching algorithm for autoradiograph alignment. *Medical Image Analysis* 1 (4), 379–398. **12, 14, 24**
- Rasband, W., Bright, D., 1995. Nih image-a public domain image-processing program for the macintosh. *Microbeam Analysis* 4 (3), 137–149. **10**
- Rey Otero, I., Delbracio, M., 2014. Anatomy of the SIFT Method. *Image Processing On Line* 4, 370–396. **11**
- Rey-Otero, I., Delbracio, M., 2015. Is repeatability an unbiased criterion for ranking feature detectors? *SIAM Journal on Imaging Sciences* 8 (4), 2558–2580. **27**
- Rey-Otero, I., Morel, J.-M., Delbracio, M., 2015. An analysis of the factors affecting keypoint stability in scale-space. *Journal of Mathematical Imaging and Vision*, 1–19. **27**
- Reyes-Aldasoro, C. C., 2009. Retrospective shading correction algorithm based on signal envelope estimation. *Electronics letters* 45 (9), 454. **8**
- Riddle, A., Dean, J., Buser, J. R., Gong, X., Maire, J., Chen, K., Ahmad, T., Cai, V., Nguyen, T., Kroenke, C. D., et al., 2011. Histopathological correlates of magnetic resonance imaging-defined chronic perinatal white matter injury. *Annals of neurology* 70 (3), 493–507. **11**
- Roberts, N., Magee, D., Song, Y., Brabazon, K., Shires, M., Crellin, D., Orsi, N. M., Quirke, R., Quirke, P., Treanor, D., 2012. Toward routine use of 3d histopathology as a research tool. *The American journal of pathology* 180 (5), 1835–1842. **24**
- Rohde, G. K., Aldroubi, A., Dawant, B. M., 2003. The adaptive bases algorithm for intensity-based nonrigid image registration. *Medical Imaging, IEEE Transactions on* 22 (11), 1470–1479. **19, 22**
- Rohlfing, T., 2012. Image similarity and tissue overlaps as surrogates for image registration accuracy: widely used but unreliable. *IEEE transactions on medical imaging* 31 (2), 153–163. **24**
- Rohr, K., Stiehl, H. S., Sprengel, R., Beil, W., Buzug, T. M., Weese, J., Kuhn, M., 1996. Point-based elastic registration of medical image data using approximating thin-plate splines. In: *Visualization in Biomedical Computing*. Springer, pp. 297–306. **21**
- Rolls, G., 2012. Fixation and fixatives (2)-factors influencing chemical fixation, formaldehyde and glutaraldehyde. Leica Biosystems. <http://www.leicabiosystems.com/pathologyleaders/fixation-and-fixatives-2-factors-influencing-chemical-fixation-formaldehyde-and-glutaraldehyde>. **3**
- Rolls, G., et al., 2008. 101 steps to better histology. Melbourne: Leica Microsystems. **5**
- Rosai, J., 2007. Why microscopy will remain a cornerstone of surgical pathology. *Laboratory investigation* 87 (5), 403–408. **3**
- Rousseeuw, P. J., 1984. Least median of squares regression. *Journal of the American statistical association* 79 (388), 871–880. **14**
- Rueckert, D., Sonoda, L. I., Hayes, C., Hill, D. L., Leach, M. O., Hawkes, D. J., 1999. Nonrigid registration using free-form deformations: application to breast mr images. *Medical Imaging, IEEE Transactions on* 18 (8), 712–721. **16, 19, 22**
- Ruiz, A., Ujjaldon, M., Cooper, L., Huang, K., 2009. Non-rigid registration for large sets of microscopic images on graphics processors. *Journal of signal processing systems* 55 (1-3), 229–250. **11, 12, 15**
- Rusu, M., Golden, T., Wang, H., Gow, A., Madabhushi, A., 2015. Framework for 3d histologic reconstruction and fusion with in vivo mri: Preliminary results of characterizing pulmonary inflammation in a mouse model. *Medical physics* 42 (8), 4822–4832. **10, 19, 24**
- Saalfeld, S., Cardona, A., Hartenstein, V., Tomančák, P., 2010. As-rigid-as-possible mosaicking and serial section registration of large sstem datasets. *Bioinformatics* 26 (12), i57–i63. **9, 11, 13**
- Saalfeld, S., Fetter, R., Cardona, A., Tomancak, P., 2012. Elastic volume reconstruction from series of ultra-thin microscopy sections. *Nature methods* 9 (7), 717–720. **9, 10, 11, 13, 15**
- Saalfeld, S., Tomančák, P., 2008. Automatic landmark correspondence detection for imagej. In: *Proceedings of the ImageJ User and Developer Conference*. pp. 128–133. **11**
- Sakoe, H., Chiba, S., 1978. Dynamic programming algorithm optimization for spoken word recognition. *Acoustics, Speech and Signal Processing, IEEE Transactions on* 26 (1), 43–49. **15**
- Saleem, K. S., Logothetis, N. K., 2012. A combined MRI and histology atlas of the rhesus monkey brain in stereotaxic coordinates. Academic Press. **25**
- Samavati, N., McGrath, D. M., Lee, J., van der Kwast, T., Jewett, M., Ménard, C., Brock, K. K., et al., 2011. Biomechanical model-based deformable registration of mri and histopathology for clinical prostatectomy. *Journal of pathology informatics* 2 (2), 10. **4, 25, 26**
- Schmitt, O., Modersitzki, J., Heldmann, S., Wirtz, S., Fischer, B., 2007. Image registration of sectioned brains. *International Journal of Computer Vision* 73 (1), 5–39. **15**
- Schneider, C. A., Rasband, W. S., Eliceiri, K. W., et al., 2012. Nih image to imagej: 25 years of image analysis. *Nat methods* 9 (7), 671–675. **10**
- Schormann, T., Dabringhaus, A., Zilles, K., 1995. Statistics of deformations in histology and application to improved alignment with mri. *Medical Imaging, IEEE Transactions on* 14 (1), 25–35. **4, 21**
- Schormann, T., von Matthey, M., Dabringhaus, A., Zilles, K., 1993. Alignment of 3-d brain data sets originating from mr and histology. *Bioimaging* 1 (2), 119–128. **21**
- Schormann, T., Zilles, K., 1998. Three-dimensional linear and nonlinear transformations: an integration of light microscopical and mri data. *Human brain mapping* 6 (5-6), 339–347. **3, 21**
- Schubert, N., Axer, M., Schober, M., Huynh, A.-M., Huyssegoms, M., Palomero-Gallagher, N., Bjaalie, J. G., Leergaard, T. B., Kirilangic, M. E., Amunts, K., et al., 2016. 3d reconstructed cyto-, muscarinic m2 receptor, and fiber architecture of the rat brain registered to the waxholm space atlas. *Frontiers in neuroanatomy* 10. **5**
- Schwier, M., Böehler, T., Hahn, H. K., Dahmen, U., Dirsch, O., et al., 2013. Registration of histological whole slide images guided by vessel structures. *Journal of pathology informatics* 4 (2), 10. **11, 13, 24**
- Sederberg, T. W., Parry, S. R., 1986. Free-form deformation of solid geometric models. *ACM SIGGRAPH computer graphics* 20 (4), 151–160. **15**
- Seeley, E. H., Wilson, K. J., Yankeelov, T. E., Johnson, R. W., Gore, J. C., Caprioli, R. M., Matrisian, L. M., Sterling, J. A., 2014. Co-registration of multi-modality imaging allows for comprehensive analysis of tumor-induced bone disease. *Bone* 61, 208–216. **5, 25**
- Seewann, A., Kooi, E.-J., Roosendaal, S., Pouwels, P., Wattjes, M., Van der Valk, P., Barkhof, F., Polman, C., Geurts, J., 2012. Postmortem verification of ms cortical lesion detection with 3d dir. *Neurology* 78 (5), 302–308. **2**
- Shepherd, T. M., Thelwall, P. E., Stanisz, G. J., Blackband, S. J., 2009. Aldehyde fixative solutions alter the water relaxation and diffusion properties of nervous tissue. *Magnetic resonance in medicine* 62 (1), 26–34. **28**
- Shi, S.-R., Key, M. E., Kalra, K. L., 1991. Antigen retrieval in formalin-fixed, paraffin-embedded tissues: an enhancement method for immunohistochemical staining based on microwave oven heating of tissue sections. *Journal of Histochemistry & Cytochemistry* 39 (6), 741–748. **4**

- Shirley, P., 2001. Color transfer between images. *IEEE Corn* 21, 34–41. [7](#)
- Shojaii, R., Bacopulos, S., Yang, W., Karavardanyan, T., Spyropoulos, D., Raouf, A., Martel, A., Seth, A., 2014. Reconstruction of 3-dimensional histology volume and its application to study mouse mammary glands. *JoVE (Journal of Visualized Experiments)* (89), e51325–e51325. [12](#)
- Shojaii, R., Martel, A. L., 2009. A novel edge point selection method for registration of histology images. In: *Optical Tissue Image analysis in Microscopy, Histopathology and Endoscopy (OPTIMHisE) Workshop, MICCAI*. [12](#), [14](#)
- Simonetti, A. W., Elezi, V. A., Farion, R., Malandain, G., Segebarth, C., Rémy, C., Barbier, E. L., 2006. A low temperature embedding and section registration strategy for 3d image reconstruction of the rat brain from autoradiographic sections. *Journal of neuroscience methods* 158 (2), 242–250. [10](#)
- Singh, M., Rajagopalan, A., Kim, T.-S., Hwang, D., Chui, H., Zhang, X.-L., Lee, A.-Y., Zarow, C., 2008. Co-registration of in vivo human mri brain images to postmortem histological microscopic images. *International journal of imaging systems and technology* 18 (5-6), 325–335. [4](#), [18](#), [23](#), [25](#)
- Singh, R. K., Barbosa-Lorenzi, V. C., Lund, F. W., Grosheva, I., Maxfield, F. R., Haka, A. S., 2016. Degradation of aggregated ldl occurs in complex extracellular sub-compartments of the lysosomal synapse. *J Cell Sci*, jcs-181743. [10](#)
- Sled, J. G., Zijdenbos, A. P., Evans, A. C., 1998. A nonparametric method for automatic correction of intensity nonuniformity in mri data. *IEEE transactions on medical imaging* 17 (1), 87–97. [8](#)
- Solomon, J., Vouga, E., Wardetzky, M., Grinspun, E., 2012. Flexible developable surfaces. In: *Computer Graphics Forum*. Vol. 31. Wiley Online Library, pp. 1567–1576. [8](#)
- Song, Y., Treanor, D., Bulpitt, A. J., Magee, D. R., et al., 2013. 3d reconstruction of multiple stained histology images. *Journal of pathology informatics* 4 (2), 7. [4](#), [12](#), [24](#)
- Song, Y., Treanor, D., Bulpitt, A. J., Wijayathunga, N., Roberts, N., Wilcox, R., Magee, D. R., 2014. Unsupervised content classification based nonrigid registration of differently stained histology images. *IEEE Transactions on Biomedical Engineering* 61 (1), 96–108. [12](#), [13](#)
- Sorzano, C. Ó. S., Thévenaz, P., Unser, M., 2005. Elastic registration of biological images using vector-spline regularization. *Biomedical Engineering, IEEE Transactions on* 52 (4), 652–663. [11](#)
- Sotiras, A., Davatzikos, C., Paragios, N., 2013. Deformable medical image registration: A survey. *IEEE transactions on medical imaging* 32 (7), 1153–1190. [9](#), [10](#)
- Steenbergen, P., Haustermans, K., Lerut, E., Oyen, R., De Wever, L., Van den Bergh, L., Kerkmeijer, L. G., Pameijer, F. A., Veldhuis, W. B., Pos, F. J., et al., 2015. Prostate tumor delineation using multiparametric magnetic resonance imaging: Inter-observer variability and pathology validation. *Radiotherapy and Oncology* 115 (2), 186–190. [17](#)
- Stille, M., Smith, E. J., Crum, W. R., Modo, M., 2013. 3d reconstruction of 2d fluorescence histology images and registration with in vivo mr images: Application in a rodent stroke model. *Journal of neuroscience methods* 219 (1), 27–40. [4](#), [5](#), [8](#), [11](#), [19](#), [25](#)
- Streicher, J., Weninger, W. J., Müller, G. B., 1997. External marker-based automatic congruencing: a new method of 3d reconstruction from serial sections. *The Anatomical Record* 248 (4), 583–602. [3](#)
- Stüben, K., Trottenberg, U., 1982. Multigrid methods: Fundamental algorithms, model problem analysis and applications. Springer. [21](#)
- Sze, G., De Armond, S. J., Brant-Zawadzki, M., Davis, R. L., Norman, D., Newton, T. H., 1986. Foci of mri signal (pseudo lesions) anterior to the frontal horns: histologic correlations of a normal finding. *American journal of neuroradiology* 7 (3), 381–387. [16](#)
- Tan, Y., Hua, J., Dong, M., 2007. Feature curve-guided volume reconstruction from 2d images. In: *Biomedical Imaging: From Nano to Macro*, 2007. ISBI 2007. 4th IEEE International Symposium on. IEEE, pp. 716–719. [12](#), [14](#)
- Taxy, J. B., 2009. Frozen section and the surgical pathologist: a point of view. *Archives of pathology & laboratory medicine* 133 (7), 1135–1138. [4](#)
- Tekalp, A. M., 1995. Digital video processing. Prentice-Hall, Inc. [9](#)
- Thevenaz, P., Ruttimann, U. E., Unser, M., 1998. A pyramid approach to subpixel registration based on intensity. *Image Processing, IEEE Transactions on* 7 (1), 27–41. [10](#), [11](#), [21](#)
- Thevenaz, P., Unser, M., 2007. User-friendly semiautomated assembly of accurate image mosaics in microscopy. *Microscopy research and technique* 70 (2), 135–146. [9](#)
- Toews, M., Wells, W., 2009. Sift-rank: Ordinal description for invariant feature correspondence. In: *Computer Vision and Pattern Recognition, 2009. CVPR* 2009. IEEE Conference on. IEEE, pp. 172–177. [11](#)
- Toews, M., Zöllei, L., Wells, W. M., 2013. Feature-based alignment of volumetric multi-modal images. In: *International Conference on Information Processing in Medical Imaging*. Springer, pp. 25–36. [27](#)
- Traboulsee, A., Simon, J., Stone, L., Fisher, E., Jones, D., Malhotra, A., Newsome, S., Oh, J., Reich, D., Richert, N., et al., 2016. Revised recommendations of the consortium of ms centers task force for a standardized mri protocol and clinical guidelines for the diagnosis and follow-up of multiple sclerosis. *American Journal of Neuroradiology* 37 (3), 394–401. [28](#)
- Trahearn, N., Epstein, D., Snead, D., Cree, I., Rajpoot, N., 2014. A fast method for approximate registration of whole-slide images of serial sections using local curvature. In: *SPIE Medical Imaging. International Society for Optics and Photonics*, pp. 90410E–90410E. [14](#)
- Trivedi, H., Turkbey, B., Rastinehad, A. R., Benjamin, C. J., Bernardo, M., Pohida, T., Shah, V., Merino, M. J., Wood, B. J., Linehan, W. M., et al., 2012. Use of patient-specific mri-based prostate mold for validation of multiparametric mri in localization of prostate cancer. *Urology* 79 (1), 233–239. [17](#)
- Uberti, M., Liu, Y., Dou, H., Mosley, R. L., Gendelman, H. E., Boska, M., 2009. Registration of in vivo mr to histology of rodent brains using blockface imaging. In: *SPIE Medical Imaging. International Society for Optics and Photonics*, pp. 726213–726213. [8](#), [22](#)
- Ulrich, C., Lobachev, O., Steiniger, B., Guthe, M., 2014. Imaging the vascular network of the human spleen from immunostained serial sections. In: *VCBM*. Citeseer, pp. 69–78. [11](#), [13](#), [24](#)
- Vahadane, A., Peng, T., Sethi, A., Albarqouni, S., Wang, L., Baust, M., Steiger, K., Schlitter, A. M., Esposito, I., Navab, N., 2016. Structure-preserving color normalization and sparse stain separation for histological images. [7](#)
- Van de Plas, R., Yang, J., Spraggins, J., Caprioli, R. M., 2015. Image fusion of mass spectrometry and microscopy: a multimodality paradigm for molecular tissue mapping. *Nature methods* 12 (4), 366–372. [28](#)
- Van Der Kolk, A., Zwanenburg, J., Denswil, N., Vink, A., Spliet, W., Daemen, M., Visser, F., Klomp, D., Luijten, P., Hendrikse, J., 2015. Imaging the intracranial atherosclerotic vessel wall using 7t mri: initial comparison with histopathology. *American Journal of Neuroradiology* 36 (4), 694–701. [17](#)
- Vandenbergh, M. E., Hérard, A.-S., Souedet, N., Sadouni, E., Santin, M. D., Briet, D., Carré, D., Schulz, J., Hantraye, P., Chabrier, P.-E., et al., 2016. High-throughput 3d whole-brain quantitative histopathology in rodents. *Scientific reports* 6. [22](#)
- Vicory, J., Couture, H. D., Thomas, N. E., Borland, D., Marron, J. S., Woosley, J., Niethammer, M., 2015. Appearance normalization of histology slides. *Computerized Medical Imaging and Graphics* 43, 89–98. [7](#)
- Viergever, M. A., Maintz, J. A., Klein, S., Murphy, K., Staring, M., Pluim, J. P., 2016. A survey of medical image registration—under review. *Medical Image Analysis*. [9](#)
- Viola, P., Wells III, W. M., 1997. Alignment by maximization of mutual information. *International journal of computer vision* 24 (2), 137–154. [22](#)
- Vovk, U., Pernus, F., Likar, B., 2007. A review of methods for correction of intensity inhomogeneity in mri. *IEEE transactions on medical imaging* 26 (3), 405–421. [8](#)
- Wang, C.-W., Chen, H.-C., 2013. Improved image alignment method in application to x-ray images and biological images. *Bioinformatics* 29 (15), 1879–1887. [11](#), [13](#)
- Wang, C.-W., Gosno, E. B., Li, Y.-S., 2015. Fully automatic and robust 3d registration of serial-section microscopic images. *Scientific reports* 5. [5](#), [11](#), [13](#)
- Wang, C.-W., Ka, S.-M., Chen, A., 2014. Robust image registration of biological microscopic images. *Scientific reports* 4. [5](#), [10](#), [11](#), [13](#)
- Wang, Y.-Y., Chang, S.-C., Wu, L.-W., Tsai, S.-T., Sun, Y.-N., 2007. A color-based approach for automated segmentation in tumor tissue classification. In: *2007 29th Annual International Conference of the IEEE Engineering in Medicine and Biology Society. IEEE*, pp. 6576–6579. [7](#)
- Ward, A. D., Cruckley, C., McKenzie, C. A., Montreuil, J., Gibson, E., Romagnoli, C., Gomez, J. A., Moussa, M., Chin, J., Bauman, G., et al., 2012. Prostate: registration of digital histopathologic images to in vivo mr images acquired by using endorectal receive coil. *Radiology* 263 (3), 856–864. [4](#), [23](#), [25](#)
- Weinstein, R. S., Graham, A. R., Richter, L. C., Barker, G. P., Krupinski, E. A., Lopez, A. M., Erps, K. A., Bhattacharyya, A. K., Yagi, Y., Gilbertson, J. R., 2009. Overview of telepathology, virtual microscopy, and whole slide imaging: prospects for the future. *Human pathology* 40 (8), 1057–1069. [5](#)
- Wells, W. M., Viola, P., Atsumi, H., Nakajima, S., Kikinis, R., 1996. Multi-

- modal volume registration by maximization of mutual information. *Medical image analysis* 1 (1), 35–51. [19](#)
- Weninger, W. J., Meng, S., Streicher, J., Müller, G. B., 1998. A new episcopic method for rapid 3-d reconstruction: applications in anatomy and embryology. *Anatomy and embryology* 197 (5), 341–348. [3](#)
- Wentzensen, N., Braumann, U.-D., Eienkel, J., Horn, L.-C., Doeberitz, M. v. K., Löffler, M., Kuska, J.-P., 2007. Combined serial section-based 3d reconstruction of cervical carcinoma invasion using h&e/p16ink4a/cd3 alternate staining. *Cytometry Part A* 71 (5), 327–333. [13](#), [24](#)
- Winkler, H., 2007. 3d reconstruction and processing of volumetric data in cryo-electron tomography. *Journal of structural biology* 157 (1), 126–137. [10](#)
- Wirtz, S., Fischer, B., Modersitzki, J., Schmitt, O., 2004. Superfast elastic registration of histologic images of a whole rat brain for 3d reconstruction. In: *Medical Imaging 2004. International Society for Optics and Photonics*, pp. 328–334. [15](#), [23](#)
- Wirtz, S., Papenberg, N., Fischer, B., Schmitt, O., 2005. Robust and staining-invariant elastic registration of a series of images from histologic slices. In: *Medical imaging. International Society for Optics and Photonics*, pp. 1256–1262. [15](#)
- Woods, R. P., Grafton, S. T., Holmes, C. J., Cherry, S. R., Mazziotta, J. C., 1998a. Automated image registration: I. general methods and intrasubject, intramodality validation. *Journal of computer assisted tomography* 22 (1), 139–152. [11](#), [19](#)
- Woods, R. P., Grafton, S. T., Watson, J. D., Sicotte, N. L., Mazziotta, J. C., 1998b. Automated image registration: II. intersubject validation of linear and nonlinear models. *Journal of computer assisted tomography* 22 (1), 153–165. [11](#)
- Xiao, G., Bloch, B. N., Chappelow, J., Genega, E. M., Rofsky, N. M., Lenkinski, R. E., Tomaszewski, J., Feldman, M. D., Rosen, M., Madabhushi, A., 2011. Determining histology-mri slice correspondences for defining mri-based disease signatures of prostate cancer. *Computerized Medical Imaging and Graphics* 35 (7), 568–578. [17](#), [25](#), [28](#)
- Xu, Y., Pickering, J. G., Nong, Z., Gibson, E., Arpino, J.-M., Yin, H., Ward, A. D., 2015. A method for 3d histopathology reconstruction supporting mouse microvasculature analysis. *PloS one* 10 (5), e0126817. [12](#), [15](#), [24](#)
- Xu, Y., Weaver, J. B., Healy, D. M., Lu, J., 1994. Wavelet transform domain filters: a spatially selective noise filtration technique. *IEEE transactions on image processing* 3 (6), 747–758. [11](#)
- Yagi, Y., Gilbertson, J. R., 2005. Digital imaging in pathology: the case for standardization. *Journal of telemedicine and telecare* 11 (3), 109–116. [6](#)
- Yang, S., Yang, Z., Fischer, K., Zhong, K., Stadler, J., Godenschweger, F., Steiner, J., Heinze, H.-J., Bernstein, H.-G., Bogerts, B., et al., 2013. Integration of ultra-high field mri and histology for connectome based research of brain disorders. *Front Neuroanat* 7 (31), 3, 7
- Yang, Z., Richards, K., Kurniawan, N. D., Petrou, S., Reutens, D. C., 2012. Mri-guided volume reconstruction of mouse brain from histological sections. *Journal of neuroscience methods* 211 (2), 210–217. [4](#), [7](#), [8](#), [19](#), [20](#), [23](#), [28](#)
- Yelnik, J., Bardin, E., Dormont, D., Malandain, G., Ourselin, S., Tandé, D., Karachi, C., Ayache, N., Cornu, P., Agid, Y., 2007. A three-dimensional, histological and deformable atlas of the human basal ganglia. i. atlas construction based on immunohistochemical and mri data. *Neuroimage* 34 (2), 618–638. [5](#), [7](#), [20](#), [22](#), [25](#)
- Yigitsoy, M., Navab, N., 2013. Structure propagation for image registration. *IEEE transactions on medical imaging* 32 (9), 1657–1670. [8](#), [9](#)
- Yoo, T. S., Ackerman, M. J., Lorensen, W. E., Schroeder, W., Chalana, V., Aylward, S., Metaxas, D., Whitaker, R., 2002. Engineering and algorithm design for an image processing api: a technical report on itk-the insight toolkit. *Studies in health technology and informatics*, 586–592. [11](#)
- Yu, W., 2004. Practical anti-vignetting methods for digital cameras. *IEEE Transactions on Consumer Electronics* 50 (4), 975–983. [8](#)
- Yushkevich, P. A., Avants, B. B., Ng, L., Hawrylycz, M., Burstein, P. D., Zhang, H., Gee, J. C., 2006. 3d mouse brain reconstruction from histology using a coarse-to-fine approach. In: *Biomedical Image Registration*. Springer, pp. 230–237. [4](#), [5](#), [8](#), [10](#), [19](#), [20](#), [25](#)
- Yushkevich, P. A., Avants, B. B., Pluta, J., Das, S., Minkoff, D., Mechanic-Hamilton, D., Glynn, S., Pickup, S., Liu, W., Gee, J. C., et al., 2009. A high-resolution computational atlas of the human hippocampus from postmortem magnetic resonance imaging at 9.4 t. *Neuroimage* 44 (2), 385–398. [2](#)
- Yushkevich, P. A., Wisse, L., Adler, D., Ittyerah, R., Pluta, J. B., Robinson, J. L., Schuck, T., Trojanowski, J. Q., Grossman, M., Detre, J. A., et al., 2016. A framework for informing segmentation of in vivo mri with information derived from ex vivo imaging: Application in the medial temporal lobe. In: *Engineering in Medicine and Biology Society (EMBC), 2016 IEEE 38th Annual International Conference of the. IEEE*, pp. 6014–6017. [10](#), [19](#), [26](#)
- Zarow, C., Kim, T.-S., Singh, M., Chui, H., 2004. A standardized method for brain-cutting suitable for both stereology and mri-brain co-registration. *Journal of neuroscience methods* 139 (2), 209–215. [18](#)
- Zhan, Y., Ou, Y., Feldman, M., Tomaszewski, J., Davatzikos, C., Shen, D., 2007. Registering histologic and mr images of prostate for image-based cancer detection. *Academic radiology* 14 (11), 1367–1381. [4](#), [25](#)
- Zhao, W., Young, T. Y., Ginsberg, M. D., 1993. Registration and three-dimensional reconstruction of autoradiographic images by the disparity analysis method. *Medical Imaging, IEEE Transactions on* 12 (4), 782–791. [10](#), [14](#), [24](#)
- Zhu, S. C., Yuille, A., 1996. Region competition: Unifying snakes, region growing, and bayes/mdl for multiband image segmentation. *IEEE transactions on pattern analysis and machine intelligence* 18 (9), 884–900. [8](#)
- Zitova, B., Flusser, J., 2003. Image registration methods: a survey. *Image and vision computing* 21 (11), 977–1000. [9](#)